



IntechOpen

Multiplexing

Recent Advances and Novel Applications

Edited by Somayeh Mohammady



Multiplexing - Recent Advances and Novel Applications

Edited by Somayeh Mohammady

Published in London, United Kingdom



IntechOpen





Supporting open minds since 2005



Multiplexing – Recent Advances and Novel Applications

<http://dx.doi.org/10.5772/intechopen.95684>

Edited by Somayeh Mohammady

Contributors

Bentahar Attaouia, Kandouci Malika, Ghouali Samir, Dinar Amina Elbatoul, Alaaeddine Rjeb, Habib Fathallah, Mohsen Machhout, Kamayani Shrivastav, Carmen Beatriz Rodriguez Estrello, Valeri Kontorovich, Fernando Ramos-Alarcon, Nguyen Huu Trung, Mogadala Vinod Kumar, Yenneti Laxmi Lavanya, Bharati Bidikar, Gottapu Sasibhushana Rao

© The Editor(s) and the Author(s) 2022

The rights of the editor(s) and the author(s) have been asserted in accordance with the Copyright, Designs and Patents Act 1988. All rights to the book as a whole are reserved by INTECHOPEN LIMITED. The book as a whole (compilation) cannot be reproduced, distributed or used for commercial or non-commercial purposes without INTECHOPEN LIMITED's written permission. Enquiries concerning the use of the book should be directed to INTECHOPEN LIMITED rights and permissions department (permissions@intechopen.com).

Violations are liable to prosecution under the governing Copyright Law.



Individual chapters of this publication are distributed under the terms of the Creative Commons Attribution 3.0 Unported License which permits commercial use, distribution and reproduction of the individual chapters, provided the original author(s) and source publication are appropriately acknowledged. If so indicated, certain images may not be included under the Creative Commons license. In such cases users will need to obtain permission from the license holder to reproduce the material. More details and guidelines concerning content reuse and adaptation can be found at <http://www.intechopen.com/copyright-policy.html>.

Notice

Statements and opinions expressed in the chapters are these of the individual contributors and not necessarily those of the editors or publisher. No responsibility is accepted for the accuracy of information contained in the published chapters. The publisher assumes no responsibility for any damage or injury to persons or property arising out of the use of any materials, instructions, methods or ideas contained in the book.

First published in London, United Kingdom, 2022 by IntechOpen

IntechOpen is the global imprint of INTECHOPEN LIMITED, registered in England and Wales, registration number: 11086078, 5 Princes Gate Court, London, SW7 2QJ, United Kingdom
Printed in Croatia

British Library Cataloguing-in-Publication Data

A catalogue record for this book is available from the British Library

Additional hard and PDF copies can be obtained from orders@intechopen.com

Multiplexing – Recent Advances and Novel Applications

Edited by Somayeh Mohammady

p. cm.

Print ISBN 978-1-80355-051-0

Online ISBN 978-1-80355-052-7

eBook (PDF) ISBN 978-1-80355-053-4

We are IntechOpen, the world's leading publisher of Open Access books Built by scientists, for scientists

5,900+

Open access books available

144,000+

International authors and editors

180M+

Downloads

156

Countries delivered to

Our authors are among the
Top 1%

most cited scientists

12.2%

Contributors from top 500 universities



WEB OF SCIENCE™

Selection of our books indexed in the Book Citation Index (BKCI)
in Web of Science Core Collection™

Interested in publishing with us?
Contact book.department@intechopen.com

Numbers displayed above are based on latest data collected.
For more information visit www.intechopen.com



Meet the editor



Somayeh Mohammady holds a bachelor's degree in Electronic Engineering (Robotics), as well as an MSc and Ph.D. in Electrical and Electronic Engineering from Universiti Putra Malaysia (UPM). She has industrial experience working at Teta, Tabesh Tablou Company, and Symmid Corporation Sdn. Bhd. She also worked as a postdoctoral researcher from 2012 to 2019. Dr. Mohammady is a lecturer at Technological University Dublin (TU Dublin). Her research interests include power amplifier linearization, signals processing for multicarrier signals, and Peak-to-Average Power Ratio (PAPR), also known as Crest Factor Reduction (CFR).

Contents

Preface	XIII
Section 1	
Multiplexing and Waveforms	1
Chapter 1	3
Waveguide Amplifier for Extended Reach of WDM/FSO <i>by Bentahar Attaouia, Kandouci Malika, Ghouali Samir and Dinar Amina Elbatoul</i>	
Chapter 2	23
Phase Noise in OFDM <i>by Kamayani Shrivastav</i>	
Section 2	
Multiplexing and Optics	39
Chapter 3	41
Multiplexing, Transmission and De-Multiplexing of OAM Modes through Specialty Fibers <i>by Alaaeddine Rjeb, Habib Fathallah and Mohsen Machhout</i>	
Chapter 4	65
Triple-Hop Hybrid FSO/mmW Based Backhaul Communication System for Wireless Networks Applications of 5G and beyond <i>by Mogadala Vinod Kumar, Yenneti Laxmi Lavanya, Bharati Bidikar and Gottapu Sasibhushana Rao</i>	
Section 3	
Multiplexing and New Designs	79
Chapter 5	81
NOMA Transmission Systems: Overview of SIC Design and New Findings <i>by Carmen Beatriz Rodríguez Estrello, Fernando Ramos-Alarcón and Valeri Kontorovich</i>	
Chapter 6	101
Multiplexing Techniques for Applications Based-on 5G Systems <i>by Nguyen Huu Trung</i>	

Preface

When multiple analog or digital signals are combined into one signal over a shared medium, it is called multiplexing or muxing. This is a well-known method in telecommunications and computer networking. It is widely applied in communication systems and the aim is to share a scarce resource, for example, a wire or optic fiber cable for telecommunication applications. The reverse process is necessary on the receiver's end to extract the information sent.

This book presents recent applications and advancements in multiplexing (MUX) and de-multiplexing (DEMUX) in optic and wireless communication applications. It examines signals and waveforms from different points of view for both orthogonal and non-orthogonal subcarrier scenarios.

I wish to acknowledge my late father. I hope this book makes him proud. I also wish to thank my mentors Prof. Max Ammann from the Technological University Dublin (TU Dublin) and Prof. Daniel Kilper from Trinity College Dublin (TCD) who helped me immensely in the last two years.

I acknowledge this publication is associated with CONNECT - the Science Foundation Ireland Research Centre for Future Networks and Communications and SFI Centre for Research Training in Advanced Networks for Sustainable Societies (ADVANCE CRT), Dublin, Ireland.

Somayeh Mohammady

School of Electrical and Electronic Engineering,
Technological University Dublin (TUDublin),
Dublin, Ireland

Section 1

Multiplexing and Waveforms

Waveguide Amplifier for Extended Reach of WDM/FSO

*Bentahar Attaouia, Kandouci Malika, Ghouali Samir
and Dinar Amina Elbatoul*

Abstract

In this chapter, EYDWA (erbium ytterbium doped waveguide amplifier) is characterized for wavelength division multiplexing (WDM) approach on free space optical (FSO) transmission systems with channels being spaced at 0.4 nm interval. Moreover, in this paper, was study different characterizations of EYDWA amplifier, which depend essentially on the opt-geometric parameters, such as concentrations of ions erbium, length of the waveguide and the effect of those parameters to optimize the performance of proposed system. Furthermore, the results reveal that the EYDWA booster (post-amplification) can improve the high performance remarkably under clear rain and the acceptable transmission can be carried out up to 26 km while it get reduced to 19.5 km by using pre-amplification.

Keywords: free space optical, BER, EDWA, WDM, atmospheric condition

1. Introduction

FSO (free space optics) is an optical communication technology in which contains three components: transmitter, free space transmitted, and receiver. The transmitter requires light, which can be focused by using either light emitting diode (LED) or laser (light amplification by stimulated emission of radiation) to transmit information through the atmosphere. At the receiver, a photodiode converts the optical intensity signal back into an electrical signal and the information is recovered [1, 2].

The FSO communication system has the advantages of unrestricted spectrum and high-speed transmission over other wireless communication systems. This system is likely to replace other wireless communication systems in many fields and become the solution for last-mile communication. The main limitation of FSO is seen in worse weather conditions where it suffers highest attenuation [3].

Optical network that apply wavelength division multiplexing (WDM) is currently widely used in existing telecommunications infrastructures and is expected to play a significant role in FSO system supporting a large variety of services having very different requirements in terms of bandwidth capacity which ensures multiservice and multicasting opportunity [4, 5].

WDM FSO systems use a single light beam to transmit the multiplexed signal through free space [6]. A multiplexer is used at the transmitter to combine different modulated carriers and a demultiplexer at the receiver to restore each one (Figure 1).

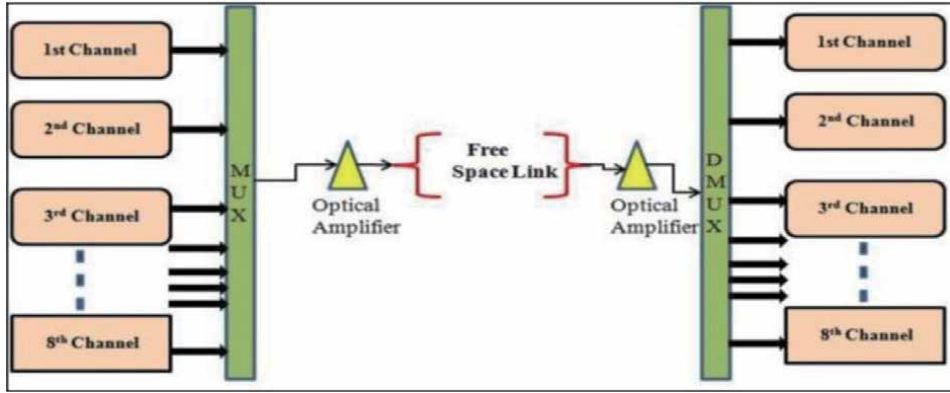


Figure 1.
The system setup of WDM-FSO.

2. Optical amplifier

An optical amplifier is a device that amplifies an optical signal directly, without the need to first convert it to an electrical signal. In the 1990's, optical amplifiers, which directly amplified the transmission signal, became widespread minimizing system intricacies and cost [7]. Many techniques have been proposed to improve the performance of FSO link like the amplification of signal [3].

To maintain the integrity of information sent from one location to another, optical amplifiers, such as doped fiber amplifiers (DFA), doped waveguide amplifiers (DWA), and semiconductor optical amplifiers (SOA), are utilized to extend transmission range for the cost-effective implementation of FSO and can be used for amplification of WDM network easily [4].

2.1 Doped fiber amplifiers

Doped fiber amplifiers (DFAs) are optical amplifiers that use a doped optical fiber as a gain medium to amplify an optical signal [8]. They are related to fiber lasers. The signal to be amplified and a pump laser are multiplexed into the doped fiber, and the signal is amplified through interaction with the doping ions. Er^{3+} is one of the most commonly used doped ions in integrated photonics and the EDFA is one effective way to amplify light signal at optical communication window between 1500 to 1600 nm.

2.1.1 Erbium doped fiber amplifier

The erbium-doped fiber amplifier (EDFA) is the most deployed fiber amplifier as its amplification window coincides with the third transmission window of silica-based optical fiber and has demonstrated high gain, low noise, and full compatibility with DWDM signals. In general, EDFA works on the principle of stimulating the emission of photons. With EDFA, an erbium-doped optical fiber at the core is pumped with a laser at or near wavelengths of 980 nm and 1480 nm, and gain is exhibited in the 1550 nm region (**Figure 2**).

2.2 Doped waveguide amplifier

Waveguide amplifiers, in particular, are new integrated optical products well suited to metro/access applications. Some of the intrinsic benefits for using this later

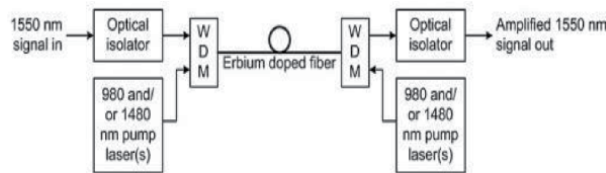


Figure 2.
 Erbium doped fiber amplifier block diagram.

include their compactness, performance, flexibility, and lower-cost processing [9]. These integrated devices offer the prospect of combining passive and active components on the same substrate while producing compact and robust devices at lower cost than commercially available fiber-based counterpart. However, the way to implement all-optical network relies on the control of gain variation of amplifiers which is sensitive to total input power variation [1, 8].

2.2.1 Erbium-doped waveguide amplifier

The erbium-doped waveguide amplifier (EDWA) are planar waveguides doped with erbium ions and are excited similar to EDFAs. EDWAs integrate several functions and components onto a mass produced integrated circuit and have recently received considerable attention as a potential high-gain medium for optical amplification in the communication band (**Figure 3**) [8, 9].

3. Concentration quenching of erbium

EDWAs are less efficient than EDFAs due to higher erbium concentration in the waveguide on the substrate. Greater erbium ion concentration causes more pumping power to quench to the system. Additionally, there is greater loss in waveguides than fibers. Concentration quenching is the reduction in quantum efficiency of a erbium ion as its concentration increases. It generally manifests itself by a shortening of the measured metastable level lifetime and occurs mostly through cross relaxation or co-operative up-conversion processes.

When the concentration levels are such that the separation between two erbium ions is greater than the diameter of an individual erbium ion then the up conversion process is called “homogeneous up conversion (HUC)”. In addition to the above-mentioned effects, another important effect that needs to be investigated is the pair induced quenching (PIQ). This later is an inhomogeneous phenomenon

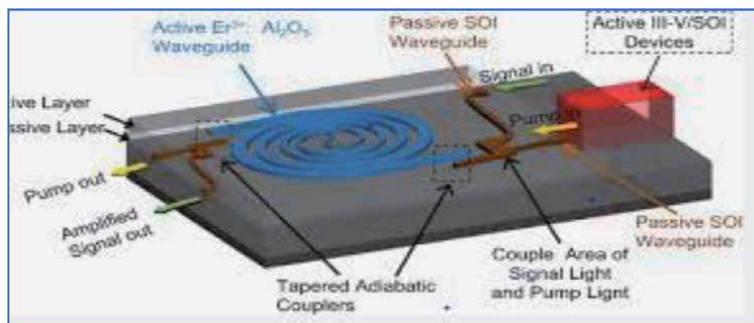


Figure 3.
 Erbium-doped waveguide amplifiers block diagram.

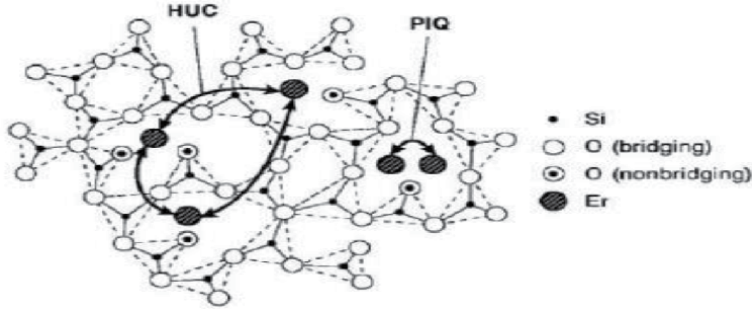


Figure 4.
Scheme of pair-induced quenching (PIQ) and up-conversion (HUC) processes in erbium-doped fiber amplifier.

caused by clustered ions when the Er^{3+} the inter-ionic distance between two erbium ions becomes less and they come much closer to each other so as to form “clusters” [10]. This issue has been addressed by co-doping the erbium by ytterbium (Yb^{3+}) (Figure 4).

4. Co doping with ytterbium ions to inhibit PIQ

To increase the absorption cross section, ytterbium ions (Yb^{3+}) are usually co-doped as a sensitizer. The introduction of ytterbium can effectively restrain the erbium Er^{3+} ion clusters, and reduce up-conversion nonlinear side effect. This can increase the total gain and the unit length gain greatly [11].

The performance of the $\text{Er}^{3+} + \text{Yb}^{3+}$ co-doped waveguide amplifiers (EYDWA) is better than that of the EDWA, and the EYDWAs are therefore expected to be an attractive high-gain medium material for optical amplification because of their use as amplifiers in optical telecommunications and as compact light sources for eye-safe range finding in the $1.55 \mu\text{m}$ spectral range (Figure 5) [12, 13].

Ytterbium offers the advantage of a high absorption cross-section and a good spectral overlap of its emission with erbium $4 I_{11/2}$ absorption, leading to an efficient energy transfer from ytterbium to erbium.

The rate equations for Er^{3+} and Yb^{3+} population can be written as [14]:

$$\frac{dN_2}{dt} = -A_{21}N_2 - 2U_{up} N_2^2 + N_1\sigma_{sa}\varphi_s - N_2\sigma_{se}\varphi_s + \gamma_{32}N_3 \quad (1)$$

$$\frac{dN_3}{dt} = -N_3\sigma_{pe}\varphi_p + N_1\sigma_{pa}\varphi_p + PN_1N_6 - P'N_3N_5 - N_3\sigma_{32} + \gamma_{43}N_4 \quad (2)$$

$$\frac{dN_4}{dt} = C_{up}N_2^2 - \gamma_{43}N_4 \quad (3)$$

$$\sum_i^4 N = N_{Er} \quad (4)$$

$$\frac{dN_3}{dt} = PN_1N_6 - P'N_3N_5 - N_5\sigma'_{pa}\varphi_p + N_6\sigma'_{pa}\varphi_p + N_6\sigma'_{pe}\varphi_p + A_{65}N_6\gamma_{43}N_4 \quad (5)$$

$$N_{Yb} = N_5 + N_6 \quad (6)$$

where, N_1, N_2, N_3 and N_4 are the Er population densities (m^{-3}) of $4I_{15/2}, 4I_{13/2}, 4I_{11/2}, 4I_{9/2}$ levels, respectively. The quantities N_5, N_6 are the Yb^{3+} population

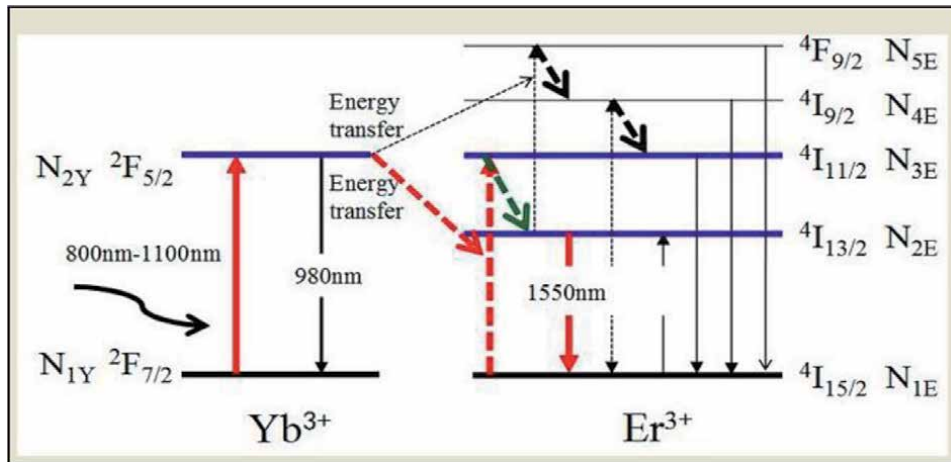


Figure 5.
Energy level diagram of erbium and ytterbium system.

densities (m^{-3}) of the $2F_{7/2}$ and $2F_{5/2}$ levels respectively. Whereas, φ_p , φ_s , σ'_{pa} , σ'_{pe} , A_{21} , A_{65} , P , P' , C_{up} are defined in **Table 1**.

The spontaneous emission rates of Er^{+3} and Yb^{+3} can be calculated by:

$$\sigma_a = \frac{h\gamma n}{C} B_{12} g_{12}(\gamma), \sigma_e = \frac{h\gamma n}{C} B_{21} g_{21}(\gamma) \quad (7)$$

where $g_{12}(\gamma)$ and $g_{21}(\gamma)$ are the normalized emission and absorption line shape respectively, n is the refractive index of the medium and B_{12} and B_{21} are the coefficients of transition. Then the signal gain G and total noise Figure NF are given by:

$$G = \exp \left[\int_0^L g(z) dz \right],$$

$$NF = 10 \log \log_{10} \left[\frac{1}{G} + \frac{P_{ASE}}{G h \gamma B_0} - \frac{P_{SSE}}{h \gamma B_0} \right] \quad (8)$$

Parameter	Definition
φ_p	The pump photon flux
φ_s	The signal photon flux
σ_{pe}	The stimulated emission cross section for Er^{+3}
σ_{pa}	The absorption cross section for Er^{+3}
σ'_{pe}	The stimulated emission cross section for Yb^{+3}
σ'_{pa}	The absorption cross section for Yb^{+3}
A_{21}	The spontaneous emission rate of Er^{+3}
A_{65}	The spontaneous emission rate Yb^{+3}
K and K'	The coefficient of energy transfer for the concentrations of Er^{+3} and Yb^{+3}
C_{up}	The up conversion coefficient

Table 1.
Parameter definition for equations.

where γ is the signal frequency, B_o is the noise bandwidth, P_{ASE} and P_{SSE} are the power of amplified spontaneous emission, and the power of source spontaneous emission, respectively.

5. Comparison of EDFA and EYDWA for WDM/FSO network

The FSO-WDM with eight input signals using EYDWA amplifier as a pre- or post-TT6Af an externally modulated WDM transmitter generating eight NRZ signals at 2.5 Gbit/s with input power of -10 dBm, the eight channels are multiplexed with a spacing set at 0.8 nm in the wavelength range 1550 to 1554.8 nm. Then the signal is ready to travel through 30 Km range of FSO. On the receiver's side, the avalanche photodiode (APD) is used followed by a low pass filter and a 3R regenerator. The performance is analyzed using BER analyzer which gives the related BER, power level and eye diagrams.

Figures 6 and 7 shows the dependence of the gain and noise figure on frequency for both optical amplifiers EDFA and EYDWA, respectively. It is evident that the EYDWA amplifier also offers a better price/performance ratio (better gain of 32 dB and high NF of 11 dB) than comparable EDFA amplifier (Gain of 15 dB and better NF of 5 dB) for WDM/FSO network applications. Most of the intrinsic advantages of EYDWAs come from their ability to provide high gain in very short optical paths than EDFA amplifier. This capability gives vendors more flexibility in the design of a compact amplifier.

5.1 Concentration quenching affects

The homogeneous up conversion tends to cause more impairment in the EDFA amplifier performance than in the EYDWA amplifier. **Figure 8** shows variation of gain as a function of the HUC coefficient [15]. It is observed that as this later increased; the gain spectrum decreased and showed larger variation especially for EDFA as compared as EYDWA amplifier. Furthermore for UHC coefficient higher of $2.10^{-22} \text{ m}^3/\text{s}$ we can notice lowest results in term of gain for EDFA, however EYDWA amplifier provides the best results (high and flat gain). Also the maximum

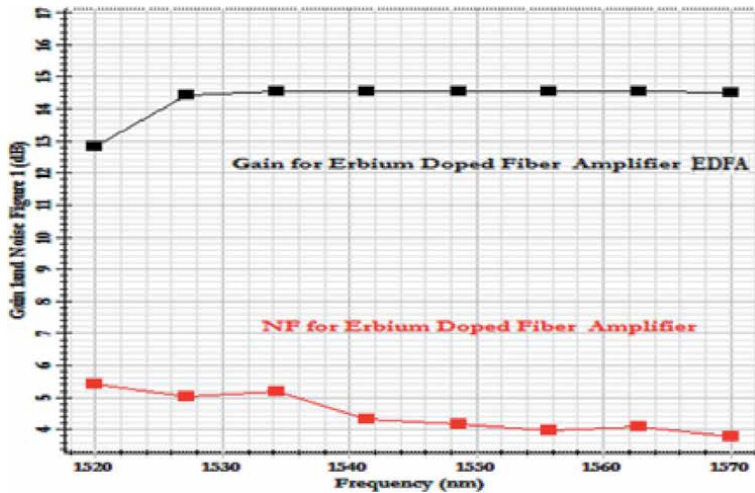


Figure 6. Gain and noise figure as a function of frequency for the erbium doped fiber amplifier (EDFA).

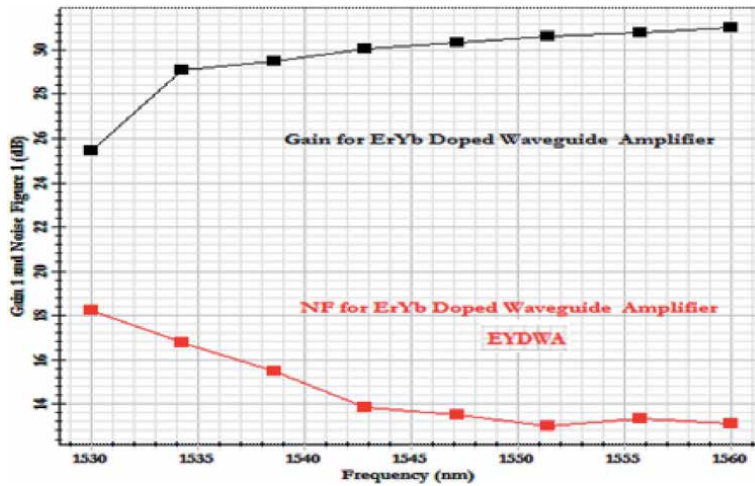


Figure 7.
 Gain and noise figure as a function of frequency for the Er-Yb doped waveguide amplifier (EYDWA).

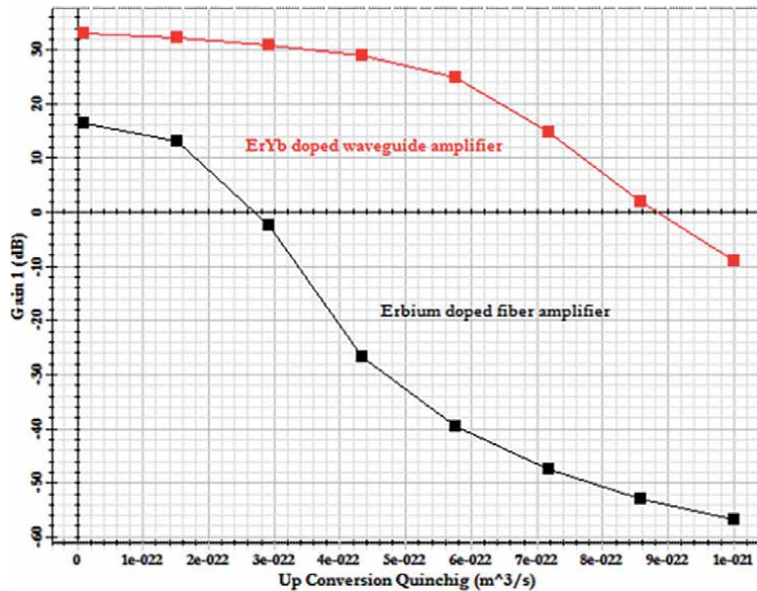


Figure 8.
 Gain as a function of up-conversion coefficient for the EYDWA and EDFA.

Q factor values occur for EYDWA amplifier and at lower HUC coefficient as compared as EDFA amplifier **Figure 9**.

5.2 Influence of length and erbium doping

The critical turning point in the EYDWA technology is finding a compromise between the high erbium ytterbium co-doping levels, which helps create large gain in a short optical length [13]. The dependence of EYDWA performance on the length and erbium ion concentration is studied **Figures 10 and 11**.

For better performance the optimization has been done and it was reported of the system amplified (WDM- FSO) under medium rain and at 2.5 Gbit/s. The EYDWA

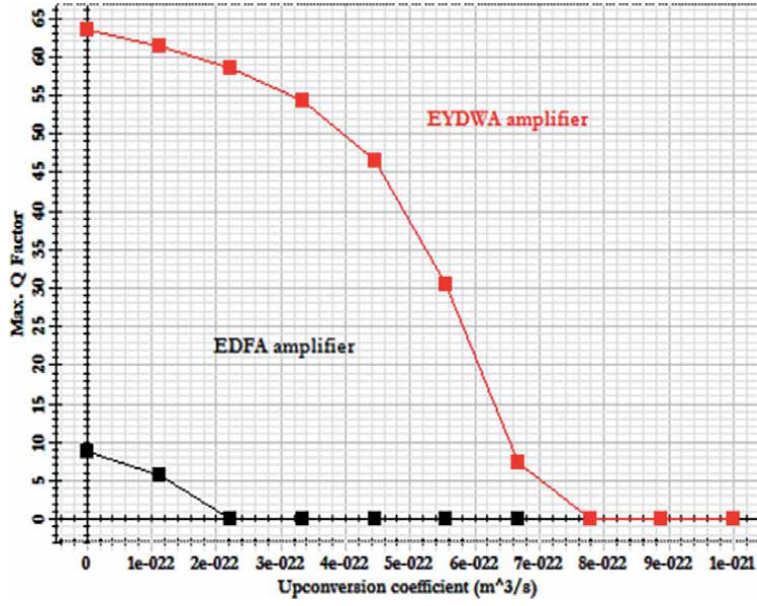


Figure 9.
Q factor as a function of up-conversion coefficient for the EYDWA and EDFA.

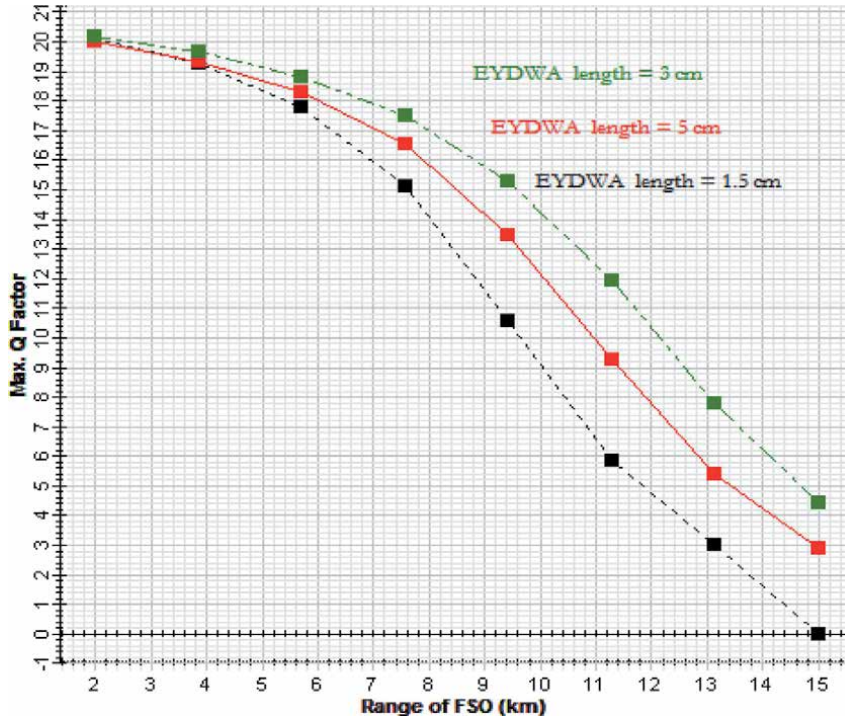


Figure 10.
Curves of Q factor versus EYDWA length for WDM-FSO system under medium rain.

amplifier can be reached higher FSO range (over 12 km) with acceptable quality factor (Q values of 6 and $\text{BER} = 10^{-9}$) by increasing the erbium concentration (up to 6.10^{26} ions/ m^3) and with optimum waveguide length (over 3.5 cm). These results proved that we can achieve high gain with a short device length.

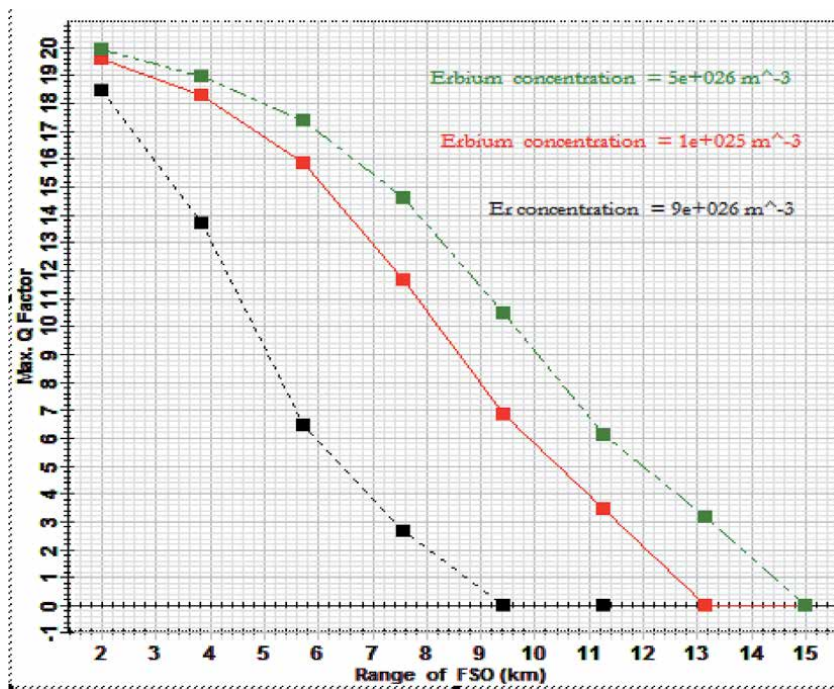


Figure 11.
Curves of maximum gain versus erbium ion concentration for WDM- FSO system under medium rain.

5.3 Influence of the position of EYDWA amplifier

The performance analysis of the system amplified under clear, medium and heavy rain conditions are shown in “Table 2”, and Max Q factor has been analyzed **Figures 12** and **13**. It can be seen that under optimized conditions of data rate, the increase in the attenuation (respective intensity of rain) causes the decrease in the maximum transmission distance (FSO range) with acceptable quality factor Q values around of 6.

We note that EYDWA as post-amplifier can be carried the link range up to 26 km at and 8 km at BER 10^{-9} under clear and heavy rain, respectively. However EYDWA preamplifier limits this distance of FSO range to 16 Km and 4.5 km at BER 10^{-9} under clear and heavy rain conditions, respectively.

6. Gain flatness of EDFA for a WDM FSO system

An amplifier does not have a flat gain curve, that is, it does not generally provide equal amplification for all wavelengths of signals transmitted over the same

Intensity of rain	System with EYDWA post-amplifier			System with EYDWA pre-amplifier		
	Q factor	BER	Range (Km)	Q factor	BER	Range (Km)
Light (clear) 3 dB	5.8	10^{-9}	27	6.12	10^{-9}	16
Medium 9 dB	6	10^{-9}	12	6.03	10^{-9}	8
Heavy 20 dB	6	10^{-9}	8	6	10^{-9}	4.5

Table 2.
Comparison of EYDWA post- and pre-amplifier.

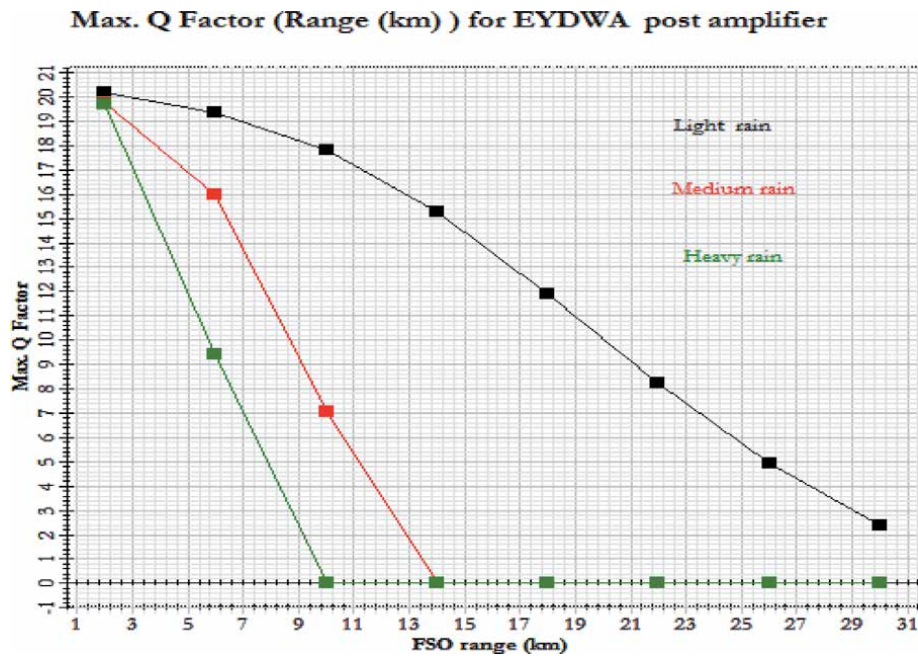


Figure 12.
Quality factor as a function of FSO range for EYDWA post- amplifier under clear (light), medium and heavy rain.

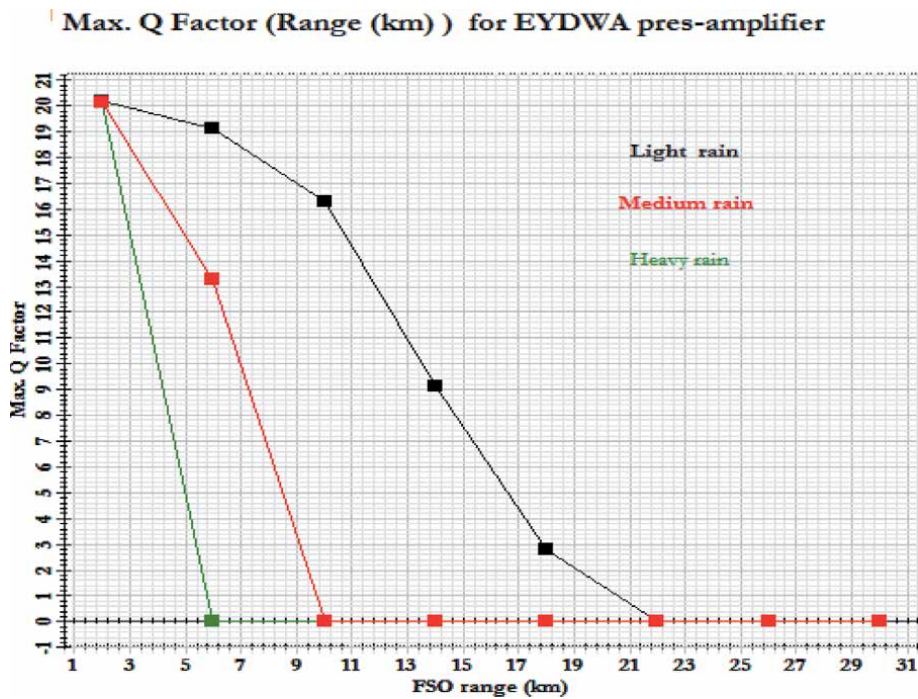


Figure 13.
Quality factor as a function of FSO range for EYDWA preamplifier under clear (light), heavy and medium rain.

transmission line (WDM). This disparity is an important limitation for wavelength division multiplexed systems. Good gain flatness requires continuous control of the input power to adjust it to its optimum value [15]. There are several methods for the design of a flat spectral EDFA gain e.g. by combining in-line amplifiers with gain equalizing filters or by controlling some internal EDFA parameters such as the length of the doped fiber, the concentration and the pump power [16].

6.1 Equalization of gain with optimization of EDFA parameters

The figures bellows show the power and noise spectrum as a function of wavelength at the output of the EDFA for different concentrations of erbium ions (from $1.10^{+24}/\text{m}^{-3}$ to $1.10^{+25}/\text{m}^{-3}$) and different lengths of the doped fiber (from 2.5 m to 12.5 m), eye diagrams of the simulated system are also shown. According to the graphs obtained, the gray wave represents the noise that decreases as the length and concentration of the doped fiber decreases, while the red symbol in the graphs indicates the sample wavelength (eight wavelengths).

The results obtained show that the concentration of de $5,5.10^{+24}/\text{m}^{-3}$ and the length of the doped fiber of 7.5 m give the best results in terms of maximum gain (around 26.63 dB) and equalization of the amplified optical spectrum.

It is noticeable that the eye aperture is well open which the quality factor is between 9 and 10 which are higher than 6 that mean that the system works correctly. The BER is higher than 10^{-12} which expresses that the transmission is error-free (Figures 14–18).

The table below summarizes the simulation results at the output of the WDM analyzer for different values of the erbium ion concentration and the length of the doped fiber, where the term R_G represents the difference between the maximum and minimum value of the EDFA gain (maximum ratio), while R_{NF} indicates the variation of the noise figure.

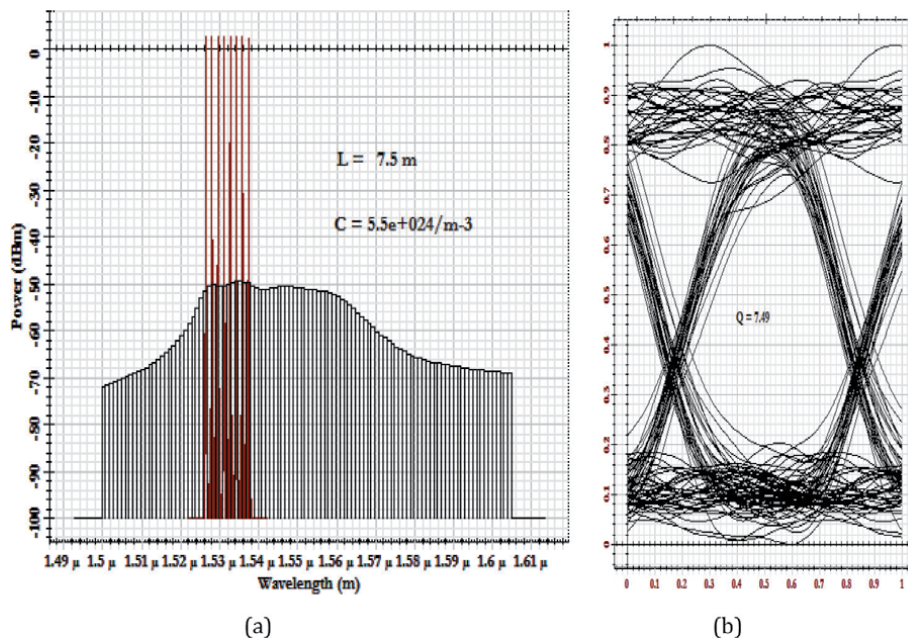


Figure 14.
 (a) Power spectrum and noise figure, (b) eye diagram for concentration and length of the doped fiber
 ($C = 5.10^{+24}/\text{m}^{-3}$ and $L = 7, 5 \text{ m}$).

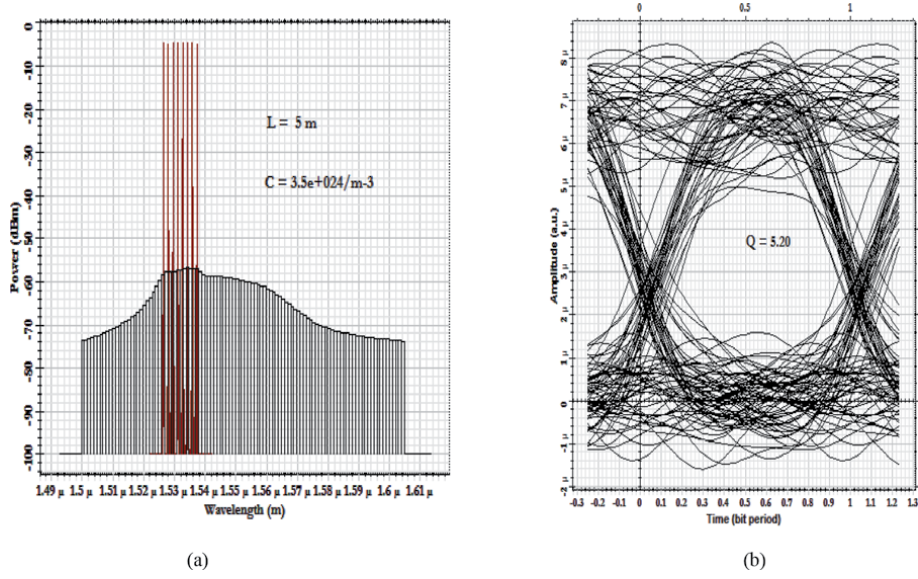


Figure 15.
(a) Power spectrum and noise figure, (b) eye diagram for concentration and length of the doped fiber ($L = 5 \text{ m}$ and $C = 3,5.10^{+24} / \text{m}^{-3}$).

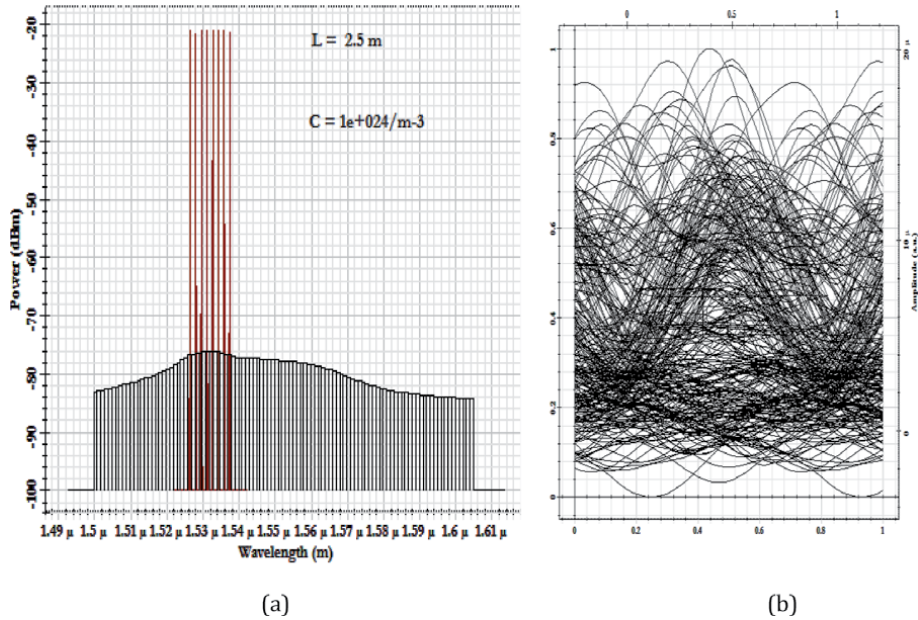


Figure 16.
(a) Power spectrum and noise figure, (b) eye diagram for concentration and length of the doped fiber ($C = 1.10^{+24} / \text{m}^{-3}$ and $L = 2.5 \text{ m}$).

Comparison of the five graphs leads to the conclusion that the gains are flattened with a $R_G = 0.7$ in the band 1537 nm to 1545 nm wavelength around a gain of 26.3 dB with a noise Figure (NF) of less than 4 dB for 8 transmission channels for a concentration of $5, 5.10^{24} / \text{m}^{-3}$ and a doped fiber length of 7.5 m the worst case (gain less equalized with a $R_G = 1.54$) is obtained with a fiber length of 12.5 m (Table 3).

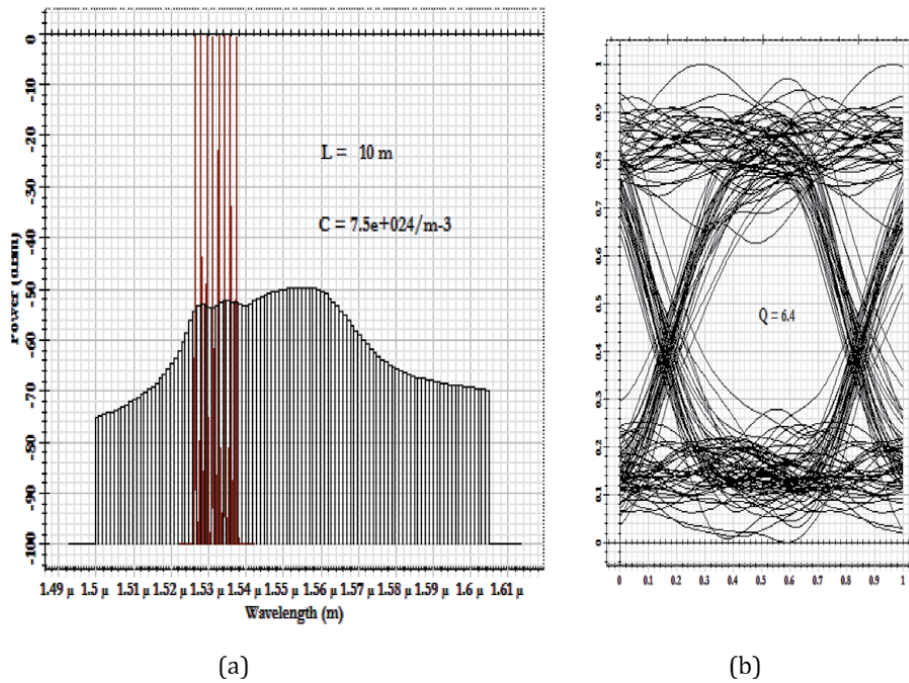


Figure 17.
 (a) Power spectrum and noise figure, (b) eye diagram for concentration and length of the doped fiber
 ($C = 7,5 \cdot 10^{+24}/m^{-3}$ and $L = 10 \text{ m}$).

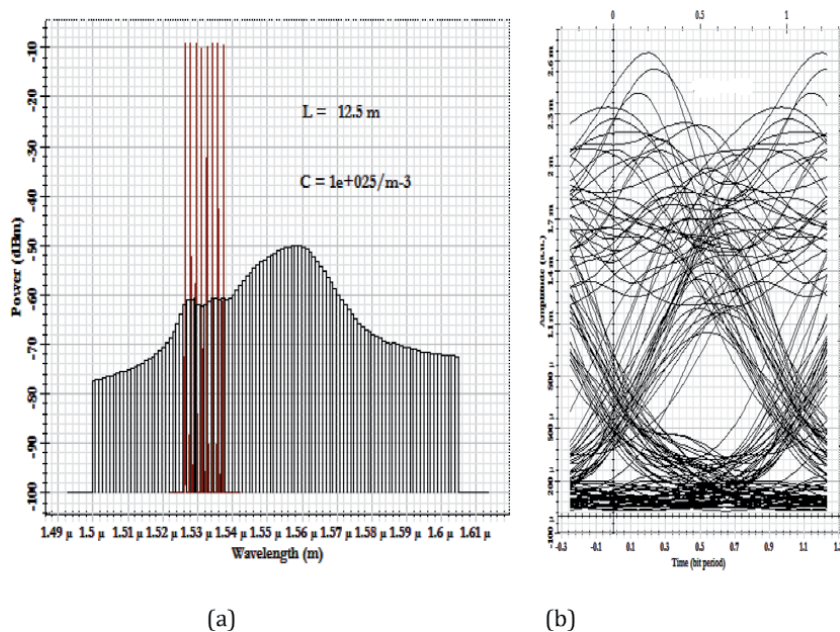


Figure 18.
 (a) Power spectrum and noise figure, (b) eye diagram for concentration and length of the doped fiber
 ($C = 1.10 \cdot 10^{+25}/m^{-3}$ and $L = 12, 5 \text{ m}$).

6.2 Gain equalization through the use of a GFF filter

Gain Equalizing Filters, also known as GFF (Gain Flattening Filters), are integrated into optical systems and are usually combined with optical amplifiers in the

Gain	NF	$R_G = G_{\max} - G_{\min}$	$R_{NF} = NF_{\max} - NF_{\min}$	Concentration "N"	L
2.95 dB	1.95 dB	0.08 dB	0.46 dB	$1.10^{24}/m^3$	2.5 m
19.44 dB	3.43 dB	0.47 dB	1.63 dB	$3.5.10^{24}/m^3$	5 m
26.63 dB	3.65 dB	0.70 dB	2.15 dB	$5.5.10^{24}/m^3$	7.5 m
23.59 dB	4.47 dB	0.98 dB	2.04 dB	$7.5.10^{24}/m^3$	10 m
14.71 dB	4.66 dB	1.54 dB	2.06 dB	$1.10^{25}/m^3$	12.5 m

Table 3.
Optimization results obtained by the WDM analyzer.

transmission chain to ensure good gain flattening. This process provides a solution to the problem of equalizing the amplifier output power of a WDM multiplexed system. This part refers to a process of combining the EDFA amplifier with a GFF filter and visualizing the power and noise spectrum.

The tables below show the results of the WDM analyzer at the output of the EDFA "Table 4" and the output of the gain equalizing filter "Table 5" in terms of wavelength, gain, noise figure and the deference between the maximum and minimum values of these figures. Comparison between the tables below leads to the conclusion that the gains are flattened with a $R_G = 0.77$ in the band 1537 nm to 1545 nm wavelength around a gain of 26.97 dB with a noise Figure (NF) of less than 2.15 dB for 8 transmission channels.

The figures below show a schematic representation of the spectrum emitted at the output of the EDFA and output of the gain equalizing filter GFF. In **Figure 19**, the different wavelengths of the multiplex at the output of the EDFA (at the input of the filter) can be recognized, represented by red symbols from 1 to 8. It can be seen that the spectrum received at the output of the EDFA has a different total

Wavelength (nm)	Gain (dB)	Noise Figure (dB)
1537.4	27.859	4.017
1535.82	29.448	3.368
1534.25	31.714	3.913
1532.68	32.990	3.382
1531.12	32.764	3.144
1529.55	31.265	2.382
1527.99	29.096	2.971
1526.44	26.298	2.063
	Gain (dB)	Noise Figure (dB)
Min value	26.197	2.0631
Max value	32.994	4.026
Total	30.712	0
Ratio Maxmin	6.698	1.954
	nm	nm
Wavelength at	1526.44	1526.44
Wavelength at	1537.40	1537.40

Table 4.
Results of the WDM analyzer at the EDFA output.

Wavelength (nm)	Gain (dB)	Noise Figure (dB)
1537.4	26.976	3.697
1535.82	26.687	3.991
1534.25	26.864	4.026
1532.68	26.634	3.297
1531.12	26.364	3.169
1529.55	26.464	2.928
1527.99	26.803	2.597
1526.44	26.197	1.871
	Gain (dB)	Noise Figure (dB)
Min value	26.197	1.871
Max value	26.864	4.026
Total	26.628	0
Ratio Maxmin	0.778	2.155
	nm	nm
Wavelength at	1526.44	1526.44
Wavelength at	1537.40	1537.40

Table 5.
 WDM analyzer filter GFF output results.

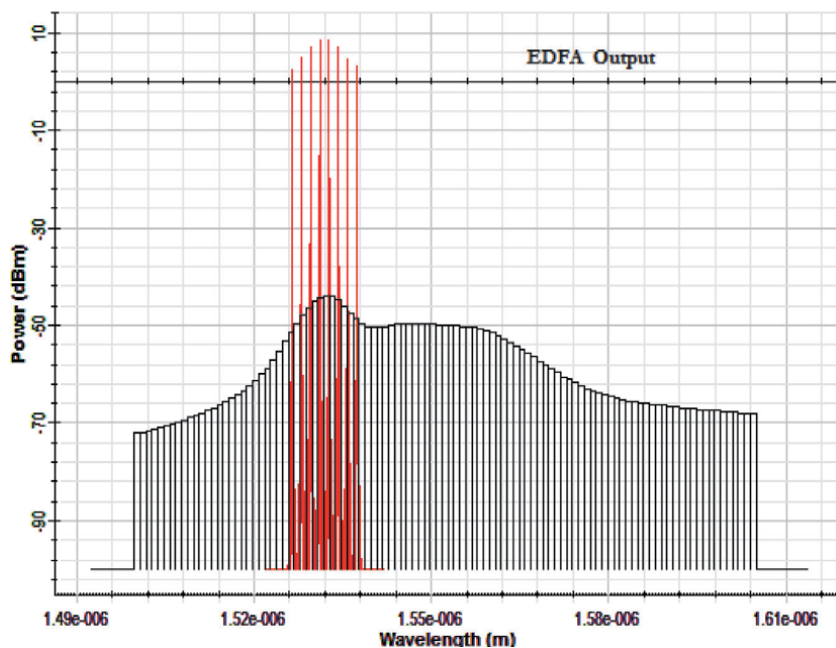


Figure 19.
 Power spectrum and noise figure at EDFA output.

power for the different wavelengths while the spectrum received at the output of the filter has a total power which is substantially equal and in particular the gain is flat over the amplification band **Figure 20**.

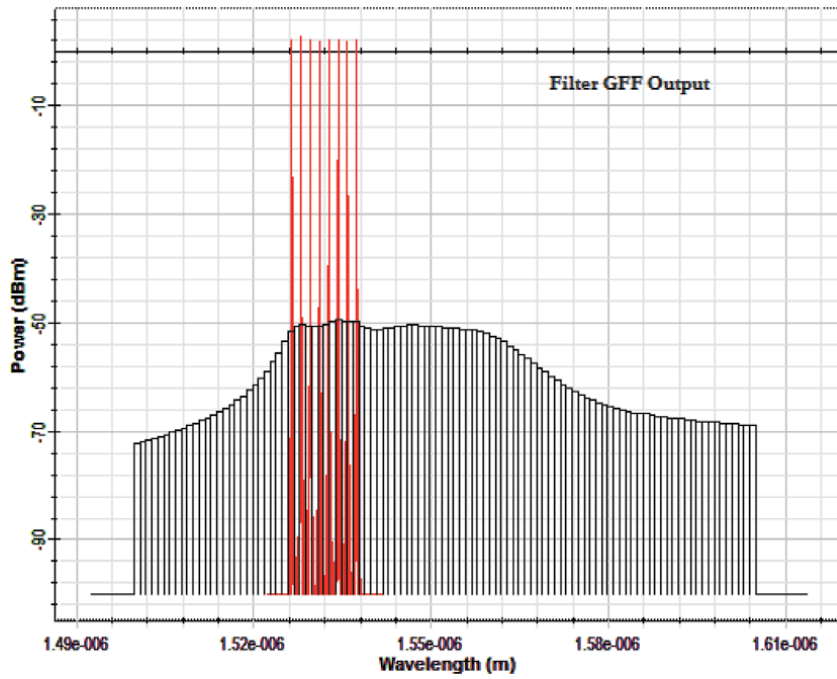


Figure 20.
Power spectrum and noise figure at filter FGG output.

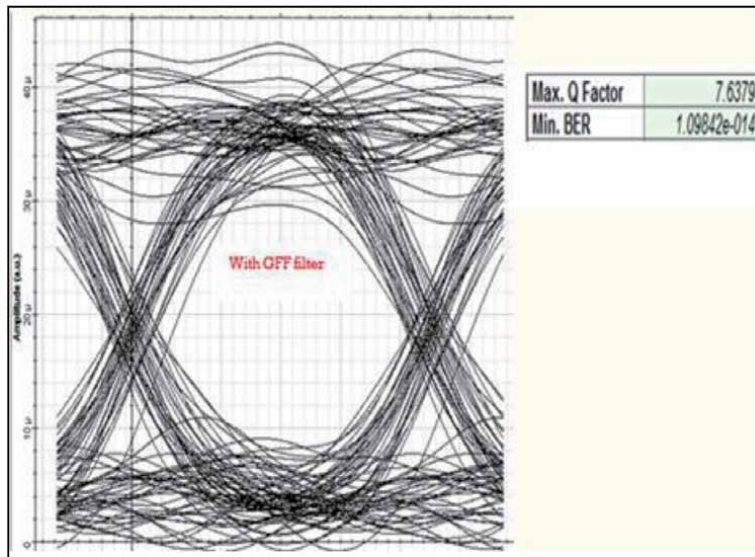


Figure 21.
Eye diagram of the WDM/FSO with GFF filter.

According to the eye diagrams for both cases we can clearly see the aperture of diagram **Figure 21** compared to diagram **Figure 22**; this confirms that the use of the gain equalizing filter GFF improves the quality of the amplified WDM system.



Figure 22.
 Eye diagram of the WDM/FSO without GFF filter.

7. Conclusion

This chapter summarizes the simulation results and their interpretations of the comparison of two configurations of EYDWA (post-and preamplifier) in the WDM/FSO system. The mentioned amplifiers were evaluated based on values of BER and the quality -factor. WDM over FSO communication system is very suitable and effective in providing high data rate transmission with low bit error rate (BER). Therefore, WDM – FSO system has achieved very good results, it has many problems, such as heavy attenuation coefficient.

For the heavy rain condition the maximum link range about 8 km at $\text{BER} = 10^{-9}$. Also, It can be noticed from simulation that the best results achieved EYDWA post-amplifier configuration, this later was able to reach transmission distance of WDM/FSO up to 26 Km however the worst results in terms of FSO range are obtained with EYDWA preamplifier and the distance of transmission is limited at 16 Km.

Furthermore the gain flatness and the noise figure of EDFA have been studied. The gain non-uniformity for each channel using the optimization of erbium doped and length fiber doped in order to equalize the amplitude gain in the WDM-FSO system have been simulated. The simulation results prove that the proposed method by optimization of erbium doped and length of fiber doped offers and improved the best performance in terms of the gain flatness $\text{GF} = 0.7$ for fiber length $L = 7.5$ m and erbium concentration $C = 5.5 \cdot 10^{+24}/\text{m}^{-3}$.

Author details

Bentahar Attaouia^{1*}, Kandouci Malika², Ghouali Samir³ and Dinar Amina Elbatoul³

1 University of Mascara, LEPO Laboratory of sidi bel abbes, Algeria

2 University of sidi bel abbes, LEPO Laboratory of sidi bel abbes, Algeria

3 University of Mascara, Algeria

*Address all correspondence to: bentaha_1011@yahoo.fr

IntechOpen

© 2022 The Author(s). Licensee IntechOpen. This chapter is distributed under the terms of the Creative Commons Attribution License (<http://creativecommons.org/licenses/by/3.0>), which permits unrestricted use, distribution, and reproduction in any medium, provided the original work is properly cited. 

References

- [1] Makowski M, Sypek M, Kolodziejczyk A. Colorful reconstructions from a thin multi-plane phase hologram. *Optics Express*. 2008; **16**:11618 Available from <http://www.opticinfobase.org/oe/abstract.cfm?URI=oe-16-15-11618>
- [2] Dat PT et al. Performance evaluation of an advanced DWDM RoFSO system for heterogeneous wireless. In: Tavel P, editor. *Modeling and Simulation Design*. AK Peters Ltd.; 2007
- [3] Arora P, Kumar S, Sharma D. Performance analysis of NRZ and RZ modulation schemes in optical fiber link using EDFA. *International Journal of Advanced Research in Computer Science and Software Engineering (IJARCSSE)*. 2017;7(8): 2277-2128
- [4] Chaudhary S, Lin B, Tang X, et al. 40 Gbps–80 GHz PSK-MDM based Ro-FSO transmission system. *Optical and Quantum Electronics*. 2018;50:321
- [5] Attaouia B, Malika K. Performance improvement by pre-amplifying with erbium, ytterbium doped devices link extenders of fiber to the home. *International Journal of Information Engineering and Electronic Business*. 2016;8(4) MECS.:26-34 Available from <http://www.mecspress.org>
- [6] Delavaux J-MP et al. Lossless 40 Channel Waveguide Demultiplexer for 10 Gbit/s DWDM Fiber Transmission Experiment. *ECOC*; 2000 paper 10.3.6
- [7] Philipsen J et al. Compact Gain-Block Consisting of an Er⁺-Doped Waveguide Amplifier (EDWA) and a Pump/Signal Multiplexer, Realized by Ion Exchange. *OAA*; 2000 paper OTuD2
- [8] Enns K, Taccheo S, Rogowski T, Shmulovich J. Efficient Erbium-doped waveguide amplifier insensitive to power fluctuations. *Optics Express*. 2006;14(22):10307-10312
- [9] Di Pasquale F, Federighi M. Improved gain characteristics in high-concentration Er³⁺/Yb³⁺ Codoped glass waveguide amplifiers. *IEEE Journal of Quantum Electronics*. 1994;30(9): 2127-2131
- [10] Muhammad OH, Hifsa S. Septechieving high gain using Er-Yb codoped waveguide/fiber optical parametric hybrid amplifier for dense wavelength division multiplexed system. *Optical Engineering*. 1994;57: 2127-2131 id. 056108 (2018)
- [11] Mahrana O, Moustafa H, et al. High performance characteristics of dual pumped Er³⁺/Yb³⁺ co-doped/raman hybrid optical amplifier. *Journal of Optoelectronics and Advanced Materials*. 2016;18(7–8):595-601
- [12] Wang XJ, Yuan G, Isshiki H, Kimura T, Zhou Z. Photoluminescence enhancement and high gain amplification of Er^xY^{2-x}SiO₅ waveguide. *J. Appl. Phys. Lett.* 2010; **108**:013506
- [13] Kaur H, Sarangal H. Simulative investigation of FSO system using 4X4 transmitter receiver combination integrated with various types of amplifiers under different weather conditions. *International Journal of Signal Processing*. 2016;9(3): 11-16
- [14] Jiang C, Zeng Q. Optimization of erbium-doped waveguide amplifier. *Optical and Laser Technology*. 2004; **36**(2):167-171
- [15] Berkedmir C, Ozsoy S. Numerical analysis of the signal gain and noise figure of Yb³⁺/Er³⁺ doped fiber amplifier

at different pumping power configurations. *Optical Materials*. 2008; **31**:229-232. DOI: 10.1016/j.optmat.2008.03.016 [Citation Time(s):1]

[16] Li JF, Duan KL, Wang YS, Zhao W, Guo YK, Lin XD. Modeling and optimizing of high-concentration erbium-doped fiber amplifiers with consideration of ion-clusters. *Optics Communications*. 2007;**277**(1):143-149

Phase Noise in OFDM

Kamayani Shrivastav

Abstract

Orthogonal frequency division multiplexing (OFDM) technique provides high data rate with high spectral efficiency for operating close to the Shanon capacity bounds. With the advantages of simple channel equalization, robustness against frequency selectivity of the channel, and efficient implementation, this is a widely deployed technique. Orthogonal frequency division multiplexing access (OFDMA), the multiple access technique using OFDM, has the great potential for providing high spectral efficiency due to its integrated space-frequency and multiuser diversity. Besides all the advantages, OFDM/A is very susceptible to transceiver's impairments such as phase noise (PHN), carrier frequency offset, and in-quadrature phase imbalance effect. Phase noise is the random fluctuation in phase of the sinusoidal waveform used for frequency up/down conversion of baseband signals to/from RF (radio frequency). This occurs due to the inherent imperfections of oscillators used for this purpose. This chapter addresses the orthogonal frequency division multiplexing/multiple access system performance under the impact of transceiver oscillator phase noise.

Keywords: multi carrier (MC), common phase error (CPE), intercarrier interference (ICI), multiuser interference (MUI), free-running oscillator (FRO), phase-locked loop (PLL)

1. Introduction

Orthogonal frequency division multiplexing (OFDM) is a multicarrier modulation technique to represent the information, which reduces the complexity of receiver digital processing unit while combating the deleterious effects of the channel with simple correction algorithms. It enables one-tap equalization by cyclic prefix (CP) insertion even in frequency selective channel and the use of discrete Fourier transform (DFT) and its extremely efficient and well-established fast Fourier transform (FFT) algorithm for implementation has made it amenable in terms of cost also [1–3]. However, some of the immediate consequences of these compelling benefits in OFDM are: limiting the spectral efficiency because of CP insertion, deleterious impact of high peak-to-average power ratio (PAPR), and serious sensitivity toward transceivers' impairments [4, 5]. The transceivers' impairments, such as phase noise (PHN), carrier frequency offset (CFO), and in-quadrature phase (IQ) imbalance effect, need to be addressed significantly to make the best possible use of limited radio spectrum to further increase throughput as well as user capacity.

While there are many transceivers' impairments that are to be taken into consideration in designing a digital communication system, there is a convincing reason to focus on the PHN precisely. While CFO and IQ imbalance is deterministic, PHN on the other hand is random perturbations in the phase of the carrier signal

generated by the transceiver oscillators [6–10]. Moreover, the multicarrier systems, such as OFDM, suffer a much loss in signal-to-noise ratio (SNR) due to PHN than single carrier systems. This is the result of longer duration of multicarrier symbol and the loss of orthogonality between the subcarriers. Further, PHN severely limits the performance of systems that employ dense constellations and degradation gets more pronounced in high-carrier-frequency systems.

2. Phase noise

The autonomous system, oscillator provides a periodic cosinusoidal reference signal used for up/down conversion of the baseband/Rf signal to/from Rf/baseband frequency. In practice, wireless digital communication systems use either oscillator in isolation, known as free-running oscillator (FRO) or phase-locked loop (PLL) oscillator because of its high stability and easy control. Either FRO or PLL voltage control oscillator (VCO), in an ideal oscillator for a perfect periodic signal: the transition of phase over a time interval should be constant, whereas practically this phase increment is a random variable. This random variation of phase is phase jitter and its instantaneous deviation is called PHN [11–13]. Thus, the output of a practical oscillator is noisy and can be written as:

$$s(t) = [A + a(t)] \sin [\omega_c t + \theta(t)] \quad (1)$$

where A and $\omega_c = 2\pi f_c$ are amplitude and angular frequency, respectively, and $a(t)$ is amplitude fluctuation, which can be kept in limit by using an automatic gain control (AGC). $\theta(t)$, the phase fluctuation (time-varying PHN), is very difficult to mitigate and can have major impact on system performance.

Phase fluctuations, resulting in the random shifting of oscillator frequency, have its origin in the noise sources present in the internal circuitry of an oscillator. These noise sources can be categorized into white (uncorrelated) and color (correlated) noise sources [14]. The white noise has the flat power spectral density (PSD) where the PSD of color noise is proportional to $1/f$. The generated PHN in an oscillator, because of these white and color noise sources, has two components. First is resulting from direct amplification/attenuation of the white and color noise, and the second is due to the phase change of white and color noise, which happens because of the time integration of white and color noise [11–14].

Resulting oscillator PHN spectrum is shown in **Figure 1** where PSD is plotted against frequency f . White PHN (flat) and white frequency-modulated (FM) PHN ($1/f^2$) spectra are resulting with white noise sources and flicker PHN ($1/f$) and flicker FM PHN ($1/f^3$) spectra are resulting with color noise sources.

For FRO:

$$\theta_{n+1} = \theta_n + \phi_n \quad (2)$$

which is Wiener process [15] with mean zero and variance, $\sigma_{\phi_n}^2 = \sigma_{\phi}^2 = 2\pi\beta T_s/N$ where $\beta = 2\Delta f_{3dB}$, double of 3 dB bandwidth.

For PLL VCO [16].

$$\theta_{n+1} = \theta_n e^{-\varphi_{\frac{T_s}{N}}} + \phi_{PLLn} \quad (3)$$

which is celebrated O-U process where ϕ_{PLLn} is a sequence of identically and independently distributed (iid) random variables with mean zero and variance:

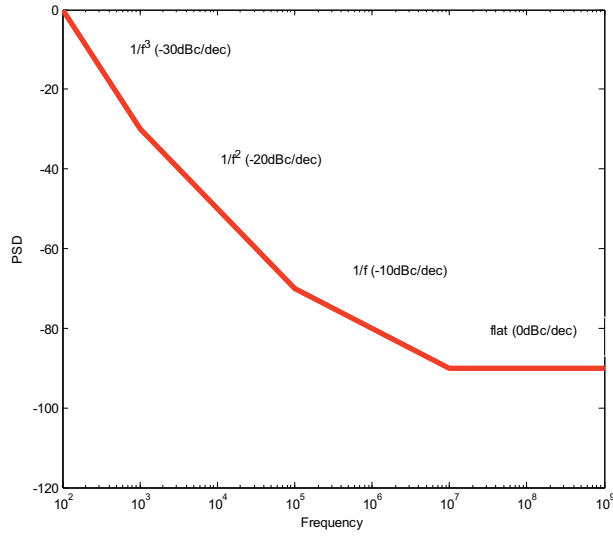


Figure 1.
 PSD of PHN in oscillator output.

$$\sigma_{\phi_{PLL,n}}^2 = 4\pi^2 f_c^2 \left(C_{RO} \frac{T_s}{N} + 2 \sum_{i=1}^2 (\xi_i + \zeta_i) \left(1 - e^{-\lambda_i \frac{T_s}{N}} \right) \right).$$

where:

$$\lambda_{1,2} = \frac{\omega_{lpf} \pm \sqrt{(\omega_{lpf}^2 - 4\omega_{lpf} \sqrt{C_{PLL}})}}{2},$$

$$\xi_1 = \frac{C_{RO}\lambda_2}{(\lambda_1 - \lambda_2)\lambda_1}, \xi_2 = \frac{-C_{RO}\lambda_1}{(\lambda_1 - \lambda_2)\lambda_2},$$

$$\zeta_1 = \frac{C_{RO} + C_{VCO}}{(\lambda_1 - \lambda_2)^2} \left(\frac{\lambda_2^2}{2\lambda_1} - \frac{\lambda_1\lambda_2}{2(\lambda_1 + \lambda_2)} \right),$$

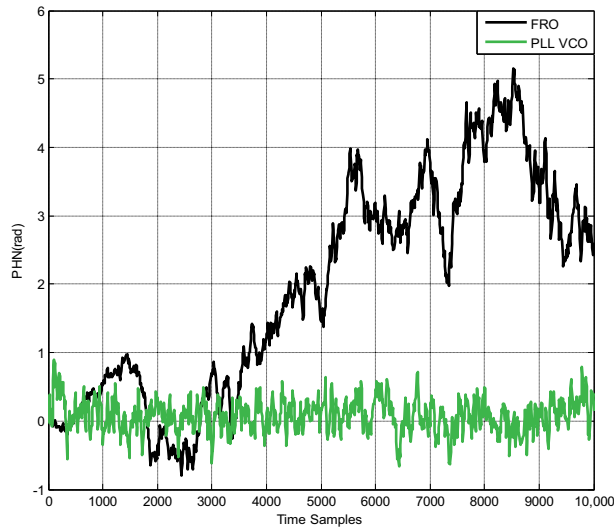


Figure 2.
 PHN time samples for FRO and PLL VCO.

f_c	5 GHz
β	20 kHz
f_{lpf}	20 kHz
C_{RO}	10^{-25} s
C_{VCO}	10^{-19} s
C_{PLL}	$4 * 10^8 / s^2$

Table 1.
PHN modeling parameters.

and

$$\zeta_2 = \frac{C_{RO} + C_{VCO}}{(\lambda_1 - \lambda_2)^2} \left(\frac{\lambda_1^2}{2\lambda_2} - \frac{\lambda_1\lambda_2}{2(\lambda_1 + \lambda_2)} \right)$$

where f_c is the center frequency of VCO in Hz, ω_{lpf} is the angular corner frequency of the low-pass filter in rad/sec, and $\sqrt{C_{PLL}}$ is the PLL bandwidth in Hz. C_{RO} and C_{VCO} are diffusion rates of the reference oscillator (RO) and VCO, respectively.

The simulated samples of PHN modeled as Wiener process and celebrated O-U process, for FRO and PLL VCO, respectively, are shown in **Figure 2**. Though the time-varying PHN process of FRO can be characterized with β only, PLL VCO requires more parameter to characterize such as given in **Table 1**, assuming that the VCO is noisier than reference oscillator.

3. OFDM

OFDM is a low complex modulation/multiplexing multicarrier (MC) technique to modulate N orthogonal sub carriers with N complex-valued source symbols $X_k, k = 0, 1, \dots, N-1$, efficiently by using digital signal processing. The source symbol is achieved after source coding, interleaving, and channel coding if applicable. The source symbol duration T_d of the serial data symbol results in the OFDM symbol duration: $T_s = N T_d$.

From the **Figure 3**, the frequency domain received signal on the k^{th} subcarrier of the m^{th} symbol is without ISI and ICI and is given by:

$$y_k^m = X_k^m h_k + W_k^m \quad 0 \leq k \leq N-1 \quad (4)$$

where X_k^m is k^{th} element of symbol vector X^m , h_k is the k^{th} element of channel vector $h = [h_0, h_1, h_2, \dots, h_{N-1}]^T$, W_k^m is AWGN in frequency domain. It is preferable to represent the signal model in matrix form as:

$$\mathbf{Y}^m = \mathbf{D}^m \mathbf{F} \mathbf{g} + \mathbf{W}^m \quad (5)$$

where $\mathbf{Y}^m = [y_0^m, y_1^m, \dots, y_{N-1}^m]^T$, \mathbf{F} is the $N \times L$ DFT matrix with $F(n, l) = \exp\left(-\frac{j2\pi nl}{N}\right)$, $\mathbf{D}^m = \text{diag}[X_0^m, X_1^m, \dots, X_{N-1}^m]$ and $\mathbf{g} = [g(0), g(1), \dots, g(L-1)]^T$ is the time domain channel vector. $\mathbf{W}^m = [W_0^m, W_1^m, \dots, W_{N-1}^m]^T$, is an uncorrelated

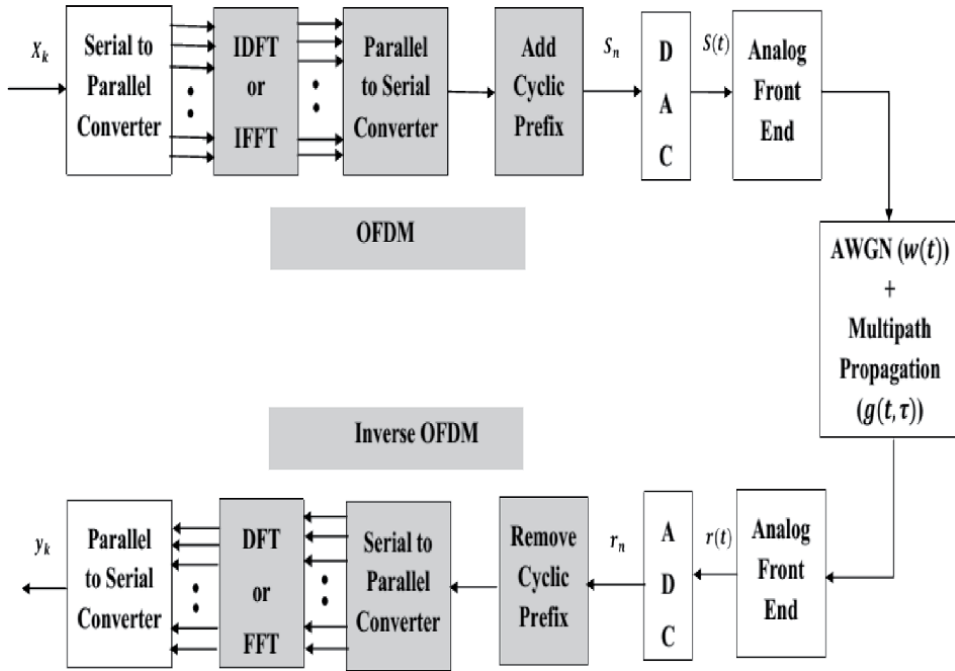


Figure 3.
 OFDM modulation and demodulation.

white noise vector distributed as, $\Pr(\mathbf{W}^m) = \mathcal{CN}(0, 2\sigma_\omega^2 \mathbf{I})$ with mean zero and covariance matrix $2\sigma_\omega^2 \mathbf{I}$, which says:

$$\Pr(\mathbf{W}^m) = \frac{1}{(2\pi)^N \sigma_\omega^{2N}} \exp\left(\frac{-1}{2\sigma_\omega^2} \mathbf{W}^{mH} \mathbf{W}^m\right). \quad (6)$$

4. Phase noise in OFDM

Further to model an OFDM system with receiver PHN consisting of N subcarriers with sampling instant T_s/N , we denote the discrete-time receiver PHN impairment to the n^{th} subcarrier of the m^{th} symbol by θ_n^m than the received OFDM signal after down conversion and CP removal can be written as [17–19]:

$$r_n^m = [S_n^m \otimes g(n)] e^{j\theta_n^m} + w_n^m, 0 \leq n \leq N-1. \quad (7)$$

If $\theta^m = [\theta_0^m, \theta_1^m, \dots, \theta_{N-1}^m]^T$, is the PHN vector for the m^{th} OFDM symbol, then:

$$\mathbf{P}^m = \left[p_{-\frac{N}{2}}^m, p_{-\frac{N}{2}+1}^m, \dots, p_0^m, \dots, p_{\frac{N}{2}-2}^m, p_{\frac{N}{2}-1}^m \right]^T \quad (8)$$

defines a vector of the DFT coefficients of one realization of $e^{j\theta_n}$ during m^{th} OFDM symbol where:

$$p_k^m = \frac{1}{N} \sum_{n=0}^{N-1} e^{j\theta_n^m} e^{-\frac{j2\pi nk}{N}}, -\frac{N}{2} \leq k \leq \frac{N}{2}-1 \quad (9)$$

After taking the FFT of r_n^m , the frequency domain received signal on the k^{th} subcarrier of the m^{th} symbol is:

$$y_k^m = \sum_{q=0}^{N-1} X_q^m h_q p_{(k-q)}^m + W_k^m, 0 \leq k \leq N-1 \quad (10)$$

where X_q^m is q^{th} element of symbol vector X^m , h_q is the q^{th} element of channel vector $\mathbf{h} = [h_0, h_1, h_2, \dots, h_{N-1}]^T$, W_k^m is AWGN in frequency domain, and $p_{(k-q)}^m$ is the $(k-q)^{th}$ spectral component of PHN spectral component vector, P^m , with modulo N indexing. Further note that with modulo N indexing, the lower-order spectral components of PHN are given by $p_0, p_1, p_{N-1}, p_2, p_{N-2}$, etc. For convenience of the later analysis, it is preferable to represent the signal model in matrix form as:

$$\mathbf{Y}^m = \mathbf{H}^m \mathbf{P}^m + \mathbf{W}^m \quad (11)$$

where

$\mathbf{Y}^m = [y_0^m, y_1^m, \dots, y_{N-1}^m]^T$, $\mathbf{P}^m = [p_0^m, p_1^m, \dots, p_{N-1}^m]^T$, $\mathbf{h} = [h_0, h_1, h_2, \dots, h_{N-1}]^T$, $\mathbf{X}^m = [X_0^m, X_1^m, \dots, X_{N-1}^m]^T$ and \mathbf{H}^m is a column-wise circulant matrix whose first column is vector $[h_0 X_0^m, h_1 X_1^m, \dots, h_{N-1} X_{N-1}^m]^T$. $\mathbf{W}^m = [W_0^m, W_1^m, \dots, W_{N-1}^m]^T$, is an uncorrelated white noise vector distributed as $\Pr(\mathbf{W}^m) = \mathcal{CN}(0, 2\sigma_\omega^2 \mathbf{I})$ as given in Eq. (6).

4.1 Common phase error

In single carrier (SC) systems, the phase noise merely causes simple random rotation in the symbol constellation known as common phase error (CPE).

Figure 4a shows the received signal constellation of an SC, 16-QAM modulation over an AWGN channel (SNR = 30 dB), whereas the effect of PHN from an FRO (PHN variance = .06 rad²), on received signal constellation, is shown in **Figure 4b**.

4.2 Inter-carrier interference

In OFDM systems, in addition to the rotational effect, PHN also causes ICI. The ICI is present because PHN causes energy of individual subcarriers to spread on the top of all the other subcarriers [20–23]. **Figure 5** shows two systems with the bandwidth of 22 MHz where first system employs the ideal oscillator without PHN with carrier frequency 2420.5 MHz, whereas second system uses a noisy FRO with carrier frequency 2433.5 MHz, which causes spectral regrowth and results in power leakage to the first band, producing the inter-carrier interference (ICI).

Figure 6a shows the received signal constellation of an OFDM system with 64 subcarriers, which are 16-QAM modulated over AWGN (SNR = 35 dB) with receiver PHN (both CPE and ICI) from an FRO (PHN variance = .06 rad²), whereas the effect of receiver as well as transmitter PHN from an FRO (PHN variance = .06 rad²) on received signal constellation is shown in **Figure 6b**. The constellation rotation is produced because of the CPE, whereas the cloudy constellation is impact of ICI.

The effect of PHN on BER of the OFDM system is shown in **Figure 7** for receiver FRO PHN (PHN variance = .06 rad²) only and for transceiver FRO PHN (PHN variance = .06 rad²) and is compared against the BER of pure AWGN channel.

OFDM symbols are generated using 16-quadrature amplitude modulation (QAM) and 64-point IFFT and then prepended by CP of length 16 samples before

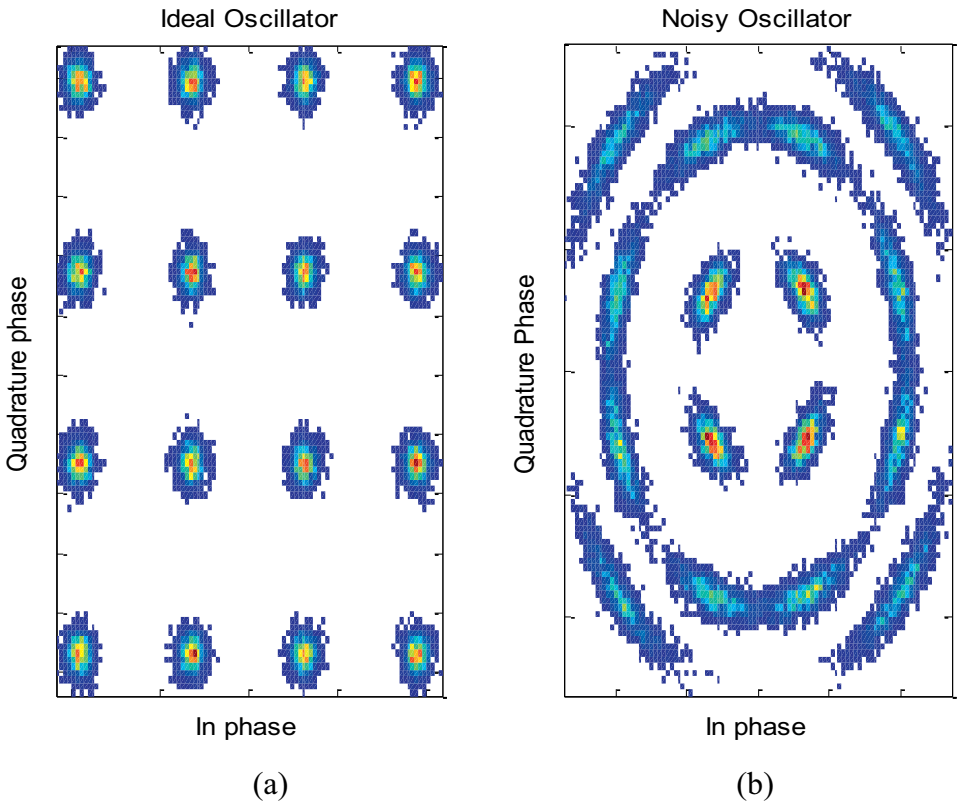


Figure 4.
Effect of phase noise in SC communication system (random rotation in constellation).

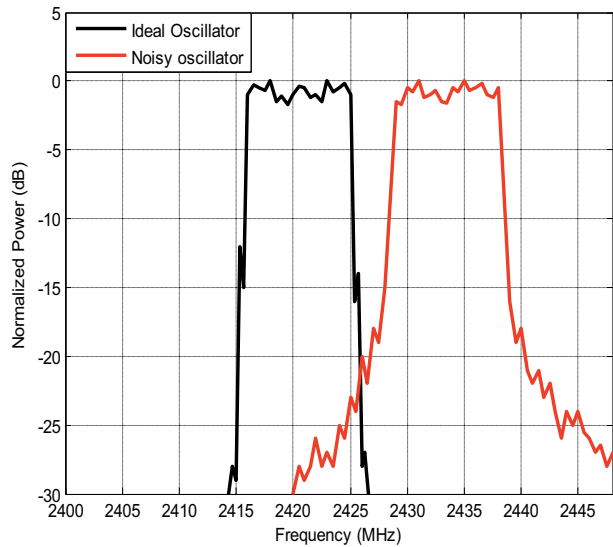


Figure 5.
Effect of phase noise in MC communication system (spectral regrowth (in-band-ICI)(out-of-band-MUI)).

transmitting over the channel. The 64-point FFT of the received signal is taken after CP removal. Simulation model is based on IEEE 802.11 g like system with parameters given in **Table 2**.

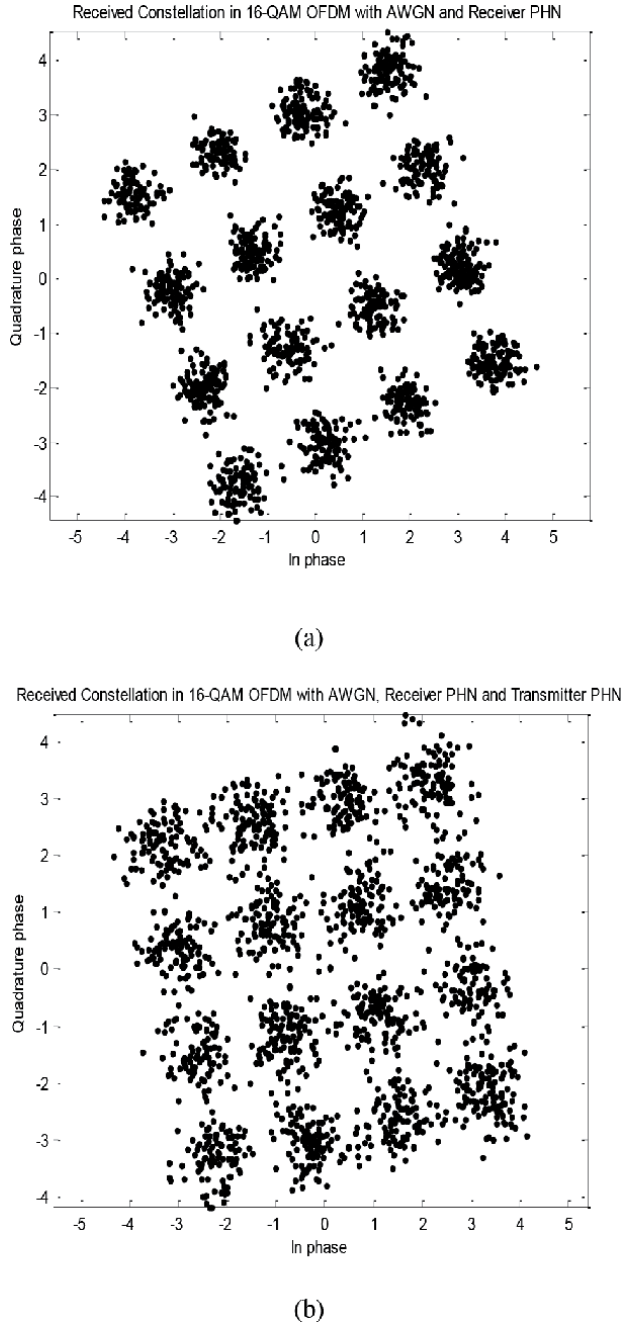


Figure 6. Received constellations in 16-QAM OFDM system with (a) receiver phase noise and (b) transceiver phase noise.

5. OFDMA

In OFDMA system, both the time and frequency resources are used to separate the multiple users. As OFDMA is typically used with burst transmission, a burst consists of many OFDM symbols. In an OFDM symbol, there are many subcarriers. So, a subcarrier in frequency domain and symbol duration in time domain are the finest units. The combination of a time unit and a frequency unit, i.e., a symbol period and a

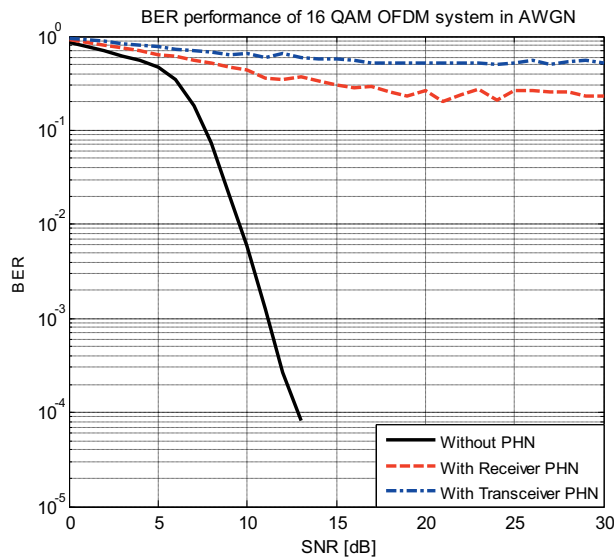


Figure 7.
 16-QAM OFDM BER performance in AWGN channel with phase noise.

F_s	20 MHz
N	64
FFT Size	64
N_g	16 Samples
Mapping	16-QAM

Table 2.
 OFDM modeling parameters.

subcarrier, is the finest slot, which or group of which is allocated to one of the multiple users. **Figure 8** shows the time frequency and power grid of OFDMA [24, 25].

Practically, in frequency domain, the allocation is not done at the level of subcarriers but on the group of subcarriers. This subcarrier's allocation is known as subchannelization. To explain the basic principle of OFDMA transceiver, we are considering here that one user is using one subcarrier in the given time slot, i.e., number of users (U) = N . With this the simplest OFDMA uplink scheme is illustrated in **Figure 9**. At the transmitter side (mobile terminal), each user is having individual transmitters. At the receiver side (base station), the received signal is the sum of U users' signal, which acts as an OFDM signal. Because of this in OFDMA receiver, a single MC demodulator (OFDM demodulator) is required than U demodulators as in case of conventional frequency division multiple access (FDMA) system. At the transmitter side, a single transmitter consists of symbol generator and OFDMA modulator. The symbol is generated with applicable channel coding and mapping. These symbols are then OFDMA modulated with subchannelization and SC modulator (in case of $U = N$) or OFDM modulator in case a single user is using group of the subcarriers.

An exact clock and carrier synchronization is must for an OFDMA system to ensure orthogonality between the unmodulated signals from different mobile terminals. This is achieved by transmitting synchronization signals from the receiver to all mobile terminals instantly. Each terminal OFDM modulator drives the carrier frequency and clock signal from these downlink signals. In case of coherent detection,

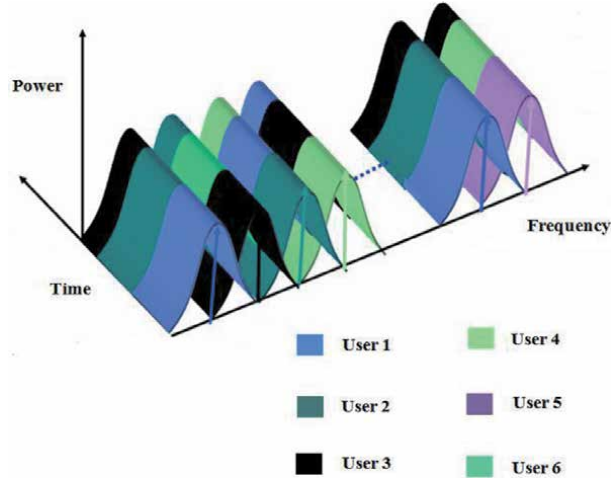


Figure 8.
OFDMA time-frequency power grids [24].

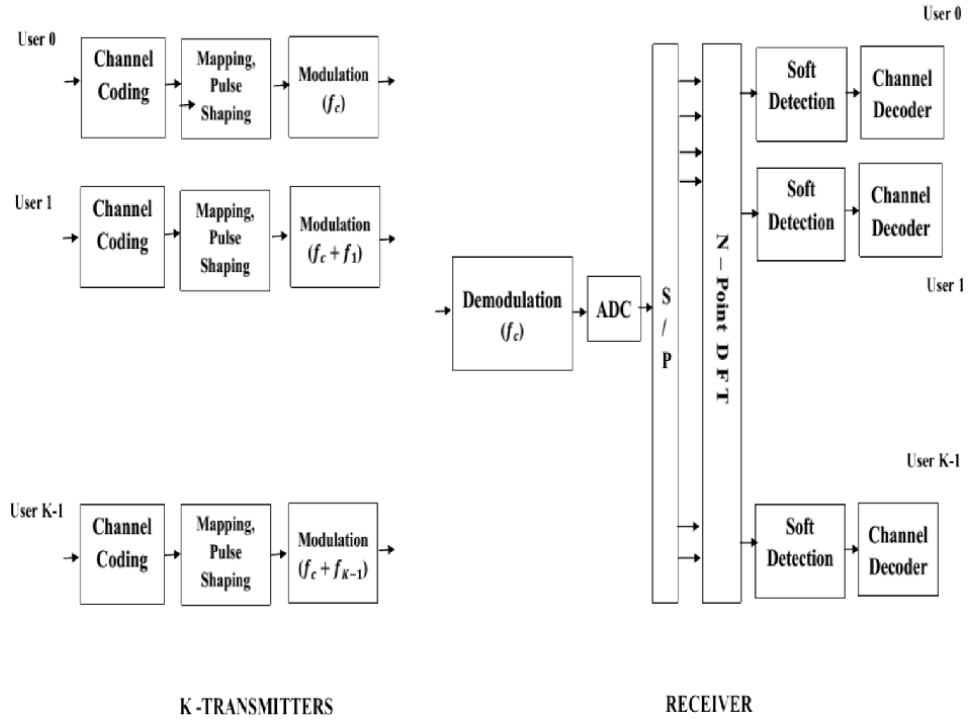


Figure 9.
OFDMA uplink.

simple carrier and clock recovery circuits are sufficient in the demodulator to extract this information from the received signal as the clock and carrier frequencies are available at the base station. This factor simplifies the OFDMA demodulator.

6. Phase noise in OFDMA

Like all other challenges of OFDM, i.e., time and frequency synchronization, high PAPR, CFO, and IQ imbalance, OFDMA also faces the challenge of transceiver

RF impairment because of time-varying PHN. In OFDMA, CPE and in-band ICI are not the only source of interference that should be considered. The multiplexing of several users in an OFDMA scenario introduces out-of-band interference from one user on another in the OFDMA symbol. This MUI is induced by the spectral spread of the energy of each user's subcarriers on the top of other users' subcarriers. The spread is more severe in case of uplink, when there are unequal power levels as well as unequal transmitter 2(PHN 3-dB BW) for different users due to different path loss effects and different oscillator nonidealities, respectively, in an uplink scenario. Additionally, in the case of transmitter PHN, ICI results not only from the higher order components of PHN but also because of the loss of the cyclic nature and so the orthogonality is destroyed of the transmitted signal as the transmitter PHN affects the samples of the CP differently than the corresponding samples in the actual OFDMA signal part [26]. Further, the transmitter PHN impairing the CP also tends to produce ICI and hence not only $N - 1$ but $N + N_g - 1$ samples of PHN realization should be considered for PHN mitigation.

In regard of PHN impaired OFDMA modeling, we consider the uplink of an OFDMA with $U(u = 1, 2, 3, \dots, U)$ users, and \mathcal{U} represents the index set of use full subcarriers with size \mathfrak{A} , means that among N subcarriers, the u^{th} user is assigned to a subset of \mathfrak{A}_u subcarriers with index set: $\mathcal{U}_u = \{\mathcal{U}_1^u \mathcal{U}_2^u \mathcal{U}_3^u \dots \mathcal{U}_{\mathfrak{A}_u}^u\}$, either contiguous or interleaved where $(.)^u$ denotes the u^{th} user. If $x^{m,u}$ is the m^{th} frequency domain symbols sent by the u^{th} user, then k^{th} entry of it, say $X_k^{m,u}$ is nonzero if $k \in \mathcal{U}_u$. Thereupon discrete-time baseband signal of the u^{th} user using IFFT can be represented as:

$$S_{k,n}^{m,u} = \frac{1}{N} \sum_{k \in \mathcal{U}_u} X_k^{m,u} e^{j2\pi \frac{kn}{N}}, 0 \leq n \leq N - 1. \quad (12)$$

As there is no ISI in between the windows of N samples, and that the whole processing can be done in a symbol-to-symbol manner, we drop the OFDMA symbol index m hereafter. After this the signal is transformed back to the serial form and is upconverted to RF with noisy transmitter oscillator and finally is sent over the channel. Let the discrete-time composite channel impulse response with order L^u between the u^{th} user and the uplink receiver be denoted by $g^u(l)$ and the channel frequency response on the k^{th} subcarrier of u^{th} user's channel be denoted by h_k^u , then we have:

$$h_k^u = \sum_{l=0}^{L_k-1} g^u(l) e^{-j2\pi \frac{kl}{N}} \quad (13)$$

Denoting the discrete-time transmitter PHN process, receiver PHN process, and AWGN impairing to the u^{th} user by $\theta_{T,n}^u$, $\theta_{R,n}^u$, and w_n , respectively, the received OFDMA symbol after downconversion and CP removal can be written as:

$$r_n = \sum_{u=1}^U [(S_{k,n}^u e^{j\theta_{T,n}^u}) \otimes g^u(l)] e^{j\theta_{R,n}^u} + w_n. \quad (14)$$

After taking the FFT, the frequency domain received symbol on the k^{th} subcarrier is:

$$y_k = p_0^u h_k^u X_k^u + \sum_{i=1}^U \sum_{\substack{q \in \mathcal{U}_i \\ q \neq k}} p_{k-q}^i h_q^i X_q^i + W_k. \quad (15)$$

As h is a circulant matrix, we can effectively map the transmitter PHN as receiver PHN, and by writing $\theta_{T,n}^u + \theta_{R,n}^u = \theta_n^u$, we have $p_q^u = \frac{1}{N} \sum_{n=0}^{N-1} e^{j\theta_n^u} e^{-j\frac{2\pi nq}{N}}$, and W_k is the AWGN noise in frequency domain.

From Eq. (15), we find the effect of phase noise in OFDMA to be different from that of single-user OFDM. First of all the CPE term (p_0^u) varies according to the index u , means that each user suffers from different CPE, and they need to be considered separately for each user to estimate and mitigate.

Secondly, the summative term, called ICI, includes the user's "in-band" ICI (self-interference (SI)) and ICI caused by MUI. While including the frequency domain dummy symbols transmitted by each active user in Eq. (15), a unified frequency domain signal model can be given by:

$$y_k = \sum_{u=1}^U \sum_{q=0}^{N-1} p_{k-q}^u h_q^u X_q^u + W_k. \quad (16)$$

Splitting the summative (ICI) term is important for our analysis purpose, as MUI takes in to account the significance of the power level of users as well as the transmitter 2(PHN 3-dB BW) as these two will be significantly different for different users precisely in case of OFDMA uplink. So the signal for u^{th} user, on his k^{th} subcarrier, is given as:

$$y_k = p_0^u h_k^u X_k^u + \sum_{\substack{q \in \mathcal{U}_u \\ q \neq k}} p_{k-q}^u h_q^u X_q^u + \sum_{\substack{i=1 \\ i \neq u}}^U \sum_{\substack{q \in \mathcal{U}_i \\ q \neq k}} p_{k-q}^i h_q^i X_q^i + W_k. \quad (17)$$

First to characterize the phase noise strength in OFDMA transmission, we adopt a parameter widely used in literature, which is the relative PHN bandwidth, $\Delta_{PN} = \frac{2(\text{PHN } 3\text{dB-BW})}{\Delta f(\text{subcarrier spacing})}$. Having the desired advantages of OFDM transmission over single-carrier transmission with "slow" PHN model restricts to have low of this ratio, which makes the assumption of complex Gaussian distribution of the ICI false, even with higher number of subcarriers. Secondly a higher $2(\text{PHN } 3\text{dB} - \text{BW})$ of the PHN process and the higher value of power level can also lead to more energy in the MUI factor of ICI terms. Considering these two facts and the OFDMA uplink scenario, not all the $U - 1$ users will produce the MUI for u^{th} user but only those who will satisfy the following inequality will be the disruptive users for u^{th} (user)

$$\sum_{a=1}^{N-1} E[|p_a^u|^2] < \sum_{a=1}^{N-1} E[|p_a^j|^2] \text{ for } j = 1 \text{ to } U \text{ and } j \neq u. \quad (18)$$

Here we define a subset of users for the u^{th} user I_u , $\forall j \in I_u$ with size I_u . Since the PSD of phase noise tapers off rapidly beyond the loop bandwidth, most of the energy in a phase noise sequence is contained in the frequency components corresponding to the first few orders. Hence, the largest contribution to interference on a particular subcarrier is likely to come from users occupying adjacent subcarriers. As a result, disruptive users who are occupying subcarriers adjacent to the u^{th} user are likely to be most disruptive users. Keeping this valid, Eq. (17) can be rewritten while using Eq. (18) as:

$$y_k = p_0^u h_k^u X_k^u + \sum_{\substack{q \in \mathcal{U}_u \\ q \neq k}} p_{k-q}^u h_q^u X_q^u + \sum_{i \in \mathcal{I}_u} \sum_{\substack{q \in \mathcal{U}_i \\ q \neq k}} p_{k-q}^i h_q^i X_q^i + W_k \quad (19)$$

where the second term is SI, and third term is MUI.

7. Conclusion

Analyzing the impact of transceiver PHN necessitates the accurate mathematical modeling of generated PHN. As the FRO model is easy to simulate mathematically and PLL is widely used in practice for digital communication systems, the PHN modeling for both of the oscillators is presented. With the white noise sources in the oscillator circuitry, the PHN is modeled as Wiener process and celebrated O-U process, for FRO and PLL VCO, respectively.

OFDM, as a low complex modulation technique, became the potential contender for MC transmission to combat the frequency selectivity of the channel. The synchronization unit (including the time and frequency synchronization units) of OFDM demodulator is performing the robust digital synchronization and channel estimation with digital algorithms. The presence of transceiver PHN degrades the OFDM system performance because of the rotational effect CPE and spectral regrowth ICI.

Being effective in mitigating the hostile channel selectivity with adaptive subchannelization and resource allocation, the OFDMA technique has gained much more interest in recent years. With transceiver PHN in OFDMA, CPE and in-band ICI are not the only sources of interference like OFDM but the multiplexing of several users introduces out-of-band interference from one user on another known as MUI [27].

Acknowledgements

Acknowledgment is made to the Department of Electronics and Communication Engineering, BIET, and Editors, IntechOpen for the support to make this book chapter possible.

Conflict of interest

The authors declare no conflict of interest.

Notes/thanks/other declarations

Thanks to Prof. R. P. Yadav for his valuable suggestions and comments that helped to improve the presentation of the book chapter.

Author details

Kamayani Shrivastav
Bharat Institute of Engineering and Technology, Hyderabad, India

*Address all correspondence to: 2014rec9012@mnit.ac.in

IntechOpen

© 2022 The Author(s). Licensee IntechOpen. This chapter is distributed under the terms of the Creative Commons Attribution License (<http://creativecommons.org/licenses/by/3.0>), which permits unrestricted use, distribution, and reproduction in any medium, provided the original work is properly cited. 

References

- [1] Cimini LJ. Analysis and simulation of a digital mobile channel using orthogonal frequency division multiplexing. *IEEE Transactions on Communications*. 1985; **COM-33**:665-675
- [2] Bingham JAC. Multicarrier modulation for data transmission: An idea whose time has come. *IEEE Communications Magazine*. 1990; **28**(5):5-14
- [3] Wu Y, Zou WY. Orthogonal frequency division multiplexing: A multi-carrier modulation scheme. *IEEE Transactions on Consumer Electronics*. 1995; **41**(3):392-399
- [4] Krondorf M, Fettweis G. OFDM link performance analysis under various receiver impairments. *EURASIP Journal on Wireless Communications and Networking*. 2008. DOI: 10.1155/2008/145279
- [5] Park MC, Han DS. Deep learning-based automatic modulation classification with blind OFDM parameter estimation. *IEEE Access*. 2021; **9**:108305-108317. DOI: 10.1109/ACCESS.2021.3102223
- [6] Robertson P, Kaiser S. Analysis of the effects of phase noise in orthogonal frequency division multiplex (OFDM) systems. In: *Proceedings of the IEEE ICC'95*. Seattle, WA; 1995. pp. 1652-1657
- [7] Armada A. Understanding the effects of phase noise in orthogonal frequency division multiplexing (OFDM). *IEEE Transactions on Broadcasting*. 2001; **47**(2):153-159
- [8] Wu S, Bar-Ness Y. OFDM systems in the presence of phase noise: Consequences and solutions. *IEEE Transactions on Communications*. 2004; **52**(11):1988-1997
- [9] Shrivastav K, Yadav RP, Jain KC. Cyclic gradient descent optimization for joint MAP estimation of channel and phase noise in OFDM. *IET Communications*. 2018; **12**(12): 1485-1490. DOI: 10.1049/iet-com.2017.0732
- [10] Mohammadian A, Tellambura C, Li GY. deep learning-based phase noise compensation in multicarrier systems. *IEEE Wireless Communications Letters*. 2021; **10**(10):2110-2114. DOI: 10.1109/LWC.2021.3093574
- [11] Demir A. Phase noise and timing jitter in oscillators with colored-noise sources. *IEEE Transactions on Circuits and Systems—I: Fundamental Theory and Applications*. 2002; **49**(12): 1782-1791
- [12] Hajimiri A, Lee T. A general theory of phase noise in electrical oscillators. *IEEE Journal of Solid-State Circuits*. 1998; **33**(2):179-194
- [13] Chorti A, Brookes M. A spectral model for RF oscillators with power-law phase noise. *IEEE Transactions on Circuits and Systems—I: Regular Papers*. 2006; **53**(9):1989-1999
- [14] Demir A. *Phase Noise in Oscillators: DAEs and Colored Noise Sources*. Bell Laboratories; 2011
- [15] Mathecken P, Riihonen T, Werner S, Wichman R. Performance analysis of OFDM with wiener phase noise and frequency selective fading channel. *IEEE Transactions on Communications*. 2011; **59**(5):1321
- [16] Ghosh AP, Qin W, Roitershtein A. Discrete-time Ornstein-Uhlenbeck process in a stationary dynamic environment. *Journal of Interdisciplinary mathematics*. 2016; **19**(1):1-35
- [17] Kamayani Shrivastav RP, Jain KC. Joint MAP detection for OFDM in

presence of phase noise from free running and phase locked loop oscillator. *Wireless Personal Communications*. 2019;**109**(6):563-577. DOI: 10.1007/s11277-019-06579-5

[18] Demir A, Mehrotra A, Roychowdhury J. Phase noise in oscillators: A unifying theory and numerical methods for characterization. *IEEE Transactions on Circuits Systems I, Fundamental, Theory & Applications*. 2000;**47**(5):655-674

[19] Ikeuchi K, Sakai M, Lin H. Compensation of phase noise in OFDM/OQAM systems. In: 2017 IEEE 86th Vehicular Technology Conference (VTC-Fall). 2017. pp. 1-5

[20] Shi Q, Wu N, Wang H, Nguyen DN, Huang X. Joint phase noise estimation and decoding in OFDM-IM. In: *GLOBECOM 2020 – 2020 IEEE Global Communications Conference*. 2020. pp. 1-6. DOI: 10.1109/GLOBECOM42002.2020.9348264

[21] Schlüter M, Dörpinghaus M, Fettweis GP. Joint phase and timing estimation with 1-bit quantization and oversampling. *IEEE Transactions on Communications*. 2022;**70**(1):71-86. DOI: 10.1109/TCOMM.2021.3113946

[22] Park CS, Gim Y, Park J, Park S. Design and implementation of a digital front-end with digital compensation for low-complexity 4G radio transceivers. *IEEE Access*. 2021;**9**:111432-111455. DOI: 10.1109/ACCESS.2021.3102949

[23] Kamayani Shrivastav RP, Jain KC. Joint MAP channel estimation and data detection for OFDM in presence of phase noise from free running and phase locked loop oscillator. *Digital Communications and Networks*. 2021; **7**(1):55-61. DOI: 10.1016/j.dcan.2020.09.007

[24] Srikanth S, Kumaran V, Manikandan C. Orthogonal frequency

division multiple access: Is it the multiple access system of the future? In: *AU-KBC Research*. India: Anna University; 2006

[25] Maeder A, Zein N. OFDMA in the field: Current and future challenges. *ACM SIGCOMM Computer Communication Review*. 2010;**40**(5): 71-76

[26] Shrivastav K, Yadav RP. Characterization of MUI for OFDMA uplink in presence of transceiver phase noise. *International Journal of Future Generation Communication and Networking*. 2017;**10**(6):23-32

[27] Mohammadian A, Tellambura C. Joint channel and phase noise estimation and data detection for GFDM. *IEEE Open Journal of the Communications Society*. 2021;**2**:915-933. DOI: 10.1109/OJCOMS.2021.3073348

Section 2

Multiplexing and Optics

Multiplexing, Transmission and De-Multiplexing of OAM Modes through Specialty Fibers

Alaaeddine Rjeb, Habib Fathallah and Mohsen Machhout

Abstract

Space division multiplexing (SDM) over fibers has introduced a new paradigm in optical communication thanks to its capability to meet the ever-renewed demand of more transmission capacity and on large spectral efficiency. This ever-increasing demand is pushed by the nonstop increase of the number of connected users, devices, processes, and data (toward internet of everything IOE). One of the most promising variants of SDM, that has recently shown great potential, is based on harnessing orbital angular momentum (OAM) modes as data carriers. These OAMs are multiplexed, transmitted over special optical fibers (OAM-fibers) then de-multiplexed. In order to highlight the potential of SDM system incorporating OAM modes through fibers, in this chapter, we disassemble an SDM system and we examine its main key elements. The potential of OAM-SDM is discussed as a promising candidate for the next generation local/global communications networks. This chapter is intended to provide a comprehensive and deep understanding of SDM, which will push R&D community to derive future research directions in the field.

Keywords: optical communication, space division multiplexing (SDM) systems, orbital angular momentum (OAM), optical fibers

1. Introduction

Over the last decade, there are unquestionably a huge demand for transmission capacity. This demand is fueling by the fast & renewed increase of the number of connected users, devices, processes, and data (e. g. According to the Annual Internet report of CISCO, there will be 5.3 billion total Internet users (66% of global population) by 2023, up from 3.9 billion (51% of global population) in 2018) [1]. This tend to create a hyper connected world. Furthermore, there are international efforts that aim to develop a concrete roadmap for “Internet Governance” targeting to both bring (i.e. to deliver) the internet to everyone (i.e. “connect the unconnected”) and provide enormous boost in performance of the actual Internet network. These efforts will put much pressure on the Internet service providers/communications actors and motivate them to reach innovative solutions and advanced technologies to deal with the growing insatiable on data capacity that will probably result in an imminent capacity crunch in the next few years [2]. On the other hand, optical fiber communication is still a milestone in the evolution of communication generally. Optical fiber is considered as the backbone of the modern

communications grid. Various research developments on optical fiber communication have been conducted showing great potential [3].

In order to cope with the huge demand of more and more data capacity, and improve the spectral efficiency, R&D optical fiber communication community has developed various technological paths based on innovative multiplexing techniques and advanced optical modulation formats. From one hand, various multiplexing techniques have been conducted based on the use of different optical signal dimensions as degrees of freedom to encode information and transmit them over optical fibers. These dimensions are the Time, as time division multiplexing (TDM: interleaving channels temporally), the polarization, Polarization division multiplexing (PDM), the wavelength, as wavelength division multiplexing (WDM: using multiple wavelength channels) and the phase (quadrature). These physical parameters help to create orthogonal signal sets even sharing the same medium (i.e. multiplexing); they do not interfere with each other (i.e. individual, separate and independent signals). **Figure 1** depicts these orthogonal dimensions. On the other hand, the improvement in modulation format is translated by the move on from the On-Off-Keying (OOK) modulation to M-ary Quadrature Amplitude Modulation (M-QAM), M-ary phase-shift keying (M-PSK) and M-ary amplitude-shift keying (M-ASK) [4–6].

Recently, researchers have oriented toward the space (Space Division Multiplexing (SDM)) as a further dimension to encode information [7]. The spatial analogue of the above cited dimensions, SDM is based on the exploitation of the spatial structure of the light (i.e. optical signal) or the spatial dimension of the physical transmission medium (e.g. optical fiber). Both strategies aim to improve the available data channels along an optical transmission link (i.e. Network). Considering these data channels, two attractive variants of SDM have shown potential interest: (1) Core Division Multiplexing (CDM) and (2) Mode Division Multiplexing (MDM). CDM is based on the increasing of the number of cores embedded in the same cladding of optical fiber [8]. These fibers are known as multicore fibers (MCFs). Other classical option that has been adopted in current optical infrastructure for several years already is based on single core fibers bundles (i.e. fibers are packed together creating a fiber bundle or

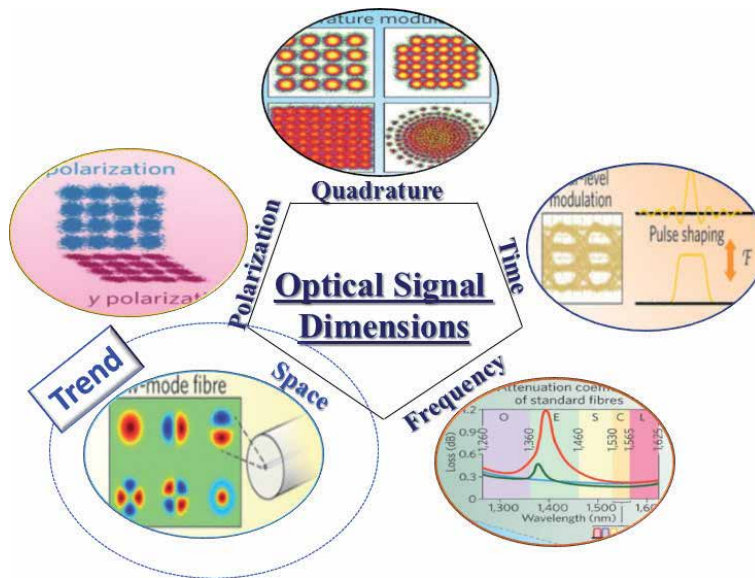


Figure 1.
Optical signal dimensions using as degrees of freedom to encode data.

ribbon cable) [9]. If we assume that one core is equivalent to one data channel hence, the transmission capacity in an optical link incorporating MCFs will be multiplied by the number of embedded cores. On other side, MDM is consisting on the transmission of several spatial optical modes (various paths or trajectories) as data channels within common physical transmission medium (within the same core) targeting to boost the capacity transmission [10]. MDM could be realized by either multimode fibers (MMFs) or few mode fibers (FMFs). MMFs are dedicated to short transmission interconnect while FMFs are used for long haul transmission links. The same as CDM, if we assume that one mode is equivalent to one data channel; the transmission capacity in an optical link incorporating MMF/FMF will be multiplied by the number of supported modes. Other promising technology is based on mixing both approaches: Multicore few modes fibers (MC-FMF) where the number of channels will be proportional to the number of embedded cores and to the number of supported modes within the same core [11]. Moreover, MDM could be realized over free space link where data are carrying on multiple parallel laser beams that propagates over free space between transceivers [12].

Considering optical fiber links, numerous mode basis have been harnessed for mode division multiplexing showing its capability & effectiveness to scale up the capacity transmission and enhance the spectral efficiency. Recently, based on the feature that light can carry Angular Momentum (AM) (i.e. AM expresses the amount of dynamical rotation presents in the electromagnetic field representing the light), the capacity transmission of optical fiber has been unleashed [13]. The AM of a light beam is composed of two forms of momentums (i.e. rotation): (1) Spin Angular Momentum (SAM), which is related to the polarization of light (e.g. right or left circular polarization). SAM provide only two different states (available data channels). (2) Orbital Angular Momentum (OAM) which is linked to the spiral aspect (twisted light) of the wave front. This is related to a phase front of $\exp(jl\varphi)$ where l is an arbitrary unlimited integer (theoretically) that indicates the degree of twist of a beam, and φ is the azimuthal angle [14]. Benefiting of two inherent features of OAM modes: first, two OAM modes with different topological charge l do not interfere (i.e. orthogonality). Second, the topological charge l is theoretically unlimited (i.e. unboundedness), exploiting the OAM of light as a further degree of freedom to encode information, is arguably one of the most promising approaches that has deserved a special attention over the last decade and showing promising achievements [15, 16]. OAM modes has been harnessed in multiplexing/de-multiplexing (OAM-SDM) or in increasing the overall optical channel capacity over optical fiber link. OAM-SDM is facing several key challenges, and lots crucial issues that it is of great importance to handle with it in order to truly realize the full potential of this promising technology and to paving the road to a robust and to a high capacity transmission operation with raised performances in next generation optical communication systems.

SDM is based on the orthogonality of spatial channels (spatial modes). Thus, mode coupling or mode mixing (e.g. channels crosstalk) is the main challenge in an SDM system and the main goals of that technology are in principle rotating around how to keep enough separation between much available modes. In order to cope with channel crosstalk, two solutions could be used. The first is the use of multiple input multiple output digital signal processing (MIMO DSP) [17] while the second is based on the optimization of fiber parameters (refractive index profile & fiber parameters) at the design stage [18]. In principle, MIMO DSP is considered as the extreme choice to decipher channels at the receiving stage since it is heavy and complex. This complexity is came from the direct proportionality between the number of required equalizer from one side and the transmission distance, the number of modes, and the difference between modes delays, from the other side. Hence, these

considering reasons allow the use of MIMO much impractical in real time and threats the scalability of optical communication SDM systems. Hence, by carefully manipulating the fiber design key parameters, it is possible to supervise/control the possible interactions between modes/channels. This better facilitates understanding each fiber parameter impact on fiber performances metrics and smooth the way of transition from the design stage to the fabrication process (e.g. MCVD as Modified Chemical Vapor Deposition) and to the deployment operation on the ground later (e.g. FTTH as Fiber To The Home and FTTX as Fiber To The x).

In this chapter, we detail the main key elements/actors (i.e. devices and parameters) that form an SDM system and allow it to become a promising approach to handle with the upcoming capacity crunch of the next generation optical communications systems. Then, we concentrate on the potential of using OAM modes over optical fibers (OAM-SDM) as a promising candidate that tend to realize the full potential for SDM technology. We provide the main generation, detection, transmission, challenges and future research directions of that technology. This aims to provide a comprehensive and deep understanding of OAM-SDM technology, which will push R&D community to derive future research directions in the field.

2. Space division multiplexing (SDM) system

In this section, we detail the optical fiber based SDM optical communication system. We describe essential devices/actors constructing a full SDM transmission line. We start by the emission side devices, then the SDM-fibers & amplifiers and at last the devices using for the reception of data at the receiver side. **Figure 2** illustrates a schematic representation of a generic SDM optical communication system.

2.1 Emission side

From the emission side, data ($Data_i$) are modulated using for example a non-return to zero (NRZ) sequence. The electrical signal (ES_i) converted into an optical signal using optical sources. These optical sources could be LED (light-emitting diode), DFB laser (distributed feedback laser), FP lasers (Fabry-Pérot laser diode), VCSEL (Vertical Cavity Surface Emitting Laser), etc. Each transmitter will couples the generated optical signal to a single mode fiber (SMF_i) in order to excite the fundamental mode (i.e. namely LP_{01} mode) [19]. All the obtained modes are multiplexed using optical multiplexers (SDM MUX). SDM Optical multiplexers (also commonly called fan-in device) are spatial multiplexers that tend to collect modes (i.e. data carriers) from SMFs and couple them to an SDM fiber. For multiplexing various modes,

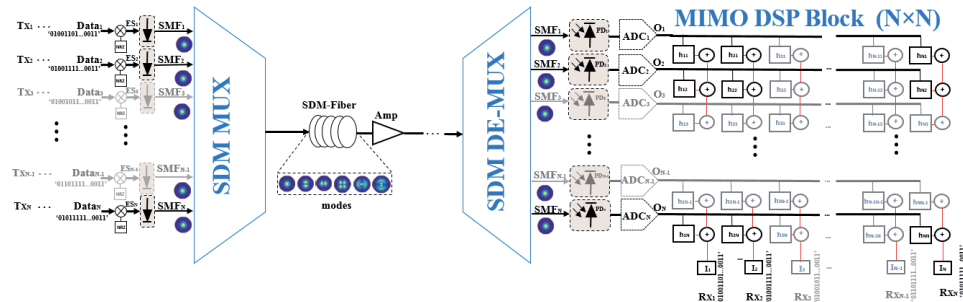


Figure 2. Schematic of a generic space division multiplexing system based on optical fiber communication.

several techniques and devices have been demonstration. Photonic lantern, Photonic integrated grating couplers waveguide optics interface, tapered multicore fibers, waveguide coupling (e.g. in case of MCFs, isolated waveguides connect each core to a particular SMF) and free space optics approaches such as phase plates, mirrors, beam splitters and special lenses [20]. In principle, the selection rule between these techniques are based on the incorporated SDM fiber (i.e. FMF, MMF MCF) and on the requirement of the lowest loss, the low susceptibility to crosstalk, the compactness, and low complexity and flexible.

2.2 SDM-optical fiber transmission

Various kinds of fibers are used for SDM communication systems. As indicated above, we divide them as CDM-fibers and MDM-fibers. Considering CDM, the first technology used as SDM fibers are based on the use of Single-core Fiber bundle (fiber ribbon) where parallels single mode fibers are packed together creating a fiber bundle or a ribbon cable. The overall diameter of these bundles varies from around 10–27 mm. Delivers up to hundreds of parallel links, fiber bundles have been commercially available [21, 22], and adopted in current optical infrastructure for several years already. Fiber ribbons are also commercially used in conjunction with several SDM transceiver technologies [23]. Another scheme is based on carrying data on single cores (single mode) embedded in the same fiber known as Multicore Fibers (MCF). Hence, each core is considered as an independent single channel. The most important constraint in MCFs is the inter-core crosstalk (XT) caused by signal power leakage from core to its adjacent cores that is controlled by core pitch (distance between adjacent cores denoted usually as Λ) [24]. There are in Principle, two main categories of MCF: weakly coupled MCFs (=uncoupled MCF) and strongly coupled MCFs (=coupled MCF) depending on the value of coupling coefficient 'K' (used to characterize the crosstalk). Using the so-called supermodes to carry data, the crosstalk in coupled MCF must be mitigated by complex digital signal processing algorithms, such as multiple-input multiple-output digital signal processing (MIMO-DSP) techniques [25]. On the contrary, due to low XT in uncoupled MCF, it is not necessary to mitigate the XT impacts via complex MIMO, (see **Table 1**). In principle, three-crosstalk suppression schemes in uncoupled MCF could be incorporated, which are trench-assisted structure, heterogeneous core arrangement, and propagation-direction interleaving (PDI) technique [26].

The first paper on communication using MCF demonstrates a transmission of 112 Tb/s over 76.8 km in a 7-cores fiber using SDM and dense WDM in the C+L ITU-T bands. The spectral efficiency was of 14 b/s/Hz [27]. The second paper [28] shows an ultra-low crosstalk level (≤ -55 dB over 17.6 km), which presents the lowest crosstalk between neighboring cores value to date. Other reported works, show high capacity (1.01 Pb/s) [29] over 52 km single span of 12-core MCF. In [30], over 7326 km, a record of 140.7 Tb/s capacity are reached. Considering MDM schemes, two types of fibers are dedicated to support that strategy. One is

	Weakly coupled MCFs	Strongly coupled MCFs
Coupling coefficient 'K' [m^{-1}]	$K < 0.01$	$K > 0.1$
Core pitch ' Λ ' [μm]	$\Lambda > 30$	$\Lambda < 30$
MIMO DSP exigence	No need	Need

Table 1.
 Classification and features of multicore fibers.

based on the use of multimode fibers (MMF) while the second exploits the well-known few-mode fibers (FMF). The main difference between both is the number of modes (available channels). Since MMF can support large number of modes (tens), the intermodal crosstalk becomes large as well as the differential mode group delay (DMGD), where each mode has its own velocity, hence reducing the number of propagating modes along the fiber becomes viable solution. This supports FMF as a viable candidate for realizing SDM [31]. **Figure 3** recapitalizes examples of SDM optical fibers.

Due to the unavoidable attenuation over the transmission operation (i.e. degradation of the spatially multiplexed optical signals powers), SDM optical amplifiers are essential for a long-haul space division multiplexing (SDM) transmission system. Two requirements should be fulfilled by optical amplifiers, which are the large mode gain and the small difference between gains over different modes. In principle, two types of optical amplifiers, optical fiber amplifier OFA (e.g. erbium-doped fiber amplifier (EDFA [32]), fiber Raman amplifier (FRA)) and semiconductor optical amplifier SOA. Other approach is based on electro-optical repeaters or regenerators where the amplification process is performed in electronic regime [33]. A repeater is consisting of optical receiver (i.e. optical signal to electrical signal), amplifier and Optical transmitter (i.e. electrical signal to optical signal). Three functions could be conducted over the amplifier known as 1R, 2R, and 3R.

- 1R: re-amplification.
- 2R: re-amplification + re-shaping.
- 3R: re-amplification + re-shaping + re-timing.

2.3 Receiver side

After propagating over the fiber, an SDM-DE-MUX which tend to disengage propagating modes (sharing the same MCF or FMF) and oriented them to particular SMFs. In principle, SDM-DE-MUX devices or techniques are the same as SDM-MUX but in the inverse sense (known also as fan-out devices).

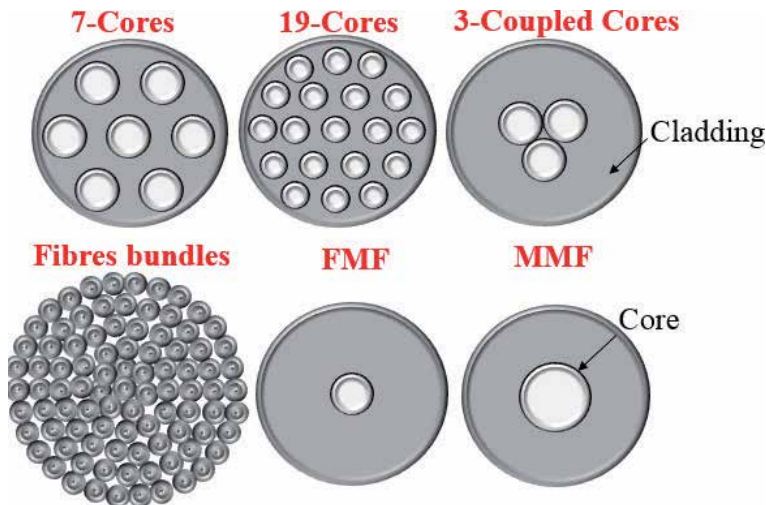


Figure 3.
Several kinds of fibers used for SDM communication system.

After retrieving the optical signal (DE-MUX), optical photodetectors are employed at the end of each SMF_i, aiming to detect each particular mode (data carrier from each SMF_i) and convert the modulated optical signal into an electrical signal. The most commonly used photodetectors are semiconductor photodiodes. Semiconductor based PIN photodiode and the Avalanche photodiode (APDs) are examples of such photodetectors. In principle, the selection of these devices is based on the following requirement: high responsivity, bandwidth, noise characteristics, low cost, and so on [34]. Thereafter, the obtained electrical signals are converted to digital ones using electrical-to-digital converters (ADCs). At the end, a MIMO DSP block is used to mitigate the crosstalk effects on different mode channels. The digital signal undergoes a normalizing/resampling and symbol synchronizing operations. Then, the obtained signals are equalized using adaptive time-domain equalization (TDE) or frequency-domain equalization (FDE). MIMO DSP are composed of equalizers (i.e. FIR filters) of coefficients h_{ij} . The number of these equalizers is related to the number of the square of the transmitted modes ($N \times N$), the length of the transmission link, and the difference between modes delays [35, 36].

3. OAM-SDM system over fibers: potential and challenges

This section highlights the potential of carrying data on OAM modes and multiplexing, transmitting them over SDM fibers & de-multiplexing them. This technology is known as OAM-SDM technology. Intuitively, Incorporating OAM modes as data carriers has shown great potential in ameliorating the performances of SDM communication system. We focus on these OAM modes, what are they? How to generate and detect these kind of modes? What are the appropriate fibers that robustly support these modes? Moreover, what are the main challenges facing this technology?

3.1 OAM beams

It is well known that an electromagnetic beam (light) possess angular momentum (AM), meaning that it can rotate around the propagation direction. Light possess a total AM of $(l + s) \cdot \hbar$ per photon, where $l\hbar$ corresponds to the orbital angular momentum (OAM) and $s\hbar$ is the spin angular momentum (SAM) (see **Figure 4a**). The orbital angular momentum (OAM) beam, depends on the field spatial distribution, characterized by a helical phase front of $\exp(il\phi)$, where l denotes the topological charge number, which is an arbitrary integer ranging from $-\infty$ to $+\infty$. ϕ is the azimuthal angle, and \hbar is the reduced Planck constant ($=1.055 \times 10^{-34}$ J s). The limitlessness of the topological charge number l indicates the unbounded states that can be modulated with OAM. In addition, two OAM lights with different l charge number are orthogonal. A series of wave fronts for various OAM modes are depicted in **Figure 4b**.

The sign of l denotes the handedness of the spiral. A clockwise rotation can be assigned to a positive l and an anticlockwise rotation to a negative l . On the other hand, the spin angular momentum (SAM) of light is related to the circular polarization state. The beam can only have bounded orthogonal states: $S = \pm 1$, which correspond to left or right circular polarization respectively. Intermediate values denote elliptical polarization. Benefiting by that inherent features (orthogonality & unbounded states), potential applications in diverse areas has exploited the OAM of light, including, but not limited to, optical trapping, tweezers, metrology, microscopy, imaging, optical speckle, astronomy, quantum entanglement, manipulation, and remote sensing (**Figure 5**) [13, 37–51]. As recent trend, Orbital

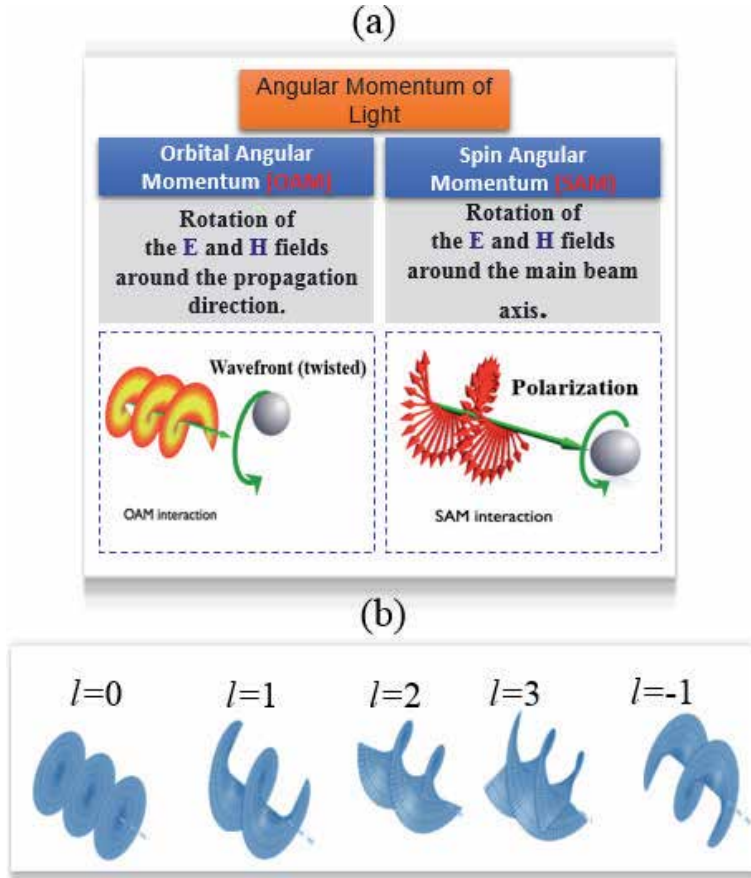


Figure 4.
(a) The OAM and the SAM of an electromagnetic beam. (b) Helical wave fronts for a set of orbital angular momentum modes.

angular momentum (OAM) has gained a widespread interest in the area of optical telecommunication due to its capability to elevate the transmission capacity and substantially improve the spectral efficiency (OAM could offer unlimited channels for data transmission) of optical communication in both free space and fiber optics links. Many families of light beams can carry orbital angular momentum including Laguerre-Gaussian beams (LGB) [52], Bessel beams [53], Bessel-Gaussian beams (BGB) [54], Hermite-Gaussian beams (HGB) [55], Mathieu beams [56], Ince-Gaussian beams [57], and vector vortex beams [58].

3.2 Devices and components for OAM-SDM over fibers

In the original and the first experiment from Allen et al. in 1992 [52], helically phased LG beam was generated from Hermite-Gaussian (HG) beams. The transformation has been based on cylindrical lens (CL). The advantage of CL is its high conversion efficiency and the high purity of generated OAM. However, CL requires high construction precision. Indeed, it has poor flexibility because it requires a very precise incident field angle.

Other obvious way to implement OAM beams is to use a spiral phase plate (SPP) [59–64]. In principle, when a Gaussian light beam passes through the phase plate, the beam experiences a different phase in the azimuth direction due to the spiral

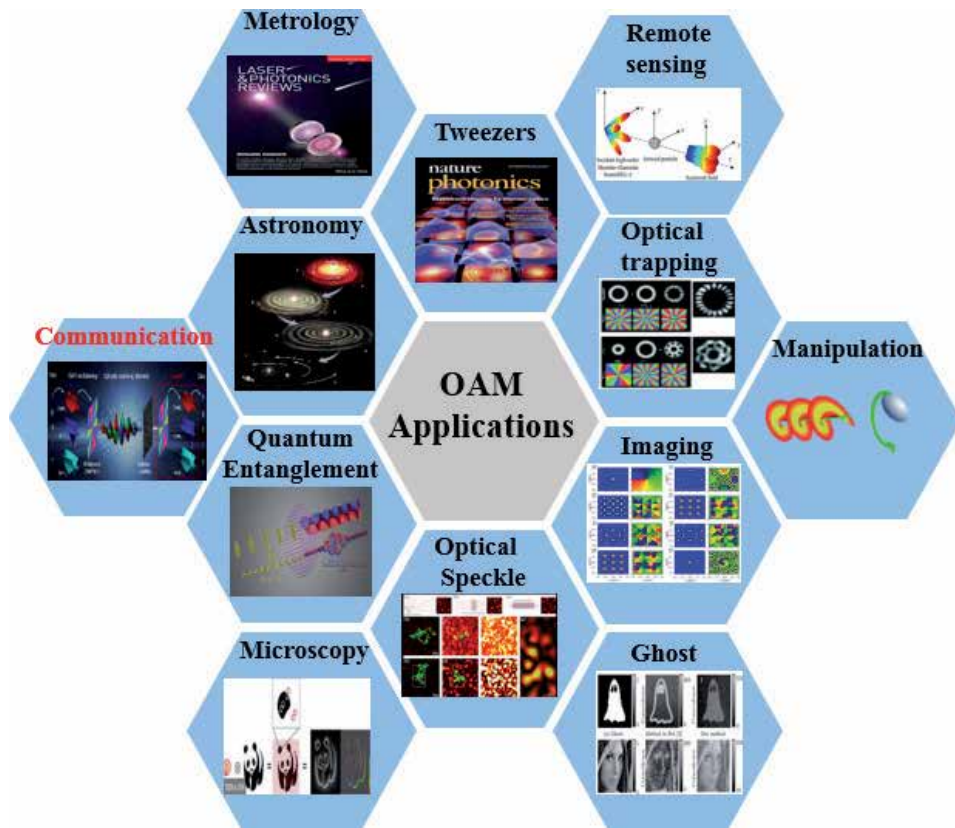


Figure 5.
 Different applications of OAM.

thickness of the phase plate and is converted into a helically phased beam with topological charge l . The advantage of SPP is that is very efficient, and allows the conversion of beams with relatively high power. However, since it is wavelength dependent, it needs extreme precision in manufacturing: different plate is needed for each kind of OAM mode (each l). Recent trend is the proposed adjustable spiral phase plate in [64]. Some diffractive optical devices or elements can be explored targeting to generate OAM light beams [65, 66]. Among these devices, fork grating are used for generating twisted light (holographic gratings). Fortunately, thanks to fork grating, we can generate multiple topological charges (different OAM beams) simultaneously (i.e. using vertical and horizontal superimposed fork gratings). However, this element seems to be inefficient and a variation of this technique has been proposed to improve its efficiency, using forked polarization grating [66]. Metamaterials (complex artificial materials) is another strategy that can make transformations in optical space [67, 68]. OAM modes are obtained by controlling the geometrical parameters (shape, size, direction, etc.) of the metamaterial to manipulate the phases of different azimuths and change the spatial phase of the incident light. A liquid crystal panel, q-plates is another promising and efficient way to generate twisted beams [69–71]. A light beam incident on q plate is modified to have a topological charge variation.

At last, one of the most convenient method to generate OAM beams is the use of spatial light modulator (SLM) [63, 72–74]. Made of liquid crystals, SLM is a programmable device that uses a computer [63]. It is composed of a matrix of pixels, and each pixel can be programmed to generate a given phase (there also exists SLMs

that act on amplitude instead of phase). By modulating the phases of Gaussian beams, we can generate a wide range of OAM modes. SLM is a versatile component, it can be reconfigured as needed. It is even possible to send different beams on different sections of the SLM, to generate several beams simultaneously. On the other hand, due to its polarization dependent, SLM accepts only limited power. Another method to generate OAM light beams, is possible to use optical fiber. Acting as a mode selector [75] or a mode converter [76, 77], optical fiber seems to be useful in OAM mode generation. Fiber coupler [78], mechanical grating [79, 80], tilted optical grating [81], helical grating [82], multicore fibers [83–86] and liquid core optical fiber [87] are example of such method. **Figure 6** presents the most of examples of OAM generation devices & schemes.

OAM beam is doughnut shaped (never has intensity at its center). This characteristic is not sufficient to identify OAM beams and their topological charge. At the receiver of a communication system, the different OAM modes can be separated easily by exploiting the orthogonality of the helical phase fronts. A variety of methods for detecting OAM has been proposed for light. In principle, the detection operation can be performed using several techniques including those used for the generation: The operation of OAM beams detection is similar to the generation but in the inverse sens (inverse SPP [88], holographic grating [51, 89]). A common way to identify OAM is to interfere (interference method) the incident beam with a Gaussian beam, and to visualize the resulting interference pattern on a camera. Two cases are resulted: If the incident beam is Gaussian, the interference pattern

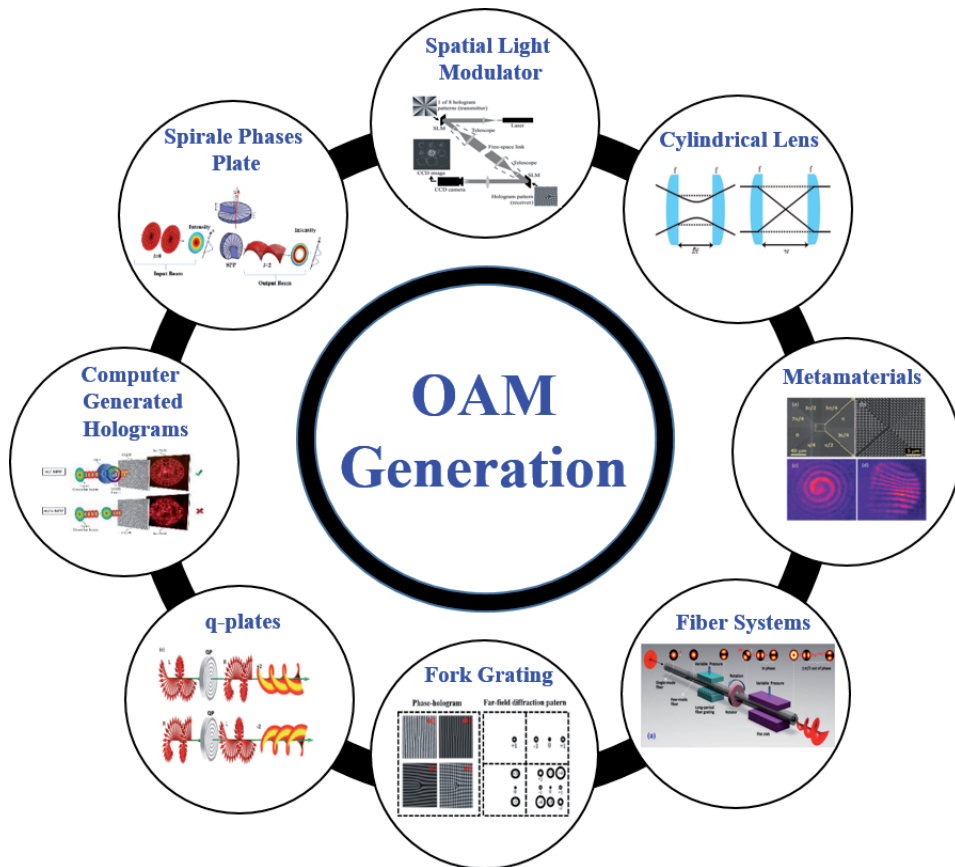


Figure 6.
OAM generation devices & components & schemes.

will look like a series of concentric circles. If the incident beam has a helical phase front, the interference pattern will be a spiral. Then, the number of arms and the direction of the spiral indicate the topological charge and the sign of l respectively. This technique is useful to validate the presence of OAM beam but it cannot be used for demultiplexing. Another efficient way, using a phase pattern or a fork grating on a glass plate or a SLM, to convert the incident beam back to Gaussian. A mode sorter was proposed to identify OAM modes, where the lateral position of the resulting beam tells the topological charge of the incident beam [90–92]. Recently, machine-learning-based approaches (ML) have been implemented in order to accurately identify OAM modes, after their propagation in free space [93, 94]. ML offer great potential in mode detection even after propagation in a turbulent medium. Many other OAM mode detection techniques are reviewed in [95, 96].

3.3 OAM-SDM-fibers: potentials and challenges

The utilization of OAM modes in optical fiber was a challenge to the optical communication community. This subsection focus on standard/special optical fibers designs that have been recently proposed investigated and incorporated in an OAM-SDM system. We start by the main designs and achievements and we will identify the main challenges that are facing this technology.

3.3.1 OAM-SDM-fibers: potentials

Aiming to guide robust OAM modes over an optical fiber, scientists have oriented to special fiber design (i.e. novel refractive index profiles). In principle, these OAM-fibers share common three criteria:

- The refractive index profile should be ring (i.e. match the ring shape of OAM modes).
- The refractive indexes between core and cladding should be high (i.e. enhance the separation between channels).
- The interface between core and the cladding should be smooth (i.e. graded index profile is preferred).

Following these recommendations, various kinds of OAM-fibers have been proposed, characterized and prototyped showing potential achievements in term of capacity transmission and spectral efficiency. Moreover, the standard existing fibers have been investigating in term of their appropriateness to support OAM modes.

The investigation of already existing fibers in OAM context has been carried out by performing a comprehensive analysis of OAM modes in the standard graded index (GIF) multimode fiber (i.e. OM3) in [97]. The refractive index of GIF is shown in **Figure 6a**. Eventhough, the standard step index fiber (e.g. ITU-TG.652) is usually used as a single mode fiber (SIF); it is investigated as an OAM fiber by the utilization of small wavelengths (i.e. visible bands) which tend to change the former fiber to a few mode fiber (**Figure 6b**) [98]. Since then, the transmission of four-OAM mode groups over OM3 MMF, the transmission of OAM modes over OM4 (8.8 km) [99], the transmission of four OAM over 5 km FMF (i.e. 4×20 Gbits/s QPSK data) [100], the high purity OAM modes ($\geq 99.9\%$) over graded index FMF [101], and the viability of 12-OAM-GI-FMF for short/medium haul interconnect [102], have been demonstrated.

Considering the above design guidelines, specialty fibers have shown their capability to handle OAM modes. At the beginning, Ramachandran group has demonstrated the multiplexing/transmission and demultiplexing of OAM modes over a special vortex fiber [80]. The transmission of OAM modes over more than 20 m-VF [16] and 1 km-VF [103], have been demonstrated. Due to the high contrast between the air and the glass (SiO_2) in term of refractive indexes, air core fibers (ACF) have been proposed, designed and prototyped (**Figure 6c**). An ACF supports 12 OAM modes over 2 m has been demonstrated in [104]. Two OAM modes supporting by an ACF was successfully transmitted over 1 km [105]. Another ACF fiber has been characterized in COPL at LAVAL University. This ACF supports 36 OAM states [106]. A capacity transmission of 10.56 Tbit/s has been demonstrated over an ACF using 12 OAM modes using WDM technology (OAM-SDM-WDM) [107]. Recently, over the O, E, S, C, and L bands, an ACF made by air, As_2S_3 and SiO_2 as material for the inner core, for the outer core and for the cladding, respectively, has been designed to support more than 1000 OAM modes [55, 108].

Ring core fibers RCF (**Figure 7d**) are another family of OAM specialty fibers that have been extensively investigated. COPL team has manufactured a family of RCFs suitable for OAM modes [109]. The transmission of two OAM mode-group has been demonstrated over a 50 km RCF [110]. Other RCF with smoothed refractive index at the interface between the core and the cladding, known as GIRCF, have been designed (**Figure 7e**). A GIRCF supporting 22 OAM modes over 10 km has been demonstrated [111]. An aggregate transmission capacity of 5.12 Tbits/s and a spectral efficiency of 9 bit/s/Hz have been reported in [112]. Over 12 km GIRCF, the transmission of two OAM modes each has 12 Gbaud (8QAM) and with 112 WDM channels has been demonstrated in [113]. Hence, a transmission capacity of 8.4 Tbits/s has been reported.

Other family of hybrid refractive index structure (i.e. inner core is graded while the outer core is step) have been proposed for OAM modes. Inverse parabolic graded

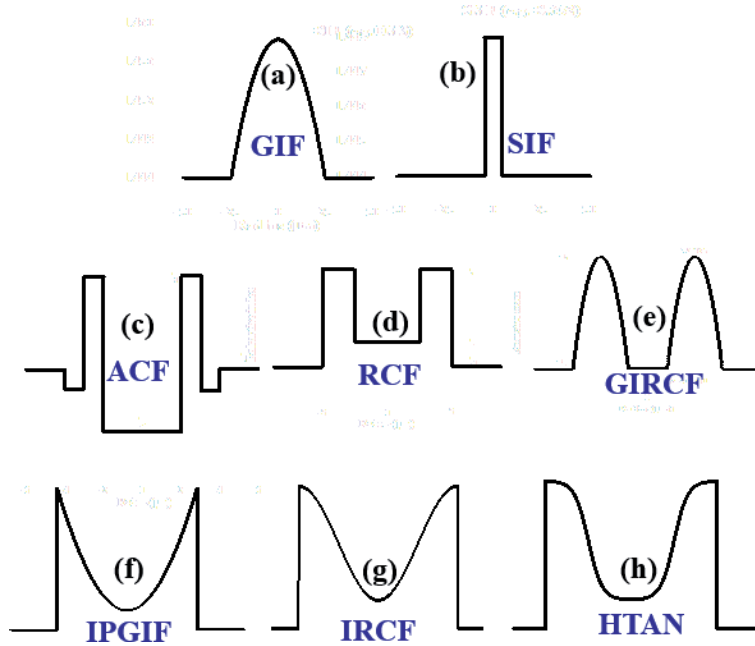


Figure 7. Various kinds of fibers that have been used in OAM-SDM systems: (a) graded index fiber, (b) step index fiber, (c) air core fiber, (d) ring core fiber, (e) graded index ring core fiber, (f) inverse parabolic graded index fiber, (g) inverse raised cosine fiber, (h) hyperbolic tangent fiber.

index fiber (IPGIF) has been designed and demonstrated experimentally (**Figure 7f**) [114]. As a first experiment, the use of IPGIF as OAM-fiber was successfully demonstrated based on the transmission of two OAM modes over 1 km. as a second step, 3.36 Tbits/s has been achieved over a IPGIF of 10 m. In that experiment, 15 wavelengths (WDM) and 4 OAM modes have been utilized [115]. In [116], we proposed inverse raised cosine fiber IRCF (**Figure 7g**) for supporting moderate and robust OAM modes. The new fiber proved the support of high pure OAM modes. Recently, we demonstrated the tolerance of IRCF in bend condition. Other usual function has been incorporated as a refractive index profile, which is the hyperbolic tangent function (HTAN). The designed fiber (**Figure 7h**) supports high pure OAM modes, with high separation among them (low crosstalk). The fiber is resilient to bending, and characterized by low chromatic dispersion and low differential group delay [117]. Recently, we designed an inverse-HTAN-MMF supporting very large number of OAM mode group (14 MG) that outperforms those supported by OM3 [118]. We designed another OAM-FMF based inverse Gaussian (IG) function. The designed IGF is favorable to transmit OAM modes in next generation OAM-MDM multiplexing optical networks [119].

The transmission of OAM modes over MCFs has been demonstrated with the aim of further increasing the capacity of an SDM links (i.e. improve the available data channels). A 7-RCF (MOMRF) has been proposed to support 22×7 modes (i.e. 154 channels) [120]. Low-level crosstalk (-30 dB) has been demonstrated over 100 km long MOMRF. A trenched multi OAM ring fiber (TA-MOMRF) has been reported in [121] showing Pbit/s as transmission capacity and hundreds bit/s/Hz as spectral efficiency. Later on, a coupled multi core fiber has been proposed in [122]. The investigated supermode fiber featured low crosstalk, low nonlinearity effects and low modal loss.

3.3.2 OAM-SDM-fibers: challenges

OAM-SDM over fibers is facing several key challenges and impediments that may curbs/slow down the transition from design process to prototyping operation and then to commercialization and standardization in the market.

Mode coupling issues are the most threads that degrade the OAM-SDM system performances. Mode coupling is the physical cause of data-channels crosstalk. Keeping these modes well separated during propagation along the fiber is a challenge in order to realize a robust OAM-SDM system and avoid the employment of additional MIMO-DSP module at the receiving stage. Even by using OAM-specialty fibers that ideally tend to appropriately support the OAM channels, there are almost some perturbations and impediments along the fiber section. These perturbations include macro & micro bending, twisting, birefringence, and core ellipticity. These imperfections may cause a mode coupling. Various linear and nonlinear effects in optical fiber could be detrimental for long distance SDM systems. Concerning linear effects, material absorption cause attenuation of optical signal (i.e. power loss). Other linear effects are the effects of dispersions during propagation. Chromatic dispersion is caused by the fact that the phase velocity and the group velocity are depending on the optical frequency. Polarization mode dispersions (PMD) are occurred because of dependency between the phase velocity of propagating mode and the polarization state. Intermodal dispersion is due to the dependency between the phase velocity and the optical mode.

On the other side, due to the intensity dependence of refractive index of optical fiber, and inelastic scattering phenomenon, different kind of nonlinearity effects can occur in optical fibers. This power material-light dependency is responsible for the Kerr-effect. Several effects are manifestations of Kerr nonlinearity. Four wave

mixing (parametric interaction among waves satisfying phases matching) arise when light components with different optical frequencies overlap in optical fiber. Stimulated Raman Scattering (SRS) is a nonlinear process that correspond to interaction between optical signals and molecular vibration in the glass-fiber (optical phonons). At last, stimulated Brillouin scattering (SBS) is very similar to Raman scattering that is correspond to interaction between optical signal and the acoustic vibration in the fiber (acoustic phonons).

4. Perspectives and future research orientations

Around a decade since the first OAM-SDM fiber, the ability of this technology has proven very fruitful in improving the optical communication networks in term of capacity, and spectral efficiency over long distances. However, it is still represent a young area of research and study that has a rich set of issues, challenges and opportunities to explore and to check it in the three regions of a communication link (emission, transmission, and reception). Starting by the emission side, important research directions are to find new materials and structures aiming to effectively generate OAM beams. These desired generation techniques or devices should feature favorable performances including low cost, high compactness, small size, high conversion efficiency, and compatibility with existing technologies. In addition, it would be important to give a significant interest in miniaturizing the devices and components at the emitter side (e.g. bringing OAM to the chip level in photonic circuits): Integrated on-chip devices on different platforms (e.g., silicon platform) could be viable candidates in next generation OAM SDM system. This helps OAM beams to be encoded & generated fast, switched freely and detected in real time. Various integrated version of devices could be widely adopted: integrated information encoders, integrated OAM modes emitters, and integrated OAM multiplexers. In spite of the price to be paid in term of cost, the development of such devices will be empowered by the rapid progress in micro and nano-fabrication technologies.

Considering optical fiber transmission phase, the perfect refractive index profile for OAM fiber is an open subject for everyone in optical communication. So far, it is unclear which kind of fiber provides the best performance in MDM, but evidently, there is no ideal OAM fiber design even if we either follow some design recommendations concluded from former proposed fibers (Section 3.3.1) or consider common electromagnetic rules. Certainly, each fiber has its pros and cons, but it is always a tradeoff between fiber key design parameters aiming to increase the number of supported modes, the separation among their refractive indexes, their purity, and their stability during transmission. Innovative designs with the former performances metrics would be an interesting direction of research. The desired designs will be motivated by the extended and the improvement of MOCVD process to support the manufacture of complex structure fibers with high refractive index contrast. Therefore, further efforts should be dedicated to develop new amplifiers. With the aim of further increasing the transmission capacity over long-haul optical fiber transmission systems, future R&D trends at the receiver side of SDM will be based on the implementation of practical coherent optical communication schemes (coherent receivers) followed, if necessary, by advanced digital signal processing (DSP) techniques. It would be valuable in next generation OAM-SDM systems to explore techniques aiming to compensate both linear & nonlinear impairments (the compensation of nonlinear impairments is an interesting research area for coherent optical communications).

In addition, machine and Deep learning (ML & DL) have risen forefront in many fields. The use of ML or DL could touch various aspects from OAM-SDM

systems including nonlinearity mitigation, optical performance monitoring (OPM), carrier recovery, in-band optical signal-to-noise ratio (OSNR) estimation and modulation format classification, and especially, advanced DSP. Hence, a full smart optical communication networks.

5. Conclusions

Multiplexing spatial modes (SDM) seems to be viable solution to cope with the upcoming capacity crunch. In this chapter, we attempted to focus on the different aspects from an SDM system (emission, transmission and reception) over optical fibers aiming to highlight their main key elements and components that allow this technology to be the desired one for next generation local/global optical communication systems/networks. We focused on the last trend of SDM communication research direction: OAM-SDM over optical fibers. We discussed the OAM modes and the main devices & schemes for the generation & detection and the transmission of them. OAM specialty fibers are highlighted with focus on, their key features, their main achievements (throughput & main contributions) and main challenges that face their progress. Perspectives and future research orientations that may touching SDM systems have been presented at the end of this chapter. From what we have attempted to present, SDM still unexhausted research area that optical communication R&D community have to derive/touch future research directions in the field.

Author details


Alaaeddine Rjeb^{1*}, Habib Fathallah² and Mohsen Machhout¹

¹ Faculty of Sciences of Monastir, Laboratory of Electronic and Microelectronic, Physics Department, University of Monastir, Monastir, Tunisia

² Faculty of Sciences of Bizerte, Laboratory of Artificial Intelligence and Data Engineering Applications, Computer Department, University of Carthage, Bizerte, Tunisia

*Address all correspondence to: alaaeddine.rjeb@gmail.com

IntechOpen

© 2022 The Author(s). Licensee IntechOpen. This chapter is distributed under the terms of the Creative Commons Attribution License (<http://creativecommons.org/licenses/by/3.0>), which permits unrestricted use, distribution, and reproduction in any medium, provided the original work is properly cited. 

References

- [1] Cisco VNI Global IP traffic forecast “2018-2023”
- [2] Chralyvy A. Plenary paper: The coming capacity crunch. In: 2009 35th European Conference on Optical Communication. Austria: Center Vienna, Austria: IEEE; 2009. pp. 1-1
- [3] Essiambre R, Tkach R. Capacity trends and limits of optical communication networks. *Proceedings of the IEEE*. 2012; **100**(5):1035-1055
- [4] Saridis GM, Alexandropoulos D, Zervas G, Simeonidou D. Survey and evaluation of space division multiplexing: From technologies to optical networks. *IEEE Communications Surveys & Tutorials*. 2015; **17**(4):2136-2156
- [5] Winzer PJ. Optical networking beyond WDM. *IEEE Photonics Journal*. 2012; **4**(2):647-651
- [6] Richardson DJ. Filling the light pipe. *Science*. 2010; **330**(6002):327-328
- [7] Richardson DJ, Fini JM, Nelson LE. Space-division multiplexing in optical fibres. *Nature Photonics*. 2013; **7**(5): 354-362
- [8] Saitoh K, Matsuo S. Multicore fiber technology. *Journal of Lightwave Technology*. 2016; **34**(1):55-66
- [9] Sumitomo Electric [Online]. Available from: <http://www.sumitomoelectric.com/>
- [10] Yaman F, Bai N, Zhu B, Wang T, Li G. Long distance transmission in few-mode fibers. *Optics Express*. 2010; **18**(12):13250-13257
- [11] Papapavlou, Charalampos, Paximadis K, Tzimas G. Progress and demonstrations on space division multiplexing. In: 2020 11th International Conference on Information, Intelligence, Systems and Applications (IISA). IEEE; 2020. pp. 1-8
- [12] Willner AE, Liu C. Perspective on using multiple orbital-angular-momentum beams for enhanced capacity in free-space optical communication links. *Nano*. 2021; **10**(1):225-233
- [13] Yao AM, Padgett MJ. Orbital angular momentum: Origins, behavior and applications. *Advances in Optics and Photonics*. 2011; **3**(2):161-204
- [14] Rusch LA, Rad M, Allahverdyan K, Fazal I, Bernier E. Carrying data on the orbital angular momentum of light. *IEEE Communications Magazine*. 2018; **56**(2):219-224
- [15] Brning R, Ndagano B, McLaren M, Schrter S, Kobelke J, Duparr M, et al. Data transmission with twisted light through a free-space to fiber optical communication link. *Journal of Optics*. 2016; **18**:03LT01
- [16] Bozinovic N, Yue Y, Ren Y, Tur M, Kristensen P, Huang H, et al. Terabit-scale orbital angular momentum mode division multiplexing in fibers. *Science*. 2013; **340**(6140):1545-1548
- [17] Yang Z, Yu W, Peng G, Liu Y, Zhang L. Recent progress on novel DSP techniques for mode division multiplexing systems: A review. *Applied Sciences*. 2021; **11**(4):1363
- [18] Brunet C, Rusch LA. Optical fibers for the transmission of orbital angular momentum modes. *Optical Fiber Technology*. 2017; **35**:2-7
- [19] Klinkowski M, Lechowicz P, Walkowiak K. Survey of resource allocation schemes and algorithms in spectrally-spatially flexible optical networking. *Optical Switching and Networking*. 2018; **27**:58-78

- [20] Wartak MS. Computational Photonics: An Introduction with MATLAB. Cambridge University Press; 2013
- [21] Reflex Photonics [Online]. Available from: <http://www.reflexphotonics.com/>
- [22] OFS [Online]. Available from: <http://www.ofsoptics.com>
- [23] Samtec [Online]. Available from: <http://www.samtec.com>
- [24] Hayashi T, Taru T, Shimakawa O, Sasaki T, Sasaoka E. Design and fabrication of ultra-low crosstalk and low-loss multi-core fiber. *Optics Express*. 2011;**19**(17):16576-16592
- [25] Kingsta RM, Selvakumari RS. A review on coupled and uncoupled multicore fibers for future ultra-high capacity optical communication. *Optik*. 2019;**199**:163341
- [26] Ortiz AM, Sáez RL. Multi-core optical fibers: Theory, applications and opportunities. In: *Selected Topics on Optical Fiber Technologies and Applications*. IntechOpen; 2017
- [27] Zhu B, Taunay TF, Fishteyn M, Liu X, Chandrasekhar S, Yan MF, et al. 112-Tb/s space-division multiplexed DWDM transmission with 14-b/s/Hz aggregate spectral efficiency over a 76.8-km seven-core fiber. *Optics Express*. 2011;**19**(17):16665-16671
- [28] Hayashi T, Taru T, Shimakawa O, Sasaki T, Sasaoka E. Low-crosstalk and low-loss multi-core fiber utilizing fiber bend. In: *Optical Fiber Communication Conference/National Fiber Optic Engineers Conference 2011*. OSA Technical Digest (CD). Los Angeles, California United States: Optical Society of America; 2011. paper OWJ3
- [29] Takara H, Sano A, Kobayashi T, Kubota H, Kawakami H, Matsuura A, et al. T. 1.01-Pb/s (12 SDM/222 WDM/456 Gb/s) crosstalk-managed transmission with 91.4-b/s/Hz aggregate spectral efficiency. Presented at the European Conf. Exhibition Optical Communication. Amsterdam, The Netherlands. Paper Th.3.C.1. 2012
- [30] Igarashi K et al. 1.03-Exabit/s-km Super-Nyquist-WDM Transmission over 7,326-km Seven-Core Fiber. *ECOC2013*. PD1.E.3
- [31] Berdague S, Facq P. Mode division multiplexing in optical fibers. *Applied Optics*. 1982;**24**(11):1950-1955
- [32] Ono H, Yamada M, Takenaga K, Matsuo S, Abe Y, Shikama K, et al. Amplification method for crosstalk reduction in a multi-core fibre amplifier. *Electronics Letters*. 2013;**49**(2): 138-140
- [33] Simon, JC, Bramerie L, Ginovart F, Roncin V, Gay M, Fève S, et al. Chares ML. All-optical regeneration techniques. In: *Annales des télécommunications* Vol. 58(11). Springer-Verlag; 2003. pp. 1708-1724
- [34] Miyamoto Y, Takenouchi H. Dense space-division-multiplexing optical communications technology for petabit-per-second class transmission. *NTT Technical Review*. 2014;**12**(12):1-7
- [35] Zhao J, Liu Y, Xu T. Advanced DSP for coherent optical fiber communication. *Applied Sciences*. 2019;**9**(19):4192
- [36] Huang H, Milione G, Lavery MP, Xie G, Ren Y, Cao Y, et al. Mode division multiplexing using an orbital angular momentum mode sorter and MIMO-DSP over a graded-index few-mode optical fibre. *Scientific Reports*. 2015;**5**(1):1-7
- [37] Padgett M. Light's twist. *Proceedings of the Royal Society A: Mathematical, Physical and Engineering Sciences*. 2014;**470**(2172):20140633

- [38] Dennis MR, O'Holleran K, Padgett MJ. Singular optics: Optical vortices and polarization singularities. In: *Progress in Optics*. Vol. 53. Amsterdam: Elsevier; 2009. pp. 293-363. DOI: 10.1016/S0079-6638(08)00205-9
- [39] Ritsch-Marte M. Orbital angular momentum light in microscopy. *Philosophical Transactions of the Royal Society A: Mathematical, Physical and Engineering Sciences*. 2017;**375**(2087): 20150437
- [40] Padgett MJ. Orbital angular momentum 25 years on. *Optics Express*. 2017;**25**(10):11265-11274
- [41] Dholakia K, Čižmár T. Shaping the future of manipulation. *Nature Photonics*. 2011;**5**(6):335
- [42] Paterson L, MacDonald MP, Arlt J, Sibbett W, Bryant PE, Dholakia K. Controlled rotation of optically trapped microscopic particles. *Science*. 2001; **292**(5518):912-914
- [43] Padgett M, Bowman R. Tweezers with a twist. *Nature Photonics*. 2011;**5**(6):343-348
- [44] Simpson NB, Dholakia K, Allen L, Padgett MJ. Mechanical equivalence of spin and orbital angular momentum of light: An optical spanner. *Optics Letters*. 1997;**22**(1):52-54
- [45] Leach J, Dennis MR, Courtial J, Padgett MJ. Knotted threads of darkness. *Nature*. 2004;**432**(7014): 165-165
- [46] Dennis MR, King RP, Jack B, O'Holleran K, Padgett MJ. Isolated optical vortex knots. *Nature Physics*. 2010;**6**(2):118-121
- [47] Lavery MP, Speirits FC, Barnett SM, Padgett MJ. Detection of a spinning object using light's orbital angular momentum. *Science*. 2013;**341**(6145): 537-540
- [48] Giovannini D, Romero J, Potoček V, Ferenczi G, Speirits F, Barnett SM, et al. Spatially structured photons that travel in free space slower than the speed of light. *Science*. 2015;**347**(6224):857-860
- [49] Bernet S, Jesacher A, Fürhapter S, Maurer C, Ritsch-Marte M. Quantitative imaging of complex samples by spiral phase contrast microscopy. *Optics Express*. 2006;**14**(9):3792-3805
- [50] Elias NM. Photon orbital angular momentum in astronomy. *Astronomy & Astrophysics*. 2008;**492**(3):883-922
- [51] Mair A, Vaziri A, Weihs G, Zeilinger A. Entanglement of the orbital angular momentum states of photons. *Nature*. 2001;**412**(6844):313-316
- [52] Allen L, Beijersbergen MW, Spreeuw RJC, Woerdman JP. Orbital angular momentum of light and the transformation of Laguerre–Gaussian laser modes. *Physical Review A*. 1992;**45**:8185-8189
- [53] Gori F, Guattari G, Padovani C. Bessel–Gauss beams. *Optics Communication*. 1987;**64**:491-495
- [54] Ahmed N, Zhao Z, Li L, Huang H, Lavery MP, Liao P, et al. Mode-division-multiplexing of multiple Bessel–Gaussian beams carrying orbital-angular-momentum for obstruction-tolerant free-space optical and millimetre-wave communication links. *Scientific Reports*. 2016;**6**:22082
- [55] Ndagano B, Mphuthi N, Milione G, Forbes A. Comparing mode-crosstalk and mode-dependent loss of laterally displaced orbital angular momentum and Hermite–Gaussian modes for free-space optical communication. *Optics Letters*. 2017;**42**(20):4175-4178
- [56] Gutiérrez-Vega JC, Iturbe-Castillo MD, Chávez-Cerda S.

Alternative formulation for invariant optical fields: Mathieu beams. *Optics Letters*. 2000;**25**:1493-1495

[57] Bandres MA, Gutierrez-Vega JC. Ince-Gaussian beams. *Optics Letters*. 2004;**29**:144-146

[58] Liu J, Chen X, He Y, Lu L, Ye H, Chai G, et al. Generation of arbitrary cylindrical vector vortex beams with cross-polarized modulation. *Results in Physics*. 2020;**19**:103455

[59] Maurer C, Jesacher A, Furhapter S, Bernet S, Ritsch-Marte M. Tailoring of arbitrary optical vector beams. *New Journal of Physics*. 2007;**9**(3):78

[60] Beijersbergen MW, Coerwinkel R, Kristensen M, Woerdman JP. Helical-wavefront laser beams produced with a spiral phaseplate. *Optics Communication*. 1994;**112**:321-327

[61] Massari M, Ruffato G, Gintoli M, Ricci F, Romanato F. Fabrication and characterization of high-quality spiral phase plates for optical applications. *Applied Optics*. 2015;**54**:4077-4083

[62] Turnbull GA, Roberson DA, Smith GM, Allen L, Padgett MJ. Generation of free-space Laguerre-Gaussian modes at millimetre-wave frequencies by use of a spiral phaseplate. *Optics Communication*. 1996;**127**:183-188

[63] Oemrawsingh S, van Houwelingen J, Eliel E, Woerdman JP, Verstegen E, Kloosterboer J, et al. Production and characterization of spiral phase plates for optical wavelengths. *Applied Optics*. 2004;**43**:688-694

[64] Sueda K, Miyaji G, Miyanaga N, Nakatsuka M. Laguerre-Gaussian beam generated with a multilevel spiral phase plate for high intensity laser pulses. *Optics Express*. 2004;**12**:3548-3553

[65] Harm W, Bernet S, Ritsch-Marte M, Harder I, Lindlein N. Adjustable

diffractive spiral phase plates. *Optics Express*. 2015;**23**(1):413-421

[66] Gibson G, Courtial J, Padgett MJ, Vasnetsov M, Pas'ko V, Barnett SM, et al. Free-space information transfer using light beams carrying orbital angular momentum. *Optics Express*. 2004;**12**(22):5448-5456

[67] Li Y, Kim J, Escuti MJ. Orbital angular momentum generation and mode transformation with high efficiency using forked polarization gratings. *Applied Optics*. 2012;**51**(34): 8236-8245

[68] Zhao Z, Wang J, Li S, Willner AE. Metamaterials-based broadband generation of orbital angular momentum carrying vector beams. *Optics Letters*. 2013;**38**:932-934

[69] Zeng J, Wang X, Sun J, Pandey A, Cartwright AN, Litchinitser NM. Manipulating complex light with metamaterials. *Scientific Reports*. 2013;**3**:2826

[70] Marrucci L, Manzo C, Paparo D. Optical spin-to-orbital angular momentum conversion in inhomogeneous anisotropic media. *Physical Review Letters*. 2006; **96**:163905

[71] Karimi E, Piccirillo B, Nagali E, Marrucci L, Santamato E. Efficient generation and sorting of orbital angular momentum eigenmodes of light by thermally tuned q-plates. *Applied Physics Letters*. 2009; **94**(23):231124

[72] Lazarev G, Hermerschmidt A, Krüger S, Osten S. LCOS spatial light modulators: Trends and applications. In: Osten W, Reingand N, editors. *Optical Imaging and Metrology: Advanced Technologies*, chap. 1. Wiley-Blackwell; 2012. pp. 1-29

[73] Heckenberg NR, McDuff R, Smith CP, White A. Generation of

- optical phase singularities by computer-generated holograms. *Optics Letters*. 1992;**17**:221-223
- [74] Ohtake Y, Ando T, Fukuchi N, Matsumoto N, Ito H, Hara T. Universal generation of higher-order multi ringed Laguerre-Gaussian beams by using a spatial light modulator. *Optics Letters*. 2007;**32**:1411-1413
- [75] Cai X, Wang J, Strain MJ, Morris BJ, Zhu J, et al. Integrated compact optical vortex beam emitters. *Science*. 2012; **338**:363-366
- [76] Volpe G, Petrov D. Generation of cylindrical vector beams with few-mode fibers excited by laguerre-gaussian beams. *Optics Communications*. 2004;**237**(1-3):89-95
- [77] Witkowska A, Leon-Saval SG, Pham A, Birks TA. All-fiber lp₁₁ mode converters. *Optics Letters*. 2008;**33**(4): 306-308
- [78] Viswanathan NK, Inavalli VVG. Generation of optical vector beams using a two-mode fiber. *Optics Letters*. 2009;**34**(8):1189-1191
- [79] Kumar R, Mehta DS, Sachdeva A, Garg A, Senthilkumaran P, Shakher C. Generation and detection of optical vortices using all fiber-optic system. *Optics Communications*. 2008;**281**(13):3414-3420
- [80] Ramachandran S, Kristensen P, Yan MF. Generation and propagation of radially polarized beams in optical fibers. *Optics Letters*. 2009;**34**(16): 2525-2527
- [81] Bozinovic N, Golowich S, Kristensen P, Ramachandran S. Control of orbital angular momentum of light with optical fibers. *Optics Letters*. 2012;**37**(13):2451-2453
- [82] Fang L, Jia H, Zhou H, Liu B. Generation of cylindrically symmetric modes and orbital-angular-momentum modes with tilted optical gratings inscribed in high-numerical-aperture fibers. *Journal of the Optical Society of America*. A. 2015;**32**(1):150-155
- [83] Fang L, Wang J. Flexible generation/conversion/exchange of fiber-guided orbital angular momentum modes using helical gratings. *Optics Letters*. 2015;**40**(17):4010-4013
- [84] Yan Y, Wang J, Zhang L, Yang J-Y, Fazal I, Ahmed N, et al. New approach for generating and (de)multiplexing oam modes in a fiber coupler consisting of a central ring and four external cores. In: 2011 37th European Conference and Exhibition on Optical Communication (ECOC). Geneva, Italy; 2011. pp. 1-3
- [85] Yan Y, Wang J, Zhang L, Yang J-Y, Fazal IM, Ahmed N, et al. Fiber coupler for generating orbital angular momentum modes. *Optics Letters*. 2011;**36**(21):4269-4271
- [86] Yan Y, Yang J-Y, Yue Y, Chitgarha MR, Huang H, Ahmed N, et al. High-purity generation and power-efficient multiplexing of optical orbital angular momentum (OAM) modes in a ring fiber for spatial-division multiplexing systems. In: Conference on Lasers and Electro-Optics 2012. San Jose, USA: Optical Society of America; 2012
- [87] Yan Y, Yue Y, Huang H, Yang J-Y, Chitgarha MR, Ahmed N, et al. Efficient generation and multiplexing of optical orbital angular momentum modes in a ring fiber by using multiple coherent inputs. *Optics Letters*. Sep. 2012;**37**(17): 3645-3647
- [88] Gao W, Hu X, Mu C, Sun P. Generation of vector vortex beams with a small core multimode liquid core optical fiber. *Optics Express*. May 2014;**22**(9):11 325-11 330

- [89] Willner AE, Huang H, Yan Y, Ren Y, Ahmed N, Xie G, et al. Optical communications using orbital angular momentum beams. *Advances in Optics Photonics*. 2015;7(1):66-106
- [90] Gao C, Zhang S, Fu S, Wang T. Integrating 5×5 dammann gratings to detect orbital angular momentum states of beams with the range of −24 to +24. *Applied Optics*. 2016;55(7):1514-1517
- [91] Berkhout GC, Lavery MP, Courtial J, Beijersbergen MW, Padgett MJ. Efficient sorting of orbital angular momentum states of light. *Physics Review Letters*. 2010;105(15):153601
- [92] Lavery MPJ, Robertson DJ, Berkhout GCG, Love GD, Padgett MJ, Courtial J. Refractive elements for the measurement of the orbital angular momentum of a single photon. *Optics Express*. 2012;20(3):2110-2115
- [93] Mirhosseini M, Malik M, Shi Z, Boyd RW. Efficient separation of the orbital angular momentum eigenstates of light. *Nature Communications*. 2013;4:2781
- [94] Doster T, Watnik AT. Machine learning approach to OAM beam demultiplexing via convolutional neural networks. *Applied Optics*. 2017;56:3386-3396
- [95] Park SR, Cattell L, Nichols JM, Watnik A, Doster T, Rohde GK. De-multiplexing vortex modes in optical communications using transport-based pattern recognition. *Optics Express*. 2018;26:4004-4022
- [96] Chen R, Zhou H, Moretti M, Wang X, Li J. Orbital angular momentum waves: Generation, detection and emerging applications. *IEEE Communications Surveys & Tutorials*. 2019;22(2):840-868
- [97] Chen S, Wang J. Theoretical analyses on orbital angular momentum modes in conventional graded-index multimode fibre. *Scientific Reports*. 2017;7(1):3990
- [98] Chen S, Wang J. Characterization of red/green/blue orbital angular momentum modes in conventional G. 652 fiber. *IEEE Journal of Quantum Electronics*. 2017;53(4):1-14
- [99] Wang A, Zhu L, Wang L, Ai J, Chen S, Wang J. Directly using 8.8-km conventional multi-mode fiber for 6-mode orbital angular momentum multiplexing transmission. *Optics Express*. 2018;26(8):10038-10047
- [100] Wang A, Zhu L, Chen S, Du C, Mo Q, Wang J. Characterization of LDPC-coded orbital angular momentum modes transmission and multiplexing over a 50-km fiber. *Optics Express*. 2016;24(11):11716-11726
- [101] Zhang Z, Gan J, Heng X, Wu Y, Li Q, Qian Q, et al. Optical fiber design with orbital angular momentum light purity higher than 99.9%. *Optics Express*. 2015;23(23):29331-29341
- [102] Rjeb A, Seleem H, Fathallah H, Machhout M. Design of 12 OAM-Graded index few mode fibers for next generation short haul interconnect transmission. *Optical Fiber Technology*. 2020;55:102148
- [103] Bozinovic N, Ramachandran S, Brodsky M, Kristensen P. Record-length transmission of entangled photons with orbital angular momentum (vortices). In: *Frontiers in Optics*. Rochester, NY: Optical Society of America; 2011. p. PDPB1
- [104] Gregg P, Kristensen P, Golowich S, Olsen J, Steinvurzel P, Ramachandran S. Stable transmission of 12 OAM states in air-core fiber. In: *CLEO*. San Jose, California: Optical Society of America; 2013
- [105] Gregg P, Kristensen P, Ramachandran S. OAM stability in fiber

- due to angular momentum conservation. In: CLEO. San Jose, California: Optical Society of America; 2014. p. 2014
- [106] Brunet C, Vaity P, Messaddeq Y, LaRochelle S, Rusch LA. Design, fabrication and validation of an OAM fiber supporting 36 states. *Optics Express*. 2014;**22**(21):26117-26127
- [107] Ingerslev K, Gregg P, Galili M, Da Ros F, Hu H, Bao F, et al. 12 mode, WDM, MIMO-free orbital angular momentum transmission. *Optics Express*. 2018;**26**:20225-20232
- [108] Wang Y, Bao C, Geng W, Lu Y, Fang Y, Mao B, et al. Air-core ring fiber with >1000 radially fundamental OAM modes across O, E, S, C, and L bands. *IEEE Access*. 2020;**8**:68280-68287
- [109] Brunet C, Ung B, Wang L, Messaddeq Y, LaRochelle S, Rusch LA. Design of a family of ring-core fibres for OAM transmission studies. *Optics Express*. 2015;**23**(8):10553-10563
- [110] Zhang R, Tan H, Zhang J, Shen L, Liu J, Liu Y, et al. A novel ring-core fiber supporting MIMO-free 50 km transmission over high-order OAM modes. In: *Proc. Opt. Fiber Commun. Conf. (OFC)*. California United States: Optical Society of America; 2019. pp. 1-3
- [111] Zhu G, Chen Y, Du C, Zhang Y, Liu J, Yu S. A graded index ring-core fiber supporting 22 OAM states. In: *Opto-Electronics and Communications Conference (OECC) and Photonics Global Conference (PGC)*. Singapore: IEEE; 2017. pp. 1-3
- [112] Zhu G et al. Scalable mode division multiplexed transmission over a 10-km ring-core fiber using high-order orbital angular momentum modes. *Optics Express*. 2018;**26**:594-604
- [113] Zhu L, Zhu G, Wang A, Wang L, Ai J, Chen S, et al. 18 km low-crosstalk OAM+WDM transmission with 224 individual channels enabled by a ring-core fiber with large high-order mode group separation. *Optics Letters*. 2018;**43**(8):1890-1893
- [114] Ung P, Vaity L, Wang Y, Messaddeq LA, LaRochelle RS. Few-mode fiber with inverse-parabolic graded-index profile for transmission of OAM-carrying modes. *Optics Express*. 2014;**22**(15):18044-18055
- [115] Wang X, Yan S, Zhu J, Ou Y, Hu Z, Messaddeq Y, et al. 3.36-tbit/s oam and wavelength multiplexed transmission over an inverse-parabolic graded index fiber. In: *2017 Conference on Lasers and Electro-Optics (CLEO)*. IEEE; 2017. pp. 1-2
- [116] Rjeb A, Guerra G, Issa K, Fathallah H, Chebaane S, Machhout M, et al. *Optics Communications*. 2020; **458**:124736
- [117] Rjeb A, Fathallah H, Khaled I, Machhout M, Alshebeili SA. A novel hyperbolic tangent profile for optical fiber for next generation OAM-MDM systems. *IEEE Access*. 2020; **8**:226737-226753
- [118] Rjeb A, Seleem H, Fathallah H, Machhout M. A novel inverse gaussian profile for orbital angular momentum mode division multiplexing optical networks. In: *2021 18th International Multi-Conference on Systems, Signals & Devices (SSD)*. Monastir, Tunisia: IEEE; 2021. pp. 480-487
- [119] Rjeb A, Fathallah H, Issa K, Machhout M, Alshebeili SA. Inverse hyperbolic tangent fiber for OAM mode/mode-group division multiplexing optical networks. *IEEE Journal of Quantum Electronics*. 2021;**57**(4):1-12. DOI: 10.1109/JQE.2021.3090993.
- [120] Li S, Wang J. Multi-orbital-angular-momentum multi-ring fiber for high-density space-division

multiplexing. IEEE Photonics Journal.
2013;5(5):7101007-7101007

[121] Li S, Wang J. A compact trench-assisted multi-orbital-angular-momentum multi-ring fiber for ultrahigh-density space-division multiplexing (19 rings \times 22 modes). Scientific Reports. 2014;4:3853

[122] Li S, Wang J. Supermode fiber for orbital angular momentum (OAM) transmission. Optics Express. 2015;23:18736-18745

Triple-Hop Hybrid FSO/mmW Based Backhaul Communication System for Wireless Networks Applications of 5G and beyond

*Mogadala Vinod Kumar, Yenneti Laxmi Lavanya,
Bharati Bidikar and Gottapu Sasibhushana Rao*

Abstract

Wireless networks applications of 5G and beyond require high throughput and high capacity. To achieve this, a macro cell is split into several small cells. When using Free Space Optics (FSO) some of the small cell base stations (BSs) which are located at the edges of a macro cell may not directly communicate with the base station of that macro cell, resulting in high outage probability (OP) and average bit error rate (ABER). Therefore, there is a need to develop a new system model to improve the OP and ABER performance. For such scenarios, triple-hop (TH) hybrid free space optics/millimeter wave (FSO/mmW) system has been proposed by considering neighboring small cell BSs as intermediate relays to forward the backhaul data. The OP and ABER of the proposed TH hybrid FSO/mmW system are derived for various channel conditions and are further verified by performing Monte-Carlo simulations. In this work, FSO link is modeled by Gamma-Gamma distribution over weak and strong turbulence channel conditions. Further the mmW link is modeled by using Nakagami-m distribution which perfectly models various fading scenarios.

Keywords: free space optics, millimeter waves, triple-hop, outage probability, average bit error rate, gamma-gamma, Nakagami-m

1. Introduction

Mobile cellular traffic has astoundingly increased during the last decade mainly due to the stunning expansion of smart wireless devices and bandwidth demanding applications (i.e., high-definition videos, gaming, social networking, etc.). The overall mobile data traffic is expected to grow up to 77 Exabyte's per month by 2022 which is about a seven-fold increase over 2017 data traffic [1]. In addition, the number of devices and connections will continue to grow exponentially. The fifth generation (5G) networks are aimed at meeting the requirements of mobile communications even beyond 2025. Current backhaul communication of cellular networks uses licensed microwave spectrum and wired copper/fiber based links. These two systems have several limitations (e.g., low data rates, security issues, and high cost of installation in urban canyons). Choosing a suitable technology in the design of the backhaul

network architecture plays a vital role in the performance of the next generation cellular networks [2]. Wireless free-space optics (FSO) and unlicensed millimeter wave (mmW) communications are being considered as the major technologies for high data rate backhaul traffic of next generation wireless networks of 5G and beyond [3]. Millimeter wave communications can achieve data rates up to 10 Gbits/s. This is because there is a large amount of bandwidth available in the mmW band (30–300 GHz), and allocating this bandwidth is an efficient approach to enhance system capacity. FSO is a line-of-sight (LOS) technology that uses light emitting diodes (LEDs) or laser to transmit information through free space medium. FSO communication has attracted significant attention due to its unlimited bandwidth, as it operates in the unlicensed Tera Hertz spectrum band [4]. However, both the FSO and mmW links are affected by different weather conditions but are complementary in nature. Therefore, hybrid system comprising of FSO/mmW communication has the advantages of both the systems and overcomes the limitations of individual systems.

In wireless networks of 5G and beyond, a given macro cell will be covered by several small cells. In such cases, some of the small cell BSs which are located at the edges of that macro cell may not be able to communicate directly with it. Hence, there is a necessity of developing a cellular system that will be based on complex interactions between small cell base stations (SBSs) and cooperation between them is necessary in order to improve the overall performance (network coverage, reduced outage probability, spectral and power efficiency) of the system. For such scenarios, triple-hop (TH) hybrid FSO/mmW system has been proposed by considering neighboring small cell BSs as intermediate relays to forward the backhaul data. This chapter mainly focuses on the performance analysis of the proposed triple-hop hybrid FSO/mmW system, which improves the reliability and coverage between SBSs and macro cell BSs over weak and strong turbulence channel conditions. This chapter is organized as follows: Section 2 introduces the proposed system model and statistical characteristics of the system is presented in Section 3. The performance analysis of the proposed system over weak and strong turbulence channel conditions is discussed in Section 4. Section 5 presents the results and discussion, and finally conclusions are presented in Section 6.

2. Proposed system and channel models

To improve the communication between a macro cell BS and small cell BS, a decode and forward (DF) relaying based triple-hop system is proposed by considering intermediate small cell BSs as relay nodes. In this, the first relay (R_1) BS will decode the received signal from the source (S) BS and then forward it to the second relay (R_2) BS. The second relay BS decodes and forwards the received signal from first relay BS to the destination (D) BS. The proposed DF relaying based triple-hop system comprising of source (S) BS, destination (D) BS, and two relay base stations (R_1 , R_2) is shown in **Figure 1**. The FSO system communicates by using intensity modulation at the transmitter and direct detection scheme (IM/DD) at the receiver [5].

2.1 Modeling of received FSO signals at different BSs

Mathematical formulation of the received signals for FSO and mmW links at R_1 , R_2 , and D base stations are presented in this section. In the case of FSO transmission, the signal received at base station R_1 from base station S is given by

$$y_{SR_1}^{FSO} = c_{SR_1} I_{SR_1} g_{SR_1} x + n_{SR_1} \quad (1)$$

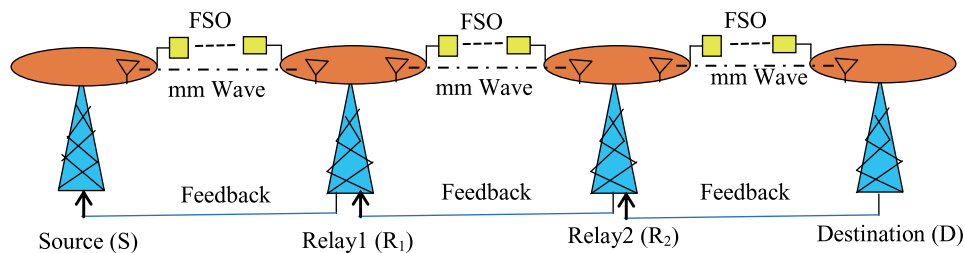


Figure 1.
Schematic of proposed triple-hop hybrid FSO/mmW system.

The signal received at base station R_1 is decoded and forwarded to base station R_2 and the signal received at base station R_2 is given by

$$y_{R_1R_2}^{FSO} = c_{R_1R_2} I_{R_1R_2} g_{R_1R_2} \tilde{x} + n_{R_1R_2} \quad (2)$$

The signal received at base station R_2 is decoded and forwarded to base station D and the signal received at base station D is given by

$$y_{R_2D}^{FSO} = c_{R_2D} I_{R_2D} g_{R_2D} \hat{x} + n_{R_2D} \quad (3)$$

where suffix SR_1 , R_1R_2 , and R_2D are source to relay1, relay1 to relay2, and relay2 to destination respectively, x is the symbol transmitted by source BS with average energy E_s , \tilde{x} is the estimate of x at R_1 , \hat{x} is the estimate of \tilde{x} at R_2 , c_j is the receiver's optical-to-electrical conversion coefficient, g_j is the average gain of the j^{th} FSO link, I_j represents the optical channel fading due to atmospheric turbulence of j^{th} link which is modeled using Gamma-Gamma distribution [6], n_j is the zero-mean circularly symmetric complex Gaussian noise of j^{th} link, where $E\{n_j n_j^*\} = \sigma_n^2$, and $j \in \{SR_1, R_1R_2, R_2D\}$. The instantaneous electrical SNR at the output of the FSO receiver denoted by γ_j^{FSO} is given as [7].

$$\gamma_j^{FSO} = \bar{\gamma}_j^{FSO} I_j^2 \quad (4)$$

where $\bar{\gamma}_j^{FSO}$ is the average SNR. By assuming perfect alignment between FSO transmitter and receiver apertures, the fading channel coefficient (I_j) probability density function (PDF) can be written as

$$f_{I_j}^{GG}(I_j) = \frac{2(\alpha\beta)^{\frac{\alpha+\beta}{2}}}{\Gamma(\alpha)\Gamma(\beta)} I_j^{\frac{\alpha+\beta}{2}-1} K_{\alpha-\beta}\left(2\sqrt{\alpha\beta I_j}\right), \quad I \geq 0 \quad (5)$$

where α and β are the small scale and large scale parameters of the scattering environment, $\Gamma(\cdot)$ is the gamma function [8], and $K_a(\cdot)$ is the modified Bessel function of the second kind of order a . The expression for the PDF of instantaneous SNR of FSO link can be obtained from Eqs. (4) and (5) as

$$f_{\gamma_j^{FSO}}^{GG}(\gamma) = \frac{\left(\frac{\alpha\beta}{\sqrt{\gamma_j^{FSO}}}\right)^{\frac{\alpha+\beta}{2}} (\gamma)^{\frac{\alpha+\beta}{4}-1}}{\Gamma(\alpha)\Gamma(\beta)} K_{\alpha-\beta}\left(2\sqrt{\frac{\alpha\beta}{\sqrt{\gamma_j^{FSO}}}(\gamma)^{\frac{1}{2}}}\right) \text{ for } \gamma \geq 0 \quad (6)$$

The above PDF expression of γ_j^{FSO} can be expressed in terms of Meijer G-function G (.) as [9].

$$f_{\gamma_j^{FSO}}^{GG}(\gamma) = P_1(\gamma)^{-1} G_{0,2}^{2,0} \left(\frac{\alpha\beta(\gamma)^{\frac{1}{2}}}{\sqrt{\gamma_j^{FSO}}} \middle| \alpha, \beta \right) \quad (7)$$

where $P_1 = \frac{1}{2\Gamma(\alpha)\Gamma(\beta)}$. The cumulative distributive function (CDF) of instantaneous SNR of FSO link is obtained by integrating the PDF of γ_j^{FSO} and is given as

$$F_{\gamma_j^{FSO}}^{GG}(\gamma) = \int_0^{\gamma} f_{\gamma_j^{FSO}}^{GG}(\gamma) d\gamma = P_2 G_{1,5}^{4,1} \left(\frac{(\alpha\beta)^2 \gamma}{16\gamma_j^{FSO}} \middle| Q_1 \right) \quad (8)$$

where $P_2 = \frac{2^{\alpha+\beta-2}}{\pi\Gamma(\alpha)\Gamma(\beta)}$ and $Q_1 = \frac{\alpha}{2}, \frac{\alpha+1}{2}, \frac{\beta}{2}, \frac{\beta+1}{2}, 0$.

2.2 Modeling of received mmW signals at different BSs

The signal received by base station R_1 from base station S, over the mmW link is given by

$$y_{SR_1}^{mmW} = h_{SR_1}x + n_{SR_1} \quad (9)$$

The decoded symbol at base station R_1 is forwarded to base station R_2 and the received signal at base station R_2 is given as

$$y_{R_1R_2}^{mmW} = h_{R_1R_2}\tilde{x} + n_{R_1R_2} \quad (10)$$

The signal received at base station R_2 is decoded and forwarded to base station D and the signal received at base station D is given by

$$y_{R_2D}^{mmW} = h_{R_2D}\hat{x} + n_{R_2D} \quad (11)$$

where h_{SR_1} , $h_{R_1R_2}$, and h_{R_2D} , are S- R_1 , R_1 - R_2 , and R_2 -D fading channel coefficients respectively. The relation between instantaneous received SNR (γ_j^{mmW}) and average SNR ($\bar{\gamma}_j^{mmW}$) of any given mmW link is given by

$$\gamma_j^{mmW} = \bar{\gamma}_j^{mmW} |h_j|^2 \quad (12)$$

where h_j is the mmW fading channel. The norm of the mmW fading channel is modeled as Nakagami-m distribution and its PDF is given by

$$f_{\gamma_j^{mmW}}(\gamma) = \left(\frac{m}{\bar{\gamma}_j^{mmW}} \right)^m \frac{(\gamma)^{m-1}}{\Gamma(m)} e^{-\frac{m\gamma}{\bar{\gamma}_j^{mmW}}} \quad (13)$$

where m indicates fading severity of the channel, $\Gamma(m)$ is the standard Gamma function, and the CDF of γ_j^{mmW} is obtained by integrating the PDF of γ_j^{mmW} and is given by

$$F_{\gamma_j^{mmW}}(\gamma) = \int_0^\gamma f_{\gamma_j^{mmW}}(\gamma) d\gamma = \frac{1}{\Gamma(m)} \gamma \left(m, \frac{\gamma m}{\gamma_j^{mmW}} \right) \quad (14)$$

where $\gamma(a, x)$ is the lower incomplete gamma function.

3. Statistical characteristics of the proposed system model

In this section, the CDF and PDF for the proposed TH hybrid FSO/mmW system over Gamma-Gamma turbulence and Nakagami-m fading channel are derived.

3.1 Derivation of CDF and PDF of TH system over G-G atmospheric channel

The CDF of γ_{TH}^{FSO} for TH FSO transmission over G-G turbulence can be derived as

$$\begin{aligned} F_{\gamma_{TH}}^{GG}(\gamma) &= 1 - \prod_j \left[1 - F_{\gamma_j}^{GG}(\gamma) \right] \\ &= F_{\gamma_{SR_1}}^{GG}(\gamma) + F_{\gamma_{R_1R_2}}^{GG}(\gamma) + F_{\gamma_{R_2D}}^{GG}(\gamma) - F_{\gamma_{SR_1}}^{GG}(\gamma)F_{\gamma_{R_1R_2}}^{GG}(\gamma) \\ &\quad - F_{\gamma_{R_1R_2}}^{GG}(\gamma)F_{\gamma_{R_2D}}^{GG}(\gamma) - F_{\gamma_{SR_1}}^{GG}(\gamma)F_{\gamma_{R_2D}}^{GG}(\gamma) + F_{\gamma_{SR_1}}^{GG}(\gamma)F_{\gamma_{R_1R_2}}^{GG}(\gamma)F_{\gamma_{R_2D}}^{GG}(\gamma) \end{aligned} \quad (15)$$

where, $F_{\gamma_{SR_1}}^{GG}(\gamma)$, $F_{\gamma_{R_1R_2}}^{GG}(\gamma)$, $F_{\gamma_{R_2D}}^{GG}(\gamma)$ are CDF's of S-R₁, R₁-R₂, and R₂-D links respectively, and are given below.

$$F_{\gamma_{SR_1}}^{GG}(\gamma) = P_2 G_{1,5}^{4,1} \left(\frac{(\alpha\beta)^2 \gamma}{16\gamma_{SR_1}^{FSO}} \middle| \frac{1}{Q_1} \right) \quad (16)$$

$$F_{\gamma_{R_1R_2}}^{GG}(\gamma) = P_2 G_{1,5}^{4,1} \left(\frac{(\alpha\beta)^2 \gamma}{16\gamma_{R_1R_2}^{FSO}} \middle| \frac{1}{Q_1} \right) \quad (17)$$

$$F_{\gamma_{R_2D}}^{GG}(\gamma) = P_2 G_{1,5}^{4,1} \left(\frac{(\alpha\beta)^2 \gamma}{16\gamma_{R_2D}^{FSO}} \middle| \frac{1}{Q_1} \right) \quad (18)$$

The PDF of γ_{TH}^{FSO} is obtained by differentiating $F_{\gamma_{TH}}^{GG}(\gamma)$ with respect to γ and its expression is given by

$$\begin{aligned} f_{\gamma_{TH}}^{GG}(\gamma) &= f_{\gamma_{SR_1}}^{GG}(\gamma) + f_{\gamma_{R_1R_2}}^{GG}(\gamma) + f_{\gamma_{R_2D}}^{GG}(\gamma) - f_{\gamma_{SR_1}}^{GG}(\gamma)f_{\gamma_{R_1R_2}}^{GG}(\gamma) \\ &\quad - f_{\gamma_{R_1R_2}}^{GG}(\gamma)f_{\gamma_{R_2D}}^{GG}(\gamma) - f_{\gamma_{SR_1}}^{GG}(\gamma)f_{\gamma_{R_2D}}^{GG}(\gamma) + f_{\gamma_{SR_1}}^{GG}(\gamma)f_{\gamma_{R_1R_2}}^{GG}(\gamma)f_{\gamma_{R_2D}}^{GG}(\gamma) \\ &\quad - f_{\gamma_{SR_1}}^{GG}(\gamma)F_{\gamma_{R_2D}}^{GG}(\gamma) - F_{\gamma_{SR_1}}^{GG}(\gamma)f_{\gamma_{R_2D}}^{GG}(\gamma) + f_{\gamma_{SR_1}}^{GG}(\gamma)F_{\gamma_{R_1R_2}}^{GG}(\gamma)F_{\gamma_{R_2D}}^{GG}(\gamma) \\ &\quad + F_{\gamma_{SR_1}}^{GG}(\gamma)f_{\gamma_{R_1R_2}}^{GG}(\gamma)F_{\gamma_{R_2D}}^{GG}(\gamma) + F_{\gamma_{SR_1}}^{GG}(\gamma)F_{\gamma_{R_1R_2}}^{GG}(\gamma)f_{\gamma_{R_2D}}^{GG}(\gamma) \end{aligned} \quad (19)$$

where $F_{\gamma_{SR_1}}^{GG}(\gamma)$, $F_{\gamma_{R_1R_2}}^{GG}(\gamma)$, $F_{\gamma_{R_2D}}^{GG}(\gamma)$ are given by Eqs. (16)–(18) respectively. $f_{\gamma_{SR_1}}^{GG}(\gamma)$, $f_{\gamma_{R_1R_2}}^{GG}(\gamma)$, $f_{\gamma_{R_2D}}^{GG}(\gamma)$ are PDF's of S-R₁, R₁-R₂, and R₂-D links respectively, and are given below.

$$f_{\gamma_{SR_1}^{FSO}}^{GG}(\gamma) = P_1(\gamma)^{-1} G_{0,2}^{2,0} \left(\frac{\alpha\beta(\gamma)^{\frac{1}{2}}}{\sqrt{\gamma_{SR_1}^{FSO}}} \middle| \begin{matrix} - \\ \alpha, \beta \end{matrix} \right) \quad (20)$$

$$f_{\gamma_{R_1R_2}^{FSO}}^{GG}(\gamma) = P_1(\gamma)^{-1} G_{0,2}^{2,0} \left(\frac{\alpha\beta(\gamma)^{\frac{1}{2}}}{\sqrt{\gamma_{R_1R_2}^{FSO}}} \middle| \begin{matrix} - \\ \alpha, \beta \end{matrix} \right) \quad (21)$$

$$f_{\gamma_{R_1D}^{FSO}}^{GG}(\gamma) = P_1(\gamma)^{-1} G_{0,2}^{2,0} \left(\frac{\alpha\beta(\gamma)^{\frac{1}{2}}}{\sqrt{\gamma_{R_2D}^{FSO}}} \middle| \begin{matrix} - \\ \alpha, \beta \end{matrix} \right) \quad (22)$$

3.2 Derivation of CDF and PDF of TH system over Nakagami-m fading channel

The cumulative distribution function of γ_{TH}^{mmW} for mmW transmission is given by

$$F_{\gamma_{TH}^{mmW}}(\gamma) = 1 - \prod_j [1 - F_{\gamma_j^{mmW}}(\gamma)] \quad (23)$$

$F_{\gamma_{TH}^{mmW}}(\gamma)$ is the CDF of γ_{TH}^{mmW} over Nakagami-m fading and is obtained by using Eq. (14) as

$$F_{\gamma_{TH}^{mmW}}(\gamma) = 1 - \left[\left(\frac{\Gamma\left(m, \frac{\gamma m}{\gamma_{SR_1}^{mmW}}\right)}{\Gamma(m)} \right) \left(\frac{\Gamma\left(m, \frac{\gamma m}{\gamma_{R_1R_2}^{mmW}}\right)}{\Gamma(m)} \right) \left(\frac{\Gamma\left(m, \frac{\gamma m}{\gamma_{R_2D}^{mmW}}\right)}{\Gamma(m)} \right) \right] \quad (24)$$

where $\Gamma(a, x)$ is the upper incomplete gamma function. The PDF of γ_{TH}^{mmW} is denoted by $f_{\gamma_{TH}^{mmW}}(\gamma)$, which is obtained by differentiating $F_{\gamma_{TH}^{mmW}}(\gamma)$ with respect to γ and its expression is given by

$$\begin{aligned} f_{\gamma_{TH}^{mmW}}(\gamma) &= \left(\frac{m}{\gamma_{SR_1}^{mmW}} \right)^m \frac{(\gamma)^{m-1}}{\Gamma(m)} e^{-\frac{m\gamma}{\gamma_{SR_1}^{mmW}}} + \left(\frac{m}{\gamma_{R_1R_2}^{mmW}} \right)^m \frac{(\gamma)^{m-1}}{\Gamma(m)} e^{-\frac{m\gamma}{\gamma_{R_1R_2}^{mmW}}} \\ &\quad + \left(\frac{m}{\gamma_{R_2D}^{mmW}} \right)^m \frac{(\gamma)^{m-1}}{\Gamma(m)} e^{-\frac{m\gamma}{\gamma_{R_2D}^{mmW}}} \end{aligned} \quad (25)$$

4. Performance analysis of the proposed TH hybrid system

The performance of the proposed TH system is evaluated by using outage probability and average BER. In this section, the expressions for outage probability and average BER of the proposed TH hybrid FSO/mmW system between source and destination BSs over Nakagami-m and Gamma-Gamma turbulence channels are derived. The outage probability expression of the proposed TH system is given by

$$P_{out}^{TH-GG} = F_{\gamma_{TH}^{FSO} GG}(\gamma_{th}^{FSO}) F_{\gamma_{TH}^{mmW}}(\gamma_{th}^{mmW}) \quad (26)$$

where $F_{\gamma_{TH}^{FSO} GG}(\gamma_{th}^{FSO})$ is obtained by replacing γ with γ_{th}^{FSO} in Eq. (15) and $F_{\gamma_{TH}^{mmW}}(\gamma_{th}^{mmW})$ is obtained by replacing γ with γ_{th}^{mmW} in Eq. (24). The transmitted data

is mapped by using BPSK modulation and then transmitted through the FSO link or the mmW link and it is assumed that both the links operate at the same data rate. The BER for BPSK modulation as a function of the instantaneous SNR is given by (Usman M., Yang H. C., and Alouini M. S., 2014)

$$p(e/\gamma) = 0.5\text{erfc}(\sqrt{\gamma}) \quad (27)$$

The average BER during non-outage period can be calculated in terms of the average BER of individual FSO and mmW links, and is given as

$$\bar{P}_b^{TH-GG} = \frac{B_{TH}^{GG}(\gamma_{th}^{FSO}) + F_{\gamma_{th}^{FSO}}^{GG}(\gamma_{th}^{FSO})B_{TH}^{mmW}(\gamma_{th}^{mmW})}{1 - P_{out}^{TH-GG}} \quad (28)$$

where, P_{out}^{TH-GG} is given by Eq. (26) and $F_{\gamma_{th}^{FSO}}^{GG}(\gamma_{th}^{FSO})$ is given by Eq. (15). The average BER of FSO link ($B_{TH}^{GG}(\gamma_{th}^{FSO})$) and mmW link ($B_{TH}^{mmW}(\gamma_{th}^{mmW})$) are given below. The average BER of FSO link is obtained by averaging the conditional BER of BPSK signal over the probability density function of γ_{th}^{FSO} based on the condition $\gamma_{th}^{FSO} > \gamma_{th}^{FSO}$ and is given as,

$$B_{TH}^{GG}(\gamma_{th}^{FSO}) = \int_{\gamma_{th}^{FSO}}^{\infty} p(e/\gamma) f_{\gamma_{th}^{FSO}}^{GG}(\gamma) d\gamma \quad (29)$$

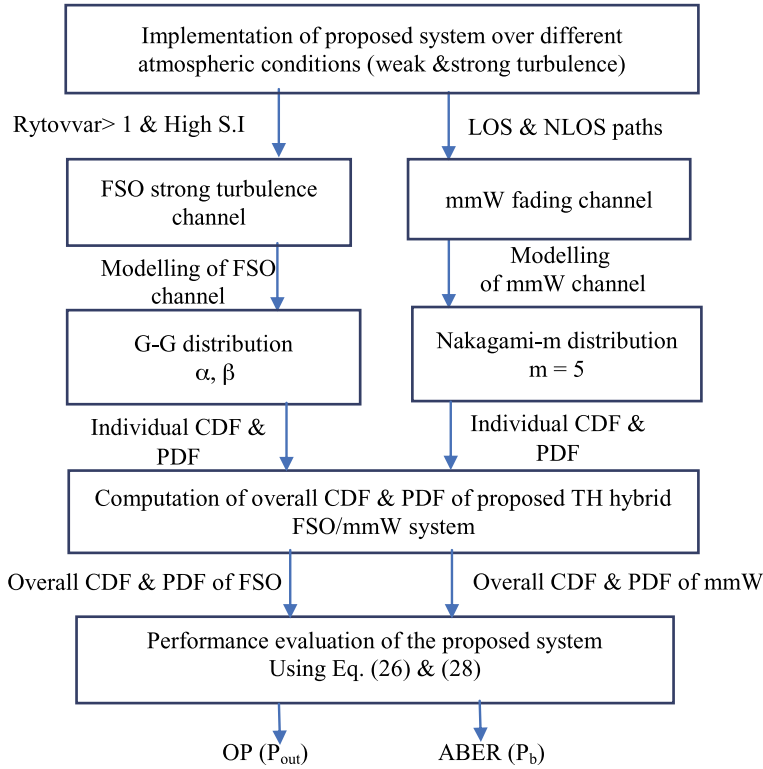
where $p(e/\gamma)$ and $f_{\gamma_{th}^{FSO}}^{GG}(\gamma)$ are given by Eqs. (27) and (19) respectively. Similarly, the average BER of mmW link is obtained by averaging the conditional BER of BPSK signal over the probability density function of γ_{th}^{mmW} based on the condition $\gamma_{th}^{mmW} > \gamma_{th}^{mmW}$ and is given as,

$$B_{TH}^{mmW}(\gamma_{th}^{mmW}) = \int_{\gamma_{th}^{mmW}}^{\infty} p(e/\gamma) f_{\gamma_{th}^{mmW}}(\gamma) d\gamma \quad (30)$$

where, $p(e/\gamma)$ and $f_{\gamma_{th}^{mmW}}(\gamma)$ are given by Eqs. (27) and (25) respectively. By substituting Eqs. (29) and (30) in Eq. (28), the average BER of the TH hybrid FSO/mmW system without direct link between source and destination BSs can be obtained.

5. Results and discussion

In this section, the performance of the proposed systems are compared by evaluating the analytical expressions which are derived for outage probability and average BER over weak and strong turbulent channel conditions. The procedure followed in the implementation of the proposed TH hybrid FSO/mmW backhaul communication system over weak and strong turbulent channels is shown in **Figure 2**. The FSO link is modeled for weak and strong turbulence conditions using Gamma-Gamma distribution. The typical values of α , β for strong turbulence are 2.064, 1.342 and for weak turbulence are 2.902, 2.51 respectively. Further, mmW channel is modeled by using Nakagami-m distribution with $m = 5$.


Figure 2.

Implementation of the TH hybrid FSO/mmW system over weak and strong turbulence conditions.

5.1 Outage probability vs. SNR of TH system over G-G atmospheric channel

The variation in the outage probability with respect to average SNR for FSO -TH and TH hybrid FSO/mmW systems at fixed threshold value of $\gamma_{th}^{mmW} = \gamma_{th}^{FSO} = 5 \text{ dB}$ is shown in **Figure 3**. As can be seen from **Figure 3**, the TH hybrid FSO/mmW system has better outage performance when compared to FSO-TH system, particularly when a high quality mmW link ($\gamma_{av}^{mmW} = 10 \text{ dB}$) is used. Even with a low quality mmW link ($\gamma_{av}^{mmW} = 5 \text{ dB}$), the TH hybrid system shows improvement over FSO-TH system. For instance, at 10 dB of average SNR, FSO-TH system achieves an outage probability of 8.6×10^{-1} , whereas TH hybrid FSO/mmW system achieves outage probabilities of 7.9×10^{-1} and 5.7×10^{-2} with low quality and high quality mmW links respectively. It is observed that from above results, TH hybrid system has low outage probability when compared to FSO-TH system and it is mainly due to adaptive transmission nature of TH hybrid system as it selects the transmission path based on threshold value.

The outage performance of the TH hybrid FSO/mmW system with respect to average SNR for different values of α, β with a high quality mmW link is shown in **Figure 4**. As can be seen from **Figure 4**, TH hybrid FSO/mmW system has better outage performance when compared to FSO-TH system. However, the outage performance deteriorates for strong turbulence conditions when compared to weak turbulence conditions, which is as expected. **Table 1** shows outage probability values of the FSO-TH and TH hybrid FSO/mmW system for different values of α, β with a high quality mmW link.

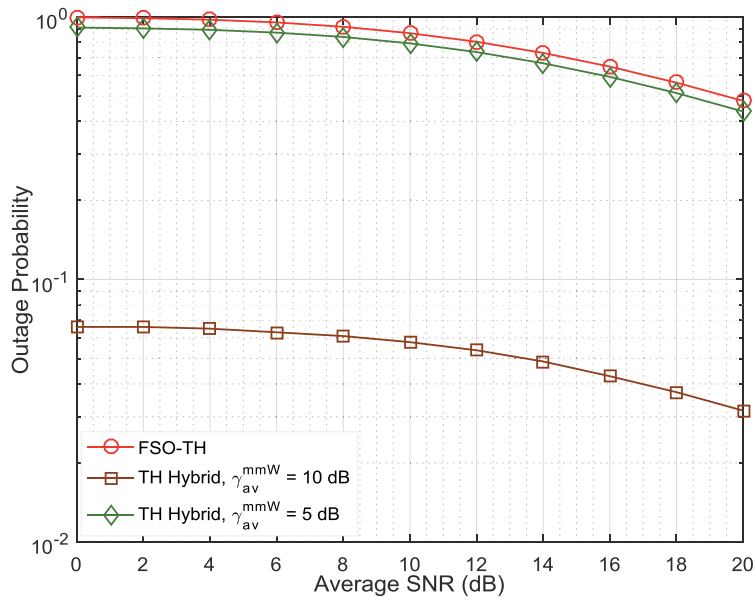


Figure 3.
 Outage probability of the TH hybrid FSO/mmW system over G-G atmospheric channel.

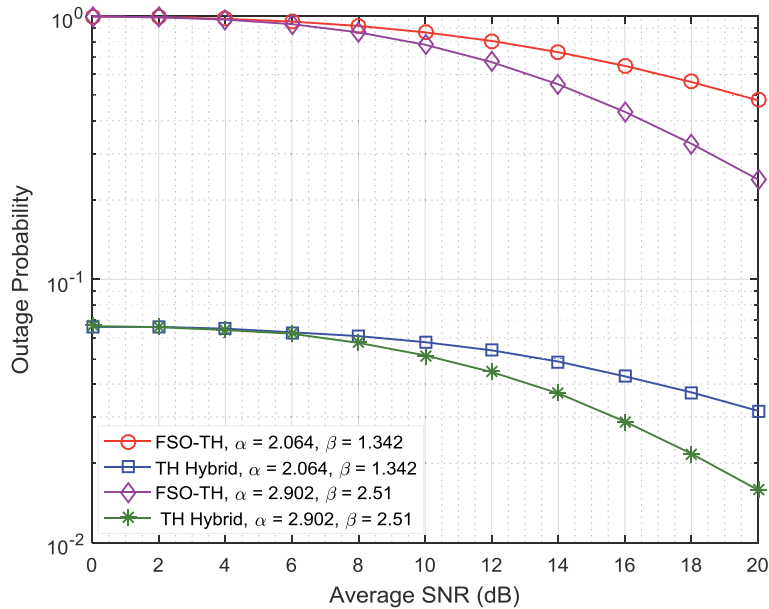


Figure 4.
 Outage probability of the TH hybrid FSO/mmW system with different values of α, β over G-G atmospheric channel.

For instance, at 10 dB average SNR, the TH hybrid FSO/mmW system achieves outage probabilities of 5.1×10^{-2} and 5.7×10^{-2} , while FSO-TH system achieves outage probabilities of 7.7×10^{-1} and 8.6×10^{-1} , respectively, for weak and strong turbulence channel conditions.

S.No.	Avg. SNR (dB)	FSO-TH system		TH hybrid system	
		$\alpha = 2.902$ $\beta = 2.51$	$\alpha = 2.064$ $\beta = 1.342$	$\alpha = 2.902$ $\beta = 2.51$	$\alpha = 2.064$ $\beta = 1.342$
1	2	9.8×10^{-1}	9.8×10^{-1}	6.5×10^{-2}	6.5×10^{-2}
2	4	9.6×10^{-1}	9.7×10^{-1}	6.4×10^{-2}	6.4×10^{-2}
3	6	9.3×10^{-1}	9.5×10^{-1}	6.2×10^{-2}	6.2×10^{-2}
4	8	8.6×10^{-1}	9.1×10^{-1}	5.7×10^{-2}	6.0×10^{-2}
5	10	7.7×10^{-1}	8.6×10^{-1}	5.1×10^{-2}	5.7×10^{-2}
6	12	6.6×10^{-1}	8.0×10^{-1}	4.4×10^{-2}	5.3×10^{-2}
7	14	5.5×10^{-1}	7.2×10^{-1}	3.6×10^{-2}	4.8×10^{-2}
8	16	4.3×10^{-1}	6.4×10^{-1}	2.8×10^{-2}	4.2×10^{-2}
9	18	3.2×10^{-1}	5.6×10^{-1}	2.1×10^{-2}	3.7×10^{-2}
10	20	2.3×10^{-1}	4.7×10^{-1}	1.5×10^{-2}	3.1×10^{-2}

Table 1.
Outage probability of FSO-TH and TH hybrid FSO/mmW vs. average SNR over G-G atmospheric channel.

5.2 ABER vs. SNR of TH system over G-G atmospheric channel

The variation in the average BER of the TH hybrid FSO/mmW system with respect to the average SNR for a fixed threshold value of $\gamma_{th}^{mmW} = \gamma_{th}^{FSO} = 5dB$ is shown in **Figure 5**. As can be seen from **Figure 5**, the TH hybrid FSO/mmW system has better ABER performance when compared to FSO-TH system. With a high quality mmW link ($\gamma_{av}^{mmW} = 10dB$), there is only marginal improvement in ABER performance, especially over low SNR region. This is because at a very low value of average SNR of FSO link, the high quality mmW link is being used more frequently. As average SNR of FSO link improves, the FSO link will be used for transmission

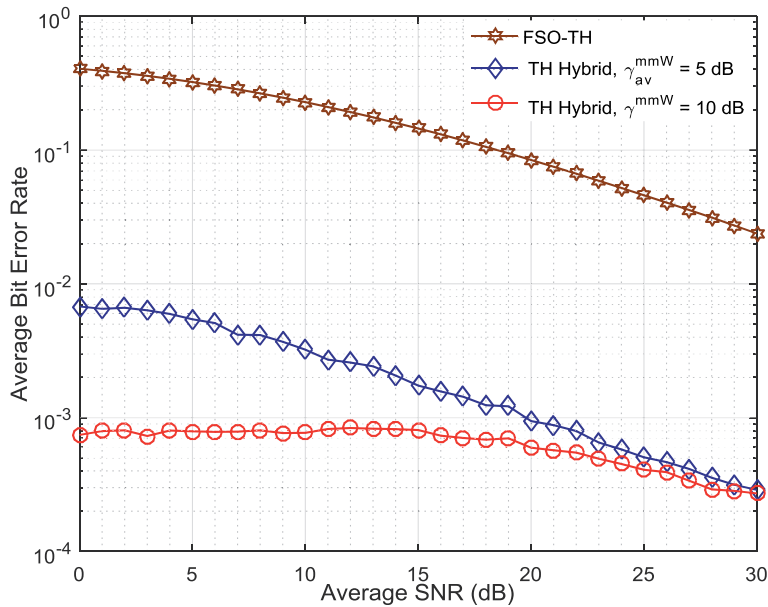


Figure 5.
ABER of the TH hybrid FSO/mmW system over G-G atmospheric channel.

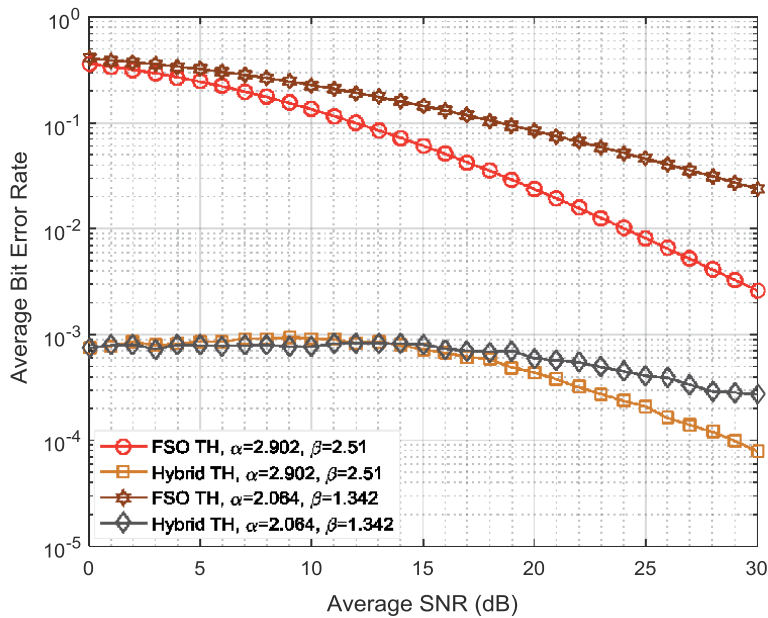


Figure 6.
ABER of the TH hybrid FSO/mmW system for different values of α , β over G-G atmospheric channel.

and hence the ABER performance of the TH hybrid FSO/mmW system improves further. For instance, at 10 dB of average SNR, FSO-TH system achieves an ABER of 2.2×10^{-1} , whereas TH hybrid FSO/mmW system achieves ABER of 3.2×10^{-3} and 7.7×10^{-4} with low quality ($\gamma_{av}^{mmW} = 5dB$) and high quality ($\gamma_{av}^{mmW} = 10dB$) mmW links respectively.

Figure 6 shows the ABER performance of the FSO-TH and TH hybrid FSO/mmW systems with respect to average SNR for different values of α and β . As can be seen from **Figure 6**, TH hybrid FSO/mmW system has better ABER performance when compared to FSO-TH system. The ABER values of FSO-TH and TH hybrid FSO/mmW systems for different values of α , β with a high quality mmW link are tabulated in **Table 2**.

S.No	Avg. SNR (dB)	FSO-TH		TH Hybrid	
		$\alpha = 2.902$ $\beta = 2.51$	$\alpha = 2.064$ $\beta = 1.342$	$\alpha = 2.902$ $\beta = 2.51$	$\alpha = 2.064$ $\beta = 1.342$
1	5	2.4×10^{-1}	3.2×10^{-1}	8.6×10^{-4}	7.9×10^{-4}
2	10	1.3×10^{-1}	2.2×10^{-1}	9.2×10^{-4}	7.7×10^{-4}
3	12	9.9×10^{-2}	1.9×10^{-1}	8.2×10^{-4}	8.3×10^{-4}
4	14	7.2×10^{-2}	1.5×10^{-1}	7.8×10^{-4}	8.2×10^{-4}
5	16	5.0×10^{-2}	1.3×10^{-1}	6.6×10^{-4}	7.3×10^{-4}
6	18	3.5×10^{-2}	1.0×10^{-1}	5.8×10^{-4}	6.8×10^{-4}
7	20	2.3×10^{-2}	8.4×10^{-2}	4.3×10^{-4}	5.9×10^{-4}
8	24	1.0×10^{-2}	5.2×10^{-2}	2.3×10^{-4}	4.5×10^{-4}
9	28	4.1×10^{-3}	3.1×10^{-2}	1.2×10^{-4}	2.9×10^{-4}
10	30	2.5×10^{-3}	2.3×10^{-2}	7.8×10^{-5}	2.7×10^{-4}

Table 2.
ABER of FSO-TH and TH hybrid FSO/mmW vs. average SNR over G-G atmospheric channel.

For instance, at 20 dB average SNR, FSO-TH system achieves ABER of 2.3×10^{-2} and 8.4×10^{-2} , while TH hybrid FSO/mmW system achieves ABER of 4.3×10^{-4} and 5.9×10^{-4} , respectively for weak and strong turbulence conditions.

6. Conclusions

Performance analysis of the proposed TH hybrid FSO/mmW system for macro-cell BS to small cell BS backhaul communication has been carried out in this chapter. The FSO link turbulence conditions ranging from weak to strong are modeled by using Gamma-Gamma distribution. Further, mmW channel is modeled by using Nakagami-m distribution with $m = 5$. Outage probability and ABER of the TH scenario have been analyzed for different values of α , β over Gamma-Gamma distribution and average SNR of mmW links. From the results, it is concluded that TH hybrid FSO/mmW system has improved outage and ABER performance when compared to FSO-TH system.

Acknowledgements

The work presented in this paper is supported by Visvesvaraya PhD scheme for Electronics and IT, Ministry of Electronics and Information Technology (Meity), Government of India, being implemented by Digital India Corporation.

Author details


Mogadala Vinod Kumar^{1*}, Yenneti Laxmi Lavanya², Bharati Bidikar²
and Gottapu Sasibhushana Rao²

¹ Department of Electronics and Communication Engineering, Bapatla Engineering College, Bapatla, Andhra Pradesh, India

² Department of Electronics and Communication Engineering, Andhra University, Visakhapatnam, Andhra Pradesh, India

*Address all correspondence to: vinodkumar.mogadala@becbapatla.ac.in

IntechOpen

© 2022 The Author(s). Licensee IntechOpen. This chapter is distributed under the terms of the Creative Commons Attribution License (<http://creativecommons.org/licenses/by/3.0>), which permits unrestricted use, distribution, and reproduction in any medium, provided the original work is properly cited. 

References

- [1] Cisco. Visual Networking Index: Forecast and Trends, 2017–2022, White Paper. [Internet] 2019. Available from: <https://s3.amazonaws.com/media.media.post.com/uploads/CiscoForecast.pdf>
- [2] Mogadala VK, Gottapu SR, Chapa BP. Dual hop hybrid FSO/RF based backhaul communication system for 5G networks. In: Proceedings of the IEEE International Conference on Wireless Communications Signal Processing and Networking (WiSPNET). Chennai, India: IEEE; 2019. pp. 229-232
- [3] Sharma S, Madhukumar AS, Swaminathan R, Sheng CJ. Performance analysis of hybrid FSO/RF transmission for DF relaying system. In: Proceedings of the IEEE Globecom Workshops (GC Wkshps). Singapore: IEEE; 2017. pp. 1-6
- [4] Ghassemlooy Z, Popoola W, Rajbhandari S. Optical Wireless Communications: System and Channel Modeling with MATLAB. 1st ed. Boca Raton: CRC Press Taylor and Francis Group; 2012. p. 497
- [5] Usman M, Yang HC, Alouini MS. Practical switching-based hybrid FSO/RF transmission and its performance analysis. IEEE Photonics Journal. 2014; 6:1-13. DOI: 10.1109/JPHOT.2014.2352629
- [6] Al-Habash MA, Andrews L, C, and Phillips R. L. Mathematical model for the irradiance probability density function of a laser beam propagating through turbulent media. Optical Engineering. 2001;8. DOI: 10.1117/1.1386641
- [7] Chatzidiamantis ND, Karagiannidis GK, Kriezis EE, Matthaiou M. Diversity combining in hybrid RF/FSO systems with PSK modulation. In: Proceedings of the IEEE International Conference on Communications (ICC). Kyoto, Japan: IEEE; 2011. pp. 1-6
- [8] Gradshteyn IS, Ryzhik IM. Table of Integrals, Series, and Products. 8th ed. Elsevier Academic Press; 2014. p. 1133. DOI: 10.1016/C2010-0-64839-5
- [9] Rakia T, Yang H, Alouini M, Gebali F. Outage analysis of practical FSO/RF hybrid system with adaptive combining. IEEE Communications Letters. 2015;19:366-369. DOI: 10.1109/LCOMM.2015.2443771

Section 3

Multiplexing and New Designs

NOMA Transmission Systems: Overview of SIC Design and New Findings

Carmen Beatriz Rodríguez Estrello,

Fernando Ramos-Alarcón and Valeri Kontorovich

Abstract

Non-Orthogonal Multiple Access (NOMA) has been recently proposed as a good alternative to meet 5G and beyond requirements in terms of high spectral efficiency, massive connectivity, and low latency. It has been demonstrated that the use of NOMA in downlink has superior performance in terms of throughput, whereas the use in uplink outperforms OMA techniques in terms of fairness. A distinctive feature of NOMA is the presence of excessive multiple-access interference due to the case of usage of power domain to multiplex signals, thus the functional implementation of NOMA implies Successive Interference Cancellation (SIC) to combat this interference. Therefore, SIC design becomes the main point in the effectiveness of NOMA systems. On the other hand, hybrid schemes, NOMA/OMA, have been recently proposed to reduce the drawbacks of pure NOMA systems. However, in these schemes, it becomes necessary to distinguish NOMA and OMA users. Cognitive Radio techniques turn to be a good option to effectively separate NOMA/OMA users as well as to distinguish NOMA users. In this chapter, a brief overview of NOMA techniques related to Cognitive Radio technology (CR-NOMA) and SIC design reported in the literature is presented. Also, new findings about NOMA/OMA users' recognition are described.

Keywords: CR-NOMA, SIC algorithms, hybrid NOMA, user separation

1. Introduction

To cover 5G and Next Generation Networks (NGN) main requirements, such as better coverage, bandwidth, reliability, and spectrum efficiency, many techniques have been proposed. Non-Orthogonal Multiple Access (NOMA), concretely power NOMA has emerged as a promising trend to improve mobility, connectivity, and spectrum efficiency through spectrum sharing of OMA-user with other multiple users. Thus, multiuser interference cancellation techniques play a predominant role to successfully mitigate excessive Multiple Access Interference (MAI). The so-called Sequential Interference Cancellation (SIC) was considered through the last decades to be the most promising approach for MAI mitigation [1–3]. It is worth mentioning as well, that SIC algorithms are recently at the center of the attention for both the research community and the industry professionals to significantly reduce excessive interferences due to the spectrum sharing.

On the other hand, hybrid NOMA / OMA schemes have been proposed [4, 5] to overcome the drawbacks of pure NOMA systems and enhance pure OMA schemes in terms of total throughput. Hybrid NOMA schemes require an effective way to separate NOMA / OMA users. Promising techniques to successfully separate NOMA/OMA users are the ones used in Cognitive Radio: a few decades ago, Cognitive Radio (CR) technology was proposed to improve spectrum utilization by allowing a secondary user (SU) to access idle spectrum allocated to a primary user (PU) [6]. Lately, the usage of Cognitive Radio-based NOMA (CR-NOMA) for power domain NOMA has been suggested to allow the SU spectrum regardless of the presence of the primary user [7] and also to separate users in NOMA/OMA hybrid schemes [4, 5].

Hereafter, the main attention will be applied to the CR-NOMA principles to effectively separate NOMA/OMA users and implementing SIC algorithms for establishing the decoding order for the multiple users but for specific conditions of Doubly Selective channels, which naturally appears when information is transmitted from High-Speed-Vehicles (HSV): trains, cars, aircrafts, etc. to the nearest base station (BS). CR-NOMA principle should be used with several significant changes in 5G and beyond networks since meticulous analysis [6, 7] of existing SIC proposals shows that if it is applied to Doubly Selective channels, some significant changes and improvements are required due to:

- The usage of the Channel State Information (CSI) or its modifications [1, 2, 8, 9] is hardly possible, due to the strong selectivity of the channels in both time and frequency domains following with severe fading as well. Though CR-NOMA Transmission at Double Selective channels is mainly incoherent and channel conditions for users use to be significantly different. Moreover, as it was pointed at [4, 5], significant differences for channel conditions for OMA and NOMA users are necessary and sufficient conditions for effective decoding for both types of users.
- Decoding algorithms should be “as fast as possible” to avoid channel selectivity in time and frequency.
- Decoding algorithms must be also of high accuracy in a wide range of fluctuations of the user’s Signal to Noise Ratio (SNR) values as the user’s channel conditions need to be sufficiently different for NOMA effective application (see above).
- Relatively large values of Doppler shifts and Frequency Offsets are present in Double Selective Channels.

In this chapter, chaos filtering is proposed for decoding hybrid NOMA/OMA signals from the combined one ($y(t)$ in **Figure 1**). Moreover, two original methods, illustrated in **Figures 2** and **3**, are proposed for separating users in the NOMA scheme. **Figure 1** shows the scenario of hybrid NOMA/OMA systems. Framework is defined as follows: OMA users are typical OFDMA users while NOMA users are generated as Non-OFDMA [10] shifting the central frequency by the factor of δ related to the original OMA signal.

As in conventional CR-NOMA, the primary user is decoded first (OMA signal) and then the set of “secondary users” (multiusers) are decoded, but contrary to conventional solutions, the OMA signal is first decoded by means of the chaos-based quasi-optimum Extended Kalman Filter (EKF) and multiusers are proposed to be decoded by one of the following methods:

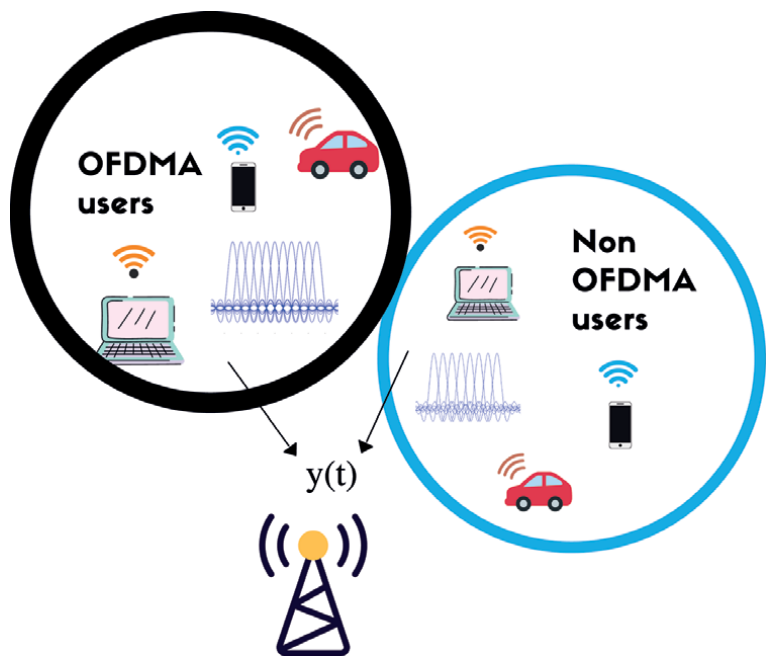


Figure 1.
A used framework of hybrid NOMA/OMA.

- Chaos-based EKF filters or

$$y(t) = \text{OMA user} + \sum \text{NOMA multiuser} + n(t)$$

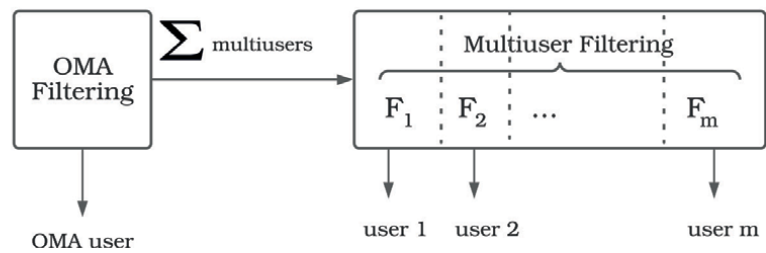


Figure 2.
Chaos-based filtering approach for NOMA users.

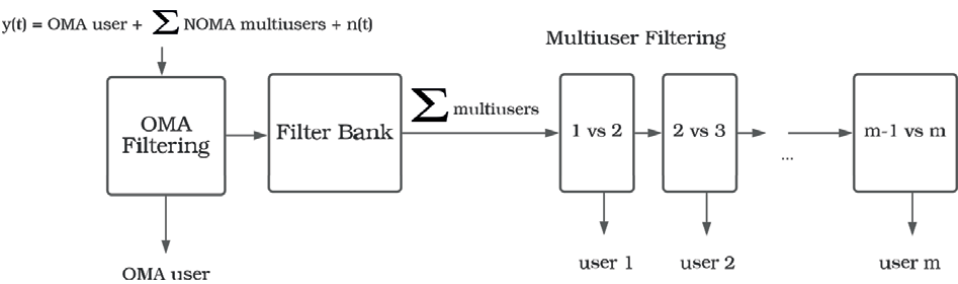


Figure 3.
Sequential m-hypothesis testing approach for NOMA users.

- Sequential m hypothesis testing.

After user's decoding, they are directed to corresponding demodulation blocks of the different services to whom they correspond. Both methods are shown to be essentially invariant to the CSI and their processing algorithms are fast and quasi-optimum. Extended Kalman Filter (EKF) might give additional "benefits" for the Chaos-based filtering approach [11] (see below).

Moreover, according to [6, 7] and our own study, shown in Section 4, OMA signal and multiuser signals can be effectively approximated by means of a Gaussian random process model. Besides, the physical nature of the Doubly Selective Channels (high selectivity in both domains) shifts signals to an "almost" Gaussian random process, no matter what service they belong to. This matter gives additional "degrees of freedom" in choosing the concrete filtering algorithms for filtering: Standard Kalman Filtering (SKF), EKF, etc. for concrete conditions of NOMA transmission. This issue will be explained in the following.

The rest of the chapter is organized as follows: In Section 1 a brief overview of SIC-NOMA techniques reported in the literature is presented, Section 2 is entirely dedicated to explain Chaos-based filtering algorithms applied both to OMA signals and for the set of multiuser interferers. Section 3 demonstrates the visibility and high precision of the Chaos-based filtering. Section 4 presents simulation results for decoding the OMA signal and the rest of the multi-users. Section 5 is devoted to the Sequential Analysis testing of m hypothesis. For the hypothesis testing each signal of the multiusers will be considered in the form of time set samples of a Gaussian process with means and variances different for each of the multiusers (conditions for all users in power NOMA must be significantly different). The way of the calculus of the characteristics of the hypothesis testing is presented as well.

2. A brief overview about SIC algorithms in NOMA systems

In the last decade, NOMA methods have gained a lot of attention to increase spectral efficiency for 5G and beyond. The usage of NOMA techniques entails a lot of multiuser interference in the system; however, these methods increase the effective throughput in the system. Hybrid NOMA/OMA systems have been proposed [4, 5] to overcome the main disadvantages caused by the MAI. Several papers have dealt with SIC algorithms [1–3] and NOMA/OMA user selection [4, 5].

Authors of [4, 5, 12, 13] suggest the usage of combined (NOMA/OMA). In [12] partial-NOMA is introduced in a large two-user downlink network to provide throughput and reliability. The associated partial overlap controls interference while still offering spectrum reuse. The nature of the partial overlap also allows them to employ receive-filtering to further suppress interference. For signal, decoding was proposed, a flexible successive interference cancelation (FSIC) decoding and compared with OMA and NOMA performance.

In [12] a problem to maximize total throughput constrained to a minimum throughput requirement for each user was formulated and proposed an algorithm to find a feasible resource allocation efficiently. The results show that partial-NOMA allows greater flexibility in terms of performance. Partial-NOMA can also serve users that NOMA cannot. Different from the proposal made in this chapter, NOMA users in [14] cannot support high transmission rate requirements.

In [13] an iterative SIC receiver architecture with the pilot- and data-based channel estimation for efficient decoding of non-orthogonal superimposed signals was proposed. It was claimed that the non-orthogonal superposition concept on top of OFDMA is a promising technique to improve cell spectral efficiency. In the

cellular case, the SIC multiuser receiver scheme is well adapted for user signal separation. However, authors in [13] do not work with high-mobility scenarios that entail Double Selective Channels.

Notice, that almost every proposed SIC technique in the literature strongly depends on the CSI. However, as it was stated before, the usage of the Channel State Information (CSI) or its modifications [14–16] is hardly possible, due to the Double Selective channels. Contrary to the previously published papers, new findings reported in this chapter consider the SIC impairments mitigation related to double selectivity troubles.

SIC methods for SISO channels have been extensively studied and reported in the literature. Nevertheless, in 5G and beyond networks MIMO techniques have been also proposed to increase capacity. Furthermore, with the employment of Massive MIMO techniques, as was mentioned before, the usage of CSI becomes challenging since the number of users goes large [17, 18]. At [17] a blind belief propagation (BP) detection for non-coherent NOMA with massive MIMO was proposed, where the transmitter of each user first performs differential modulation on PSK symbols, and then spreads its symbols using low-density spreading (LDS); the receiver of the base station (BS) employs differential demodulation and then detects all users' symbols using a blind BP detection without knowledge of CSI. Strictly speaking, this approach is not related to power domain NOMA, it rather belongs to CDMA-NOMA, but it was included here because of the idea of Incoherent transmission applications rarely considered in the NOMA design.

The new findings proposed hereafter use CR-NOMA principles and could be successfully applied to separate users in scenarios where the Channel State Information cannot be used, which corresponds to the incoherent ideology of NOMA transmission.

3. Chaos-based filtering algorithms outline

Real physical phenomena modeling through chaotic signals have been widely employed during the last decades and it has been recently used particularly for the purposes of interference mitigation [11, 19–21]. In this chapter OMA users, aggregated signal is modeled as a chaotic signal to efficiently separate NOMA/OMA users, as well as to differentiate between NOMA users.

Chaos modeling of physical phenomena has demonstrated to show very attractive characteristics regarding filtering precision and efficient interference suppression. As an example, in [20, 21] processing algorithms based on chaos filtering are used for mitigation of Radio Frequency Interference (RFI) produced by desktops and laptops. In this regard, the intention of the implementation of Chaos-based filtering for decoding OMA and multiusers looks almost natural. Considering that ideas of Chaos filtering were already widely published and discussed, hereafter only a brief outline will be presented, and details can be found at the cited references.

Continuous chaotic signals are generated by deterministic nonlinear systems (strange attractors) and are described generally by Ordinary Differential Equations (ODE) of the type:

$$\dot{x} = F(x, t) \quad (1)$$

Where x is an n -dimensional vector of the attractors output signals, $F(\bullet)$ is a known n -dimensional vector function and $x(t_0) = x_0$ is the initial condition. Thanks to the fundamental ideas of A. N. Kolmogorov and M. Born (see references at [22, 23] the statistical characterization of the deterministic systems (1) is well established.

In the following, three concrete types of attractors will be used: Lorenz, Chua, and Rössler; their statistical features are completely presented at [20]. Special cases for (1) applied hereafter (in discrete time) are:

Rössler attractor

$$\begin{aligned} x_{k+1} &= x_k + T_s(-y_k - z_k) \\ y_{k+1} &= y_k + T_s(x_k + 0.2y_k) \\ z_{k+1} &= z_k + T_s(0.2 - z_k(5.7 - x_k)) \end{aligned} \quad (2)$$

Lorenz attractor

$$\begin{aligned} x_{k+1} &= x_k + T_s(10(x_k - y_k)) \\ y_{k+1} &= y_k + T_s(28x_k - y_k + x_k z_k) \\ z_{k+1} &= z_k + T_s\left(x_k y_k - \frac{8}{3}z_k\right) \end{aligned} \quad (3)$$

Chua attractor

$$\begin{aligned} x_{k+1} &= x_k + T_s(9.205(y_k - V(x_k))) \\ y_{k+1} &= y_k + T_s(x_k - y_k + z_k) \\ z_{k+1} &= z_k - T_s(14.3y_k) \end{aligned} \quad (4)$$

Where $V(x_k) = m_1 x_k + \frac{1}{2}(m_0 - m_1)(|x_k + 1| - |x_k - 1|)$; $m_0 = -\frac{1}{7}$, $m_1 = \frac{2}{7}$. At (2)–(4) T_s is the sampling time.

Due to the lack of space, we take advantage that the theory and practice of Chaos-based filtering algorithms for different signals are exhaustively described and discussed at the cited references [20, 21], so there is no sense to repeat it here. Though only the concrete filtering algorithms for attractors (2)–(4) will be presented and some important conclusions are listed here [19–21]:

- Extended Kalman filter, implemented in the so-called “one-moment” (1MM EKF) and two-moment (2MM EKF) time fashion can be chosen as a “reasonable” option due to its balance between the filtering accuracy and computational complexity. Multi-moment implementations for more than two instants of time are still rather complex.
- The standard (optimum) Kalman filter (SKF) can be applied as well considering that both, OMA, and the set of multiusers can be well approximated via Gaussian models (see also Section 4), but the preference of the EKF for some scenarios will be explained below. One can suspect some “controversy” here, but it is not the case, and it does not have anything undermining of optimality of SKF for Gaussian scenarios. This issue must be explained more precisely.
- Linear SKF is strongly optimum for the linear Gaussian process models which are characterized by multidimensional Gaussian distributions with their dimensionality tending to infinity! As it will be illustrated in Section 4 it is not the case here! Hereafter, all the users are statistically described only by one-dimensional Gaussian distribution which can be approximately generated by nonlinear attractors.
- Though the above-mentioned controversy depends only on one side to the nonlinearity of Chaotic modeling of the signals and on the one-dimensional Gaussian approximation of its statistical characteristics on the other side.
- One-moment time instant (1MM) and two-moment time instants (2MM) algorithms [11, 19–21] differ in filtering accuracy, but they differ very lightly in

terms of computational complexity. So, their implementation depends mainly on the concrete NOMA transmission system requirements.

- An analytical comparison of the accuracy between the EKF and the SKF in this regard is difficult to obtain but considering that models (1)–(4) are significantly nonlinear, the accuracy of the EKF might be sometimes better than the accuracy of SKF, for the Chaotic filtering. Reasons for this matter were “hinted” above and details can be found at [20].

EKF (1MM and 2MM) algorithms for chaotic attractors.

Let us present concrete algorithms of Chaos-based filtering which will be tested in the next section to choose the appropriate attractor model and the discrete-time algorithm for filtering OMA and multiuser interferences. The theory of 1MM SKF and EKF is well known and developed at [19–21], then only the corresponding results will be reproduced.

As it follows from [19–21] the SKF algorithm is optimum for a linear dynamic system, and it consists of two cycles:

Prediction:

$$\begin{cases} \hat{x}_{k+1}^- = f(\hat{x}_k^+) \\ P_k^- = A_k P_k^+ A_k^T + Q_k \end{cases} \quad (5)$$

Correction

$$\begin{cases} G_k = P_k^- H_k^T [H_k P_k^- H_k^T + N_{0_k}]^{-1} \\ \hat{x}_k^+ = \hat{x}_k^- + G_k [y_k - s(x_k^-)] \\ P_k^+ = P_k^- + G_k H_k P_k^- \end{cases} \quad (6)$$

The algorithm for EKF 1MM is the same as (5) and (6) but with a small modification due to its quasi-linearity, as shown in the following. It must be stressed that the SKF is an optimum algorithm for the strongly Gaussian signals and the 1MM EKF algorithm is quasi-optimum for nonlinear Chaos models, so the accuracy of its filtering (in our case in terms of Normalized Mean Squared error MSE) is not the highest one for the Gaussian approximations of its statistics, but as it is shown at [19] it is practically acceptable for most applications. The 2MM EKF algorithm was proposed recently [19–21] and is totally heuristic; besides it is quasi-optimum as well.

It is time to stress that optimum (or quasi-optimum) filtering algorithms for Chaos Filtering demonstrate (with different grade) so-called **singular** features (see [19–21]) which practically belongs to the low dependence of the precision of filtering (in our case of MSE) to the input value of the Signal to Noise Ratio (SNR).

Meantime, the accuracy of the 1MM EKF and 2MM EKF does not demonstrate totally their “singular” properties as optimum ones (see [19–21]), but anyway those algorithms are accurate and highly recommended. Why it happens actually?

One must notice that Eqs. (1)–(4) and generally all attractors considered hereafter (see [19–21]) describe the deterministic system dynamics. In order to apply so-called statistical dynamics of the deterministic systems according to A. Kolmogorov and M. Born all dynamics of attractors (2)–(4) and the measurement of the state of the system are tied to the statistically independent noises with the a priori known covariance matrixes given by additive white noise with the intensity N_{0_k} and

very small “process noise” for Eqs. (1)–(4) with the matrix Q_k ¹ respectively. So, one can see that the ordinary differential Eqs. (OE) of attractors turn to the Stochastic Differential Equations (SDE), for which all the filtering theory is developed [22, 23].

In (5), (6) G_k is the so-called Kalman gain, \hat{x}_k^- is the a priori state estimate in the k -th update cycle, \hat{x}_k^+ is the a posteriori state estimate in the k -th update cycle, P_k^-, P_k^+ are respectively the a priori and the a posteriori error covariance matrix estimate in the k -th cycle, A_k is the fix state transition Matrix (for SKF) or for the 1MM EKF the linearization matrix (Jacobian) $A_k = \frac{\partial f(x_k)}{\partial x_k}$ denotes “quasi-linearity” for 1MM EKF.

For 2MM EKF, P_k^- in (5), becomes [19]:

$$P_k^- = A_k P_k^+ (1 - \rho^2) A_k^T + Q_k \quad (7)$$

where ρ is the correlation coefficient of two adjacent samples.

Though if the intensity of the process noise (by definition) is always much less than intensities of the channel additive white noise (AWGN) influence of the “correction” part on the estimations of the signal is almost invariant to SNR (to which depends on a-priori and a-posteriori error matrixes) and practically follows the a-priori data. In other words, the filtered signals are “tuned” to the a-priori data or to processes generated by Eqs. (1)–(4). It is a brief “physical” explanation for the singularity of chaos filtering. For sure at [19–21] the interested reader might find more rigorous proof.

The rest of the equations in (5) and (6) remain unchanged and it can be easily seen that the filtering algorithm, in general, is the same [19–21]. Thus, the processing time (number of samples) for 1MM EKF and 2MM EKF are almost the same but filtering accuracy might differ significantly. The latter was illustrated for signals of different physical nature at [19–21] and at Section 4.

It is worth mentioning once more to conclude, that chaos-based algorithms (including certainly SKF and EKF) are based on Ordinary Differential Equations (ODE) of chaotic deterministic dynamics and they have a very important and spectacular property, the so-called “singularity” for their solutions. In other words, the filter’s output signal is somehow “tuned” to its a-priori dynamics or to its mathematical model applied in the filtering algorithm, while the influence of the “correction” component of the algorithm is negligible for any reasonable value of the additive channel noise (AWGN) intensity. That is why the filtering accuracy is high, even for quasi-optimum algorithms and the filtering fidelity (in terms of the Normalized Mean Square Error, MSE) shows a rather low dependence on the input SNR. All those features will be illustrated in the next section.

4. Simulation results

Simulations presented in this section are dedicated to simulating a hybrid NOMA/OMA system using chaos-based filtering for recovery of the primary OMA signal. The process is simulated as indicated in **Figure 8**; the aggregated signal of OMA signal, NOMA signal, and AWGN noise. NOMA interference is the sum of non-orthogonal (NOMA) carriers [10]². EKF-1MM algorithm (5)–(6) is used to

¹ Once more: introducing the processing noise according to A. N. Kolmogorov and M. Born is fundamental for statistical characterization of the deterministic systems (see references at [22–24]).

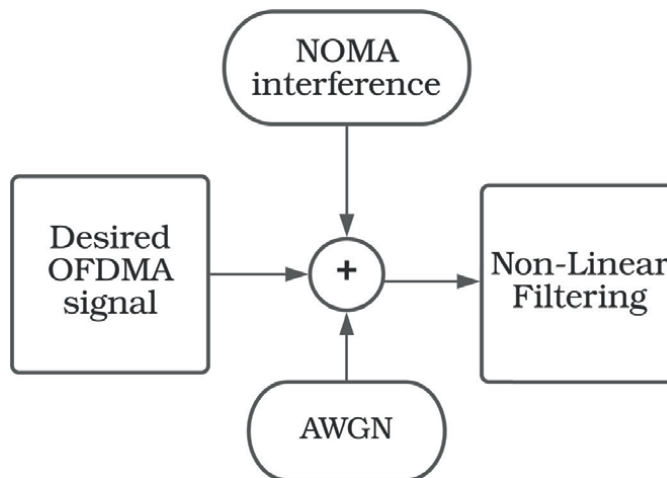


Figure 4.
 Filtering scenario.

non-linear filtering OMA signal as indicated in **Figures 2, 3, and 4**. As a reference, the IEEE 802.11a standard is considered here, where 52 carriers are used for modulated data, 4 pilot carriers, and 8 guard band carriers.

Generation of orthogonal and non-orthogonal signals.

Typical orthogonal signals are OFDMA symbols that are formed using IFFT as illustrated in the following figure.

In **Figure 5**, b_k is a set of binary pulses suitable for typical modulations such as BPSK, QPSK, etc. The pulses are passed from serial to parallel form and then multiplied by N orthogonal subcarriers using the IFFT, k is an integer number that goes from 0 to $N - 1$, $\Delta f = 1/T$, T is the OFDMA symbol period which it can be set to 1 without loss of generality. The set of $N - 1$ orthogonally modulated carriers are then summed to finally yield the orthogonal OFDMA signal $x(t)$.

In our case, the generation of the orthogonal signal was made by using the following scheme as is explained below.

The scheme of **Figure 5** uses IFFT and so the resulting signal $x(t)$ is complex, while in **Figure 6**, signals are real which makes the subsequent processing much simpler. Moreover, in the scheme of **Figure 6**, it is much easier to manipulate f_k to make it not to be an integer. This is useful for the next set of signals that would be part of the experimental setting. In our case, OFDMA and No-OFDMA multicarrier signals are simulated in the same way by using the scheme presented in **Figure 5**. Manipulating the carrier central frequencies with constant integers (OFDMA case) or non-integer constants δ (NOMA case).

The next set of signals that will be used are non-orthogonal (NOMA signals), and this is achieved using the scheme of **Figure 6** by multiply f_k by a non-integer constant, say $\delta = 0.8$.

As it was established previously, Doubly Selective Channels (high selectivity in both domains) shift signals to an “almost” Gaussian random process due to their physical nature, no matter what service they belong to. Thus, the set of corresponding signals that are considered in this chapter was processed to obtain

² The scenario in which multiuser signals are filtered by the bank of the Chaos-based filters and each element belongs to the specific multiuser could be also considered. This case might be treated in the same way, assuming that the OMA signal is extracted from the input.

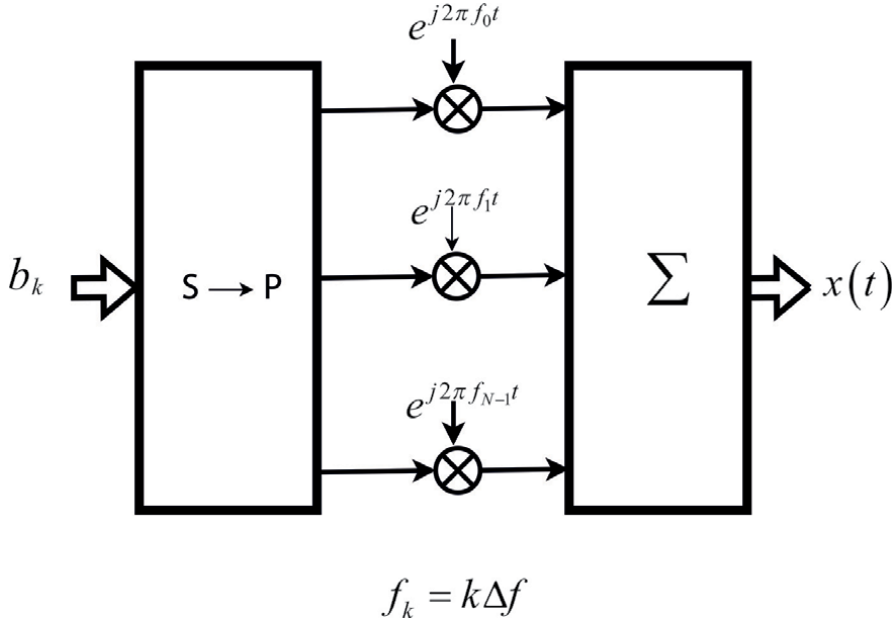


Figure 5.
OFDMA symbol forming.

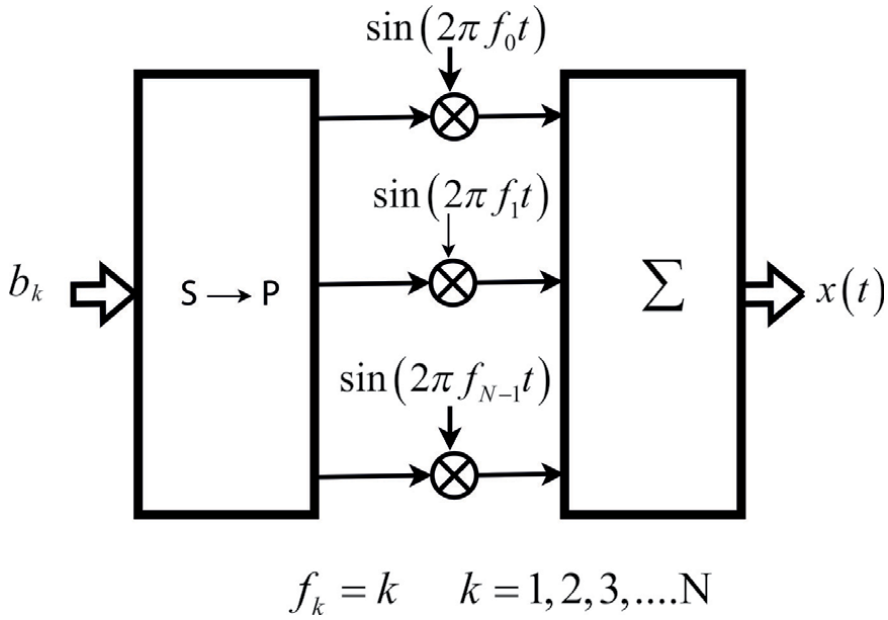


Figure 6.
OFDMA symbol forming used in simulations.

their statistical characteristics: PDF and autocorrelation function shown in **Figures 7 and 8**.

In the following, we explore how effective the EKF-based non-linear filtering (IMM and 2MM) can be, when it is applied to OFDMA(OMA) signals under the influence of AWGN and NOMA interference.

From now on, it will be considered, that the AWGN noise contributes with 50% of the total noise power and the ACGN contributes with the other 50% of the total

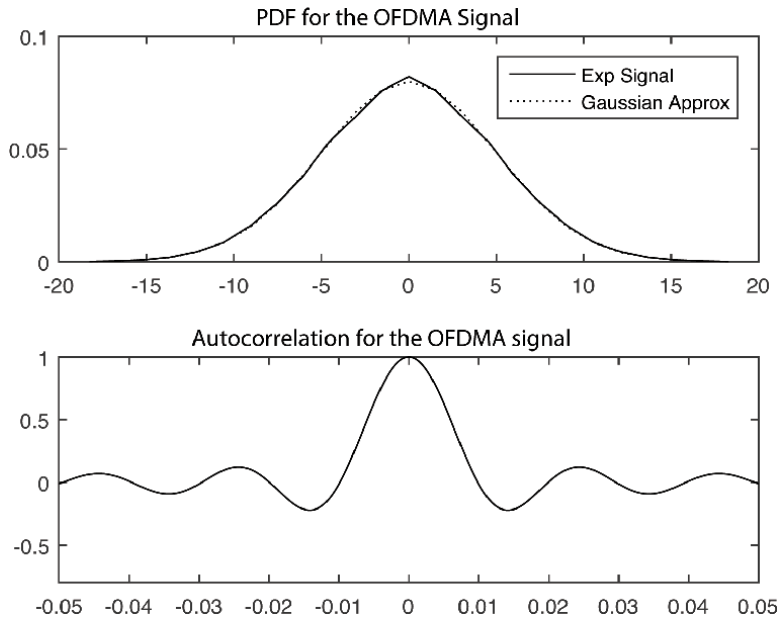


Figure 7.
 PDF and autocorrelation for the OMA signal.

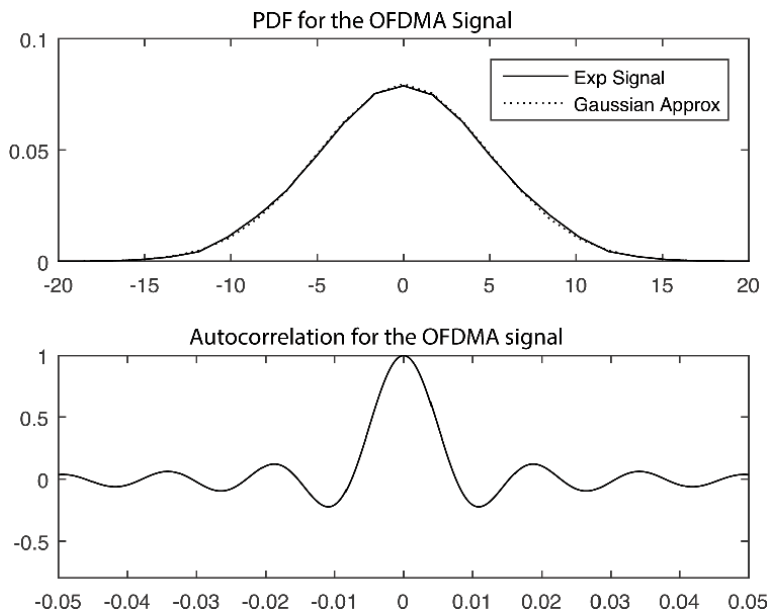


Figure 8.
 PDF and autocorrelation for the NOMA signal.

noise power. Then, we will shape the SNIR (Signal to Noise to Interference Ratio) which is used in the EKF structure.

Two different experiments were conducted to test the Normalized Mean Square Error in terms of the SNIR. The experiments consider an OFDMA signal with 52 carriers as an OMA signal. The NOMA interferences were generated according to two proposed scenarios:

Scenario 1:

NOMA Signal: Non- Orthogonal FDMA with 52 carriers separated with $\delta = 0.8$ between carriers

OMA Signal: OFDMA with 52 carriers

Scenario 2:

Two OFDMA signal blocks with 52 carriers each, with a factor of 2.4 between central frequencies of each block.

The number of carriers was chosen rather high to guarantee the Gaussianity of the PDF of the signal, but one must notice, that it rather “arbitrary” and not critical.

After testing the x , y and z components of the Rössler, and Chua Attractors, it was found by comparing the correspondent statistical characteristics that only the x component of the Rössler and Chua attractors could be used for modeling and filtering. 1MM and 2MM filtering was processed according to algorithms (5)–(7) and the results obtained are almost similar to the ones presented at [19].

Tables 1 and **2** show the results for experiments 1 and 2 respectively in terms of the SNIR vs. normalized MSE (Mean Square Error). Both tables also show the results in terms of the MSE for the filtering using Rössler’s and Chua’s x components. Note that the theoretical filtering according to (5)–(7) includes the influence of process noise Q . **Tables 1** and **2** also show the process noise values that allow adequate filtering (small MSE values) for the different SNIR values and the two attractors.

It must be noticed that Intensity Matrix for process noises Q is rather small (much less, than one) and even for very low SINR values (-10 dB) the MSE is much less than 10% and for SINR- 0 dB it was much less than 1%. Though, the accuracy of filtering is high enough for separating(classification) signals of OMA and multi-users. The explanation of the latter is simple: if the MSE is about of several percentages it means that close to 100% of the energy of the desired signal for its further demodulation is preserved and therefore bit-error-rate practically does not decrease. This “benefit” takes place because of the singular properties of Chaos-based algorithms for filtering (see above) which are somehow valid even for quasi-optimum EKF filtering in very hard interference scenarios.

It can be seen from **Figures 2** and **3** that the proposed SIC filtering algorithms are working not as a decoder but as a classifier for OMA and NOMA signals and when the OMA signal is well filtered (identified), then the multiuser interference

SINR	EKF Rössler X		EKF Chua X	
	-3 dB ($Q = 0.12521$)	10 dB ($Q = 0.2$)	-3 dB ($Q = 0.0925$)	-10 dB ($Q = 0.25$)
1MM	0.0109	0.052	0.0139	0.0705
2MM	0.0103	0.047	0.0138	0.0672

Table 1.
MSE results for experiment 1.

SINR	EKF Rössler X		EKF Chua X	
	-3 dB ($Q = 0.25$)	-10 dB ($Q = 0.2$)	-3 dB ($Q = 0.125$)	-10 dB ($Q = 0.325$)
1MM	0.0119	0.0504	0.0143	0.0730
2MM	0.0107	0.0487	0.0134	0.0677

Table 2.
MSE results for experiment 2.

separation or classification might be evaluated by the probability of classification error P_{cl} . The latter obviously affects the final bit-error-rate of the demodulation for all users (P_{err}).

One of the possible ways of evaluating P_{cl} for multiusers classification or for OMA-multiuser classification is applying the so-called DGL, or Chernoff upper bound in the way [24]:

$$P_{cl} \leq 2m(m-1)^2 e^{-n\frac{\Delta^2}{2}} \quad (8)$$

where Δ is the minimum Kullback–Leibler distance between “closest” Gaussian distributions of the multiusers, n is the number of samples and m is the number of multiusers. For OMA-multiusers classification the total number of users is $m' = m + 1$.

If $\forall P_{err}, P_{cl} < 1$ then it is easy to show that the resulting demodulation error P for each signal is:

$$P \approx P_{err} + P_{cl} \quad (9)$$

and if practically $P_{cl} \geq P_{err}$, then approximately $P_{cl} < P < 2P_{cl}$, i.e. it is defined mainly by errors of the multiuser classification. So, from (9) it follows that minimization of P_{cl} is crucial for the noise immunity of the NOMA transmission.

In this regard, the important question arises: what signal must be filtered first: OMA or multiusers? At the material presented above it was stated that the OMA signal needs to be filtered first, however, this is an open question that must be thoroughly investigated in the future. In the meantime, some recent simulations show that filtering NOMA interferences first to “clean” the OMA signal (before its filtering) might be a rather complex issue, but it can give significant benefits in terms of reducing the MSE for the OMA signal decoding.

5. Multiuser classification by means of m sequential hypothesis testing algorithms

As it was established before, OMA signal is recovered through EKF filtering and then, NOMA users could be efficiently decoded by one of the following methods:

- Chaos-based EKF filters, using the same procedure as described before.
- Sequential m -hypothesis testing: due to the sequential character of multiuser decoding with SIC algorithms for the CR-NOMA it seems reasonable to apply here an adequate implementation of the decoding strategy, i.e. m -sequential hypothesis testing algorithms. To the best of our knowledge, this option for SIC design wasn't discussed before in the literature.

The advantages of these algorithms for binary testing are well known long ago from A. Wald [25], but the results of their generalizations for the case of m hypothesis testing are mainly addressed to its tiny mathematical problems [24–29] and very few to its implementation.

For practical implementation, their solutions seem rather complex except in a few special cases. Other options (“ad-hoc”) so far are based on the heuristic extensions of the binary test to the case of the m hypothesis (see also below).

In this regard it was found reasonable to invoke the results from [29] together with the approach stated at [26] where the asymptotic approximates for the optimum Bayesian algorithms for testing are presented for the case of small probabilities of decoding errors and an expected rather long testing time, particularly for low SNR cases. Both those assumptions might be realistic for SIC design at Doubly Selective channels, applying the Gaussian statistics as well.

Here, it is time to remind, that NOMA transmission, as it was commented above, needs sufficiently different channel conditions for the users, including certainly multiusers as well. Though channel conditions for OMA and multiusers are assumed as significantly different, but between multiusers it is not always the case, i.e. hypothesis for multiusers might be “close”, therefore testing time might be large!

The extractions from [26, 29] for the asymptotic characteristics of the algorithm are as following:

$$\langle N_k \rangle = - \frac{\log A_k}{\min_{j:j \neq k} D(f_k, f_j)} \quad \alpha_k = \pi_k A_k \gamma_k \quad \alpha = \sum_{k=0}^{m-1} \pi_k A_k \gamma_k \quad (10)$$

Where $D(f, g) = \int f(x) \log \frac{f(x)}{g(x)} dx$ is the Kullback-Liebler distance between the PDFs $f(x)$ and $g(x)$; $\langle N_A \rangle = \bar{N}_A$ is the average value of the first $n \geq 1$ when the decision for the hypothesis is taken; $\{\pi_k\}$ a priori probabilities of hypothesis. ($k = 1, m$), $\{\gamma_k\}$ and $\{A_k\}$ are detailed below.

In the usual case when the value of the probability α is predefined, from (10) it follows:

$$c = \frac{\alpha}{\sum_{k=0}^{m-1} \frac{\pi_k}{\delta_k}}, \quad \delta_k = \min_{j:j \neq k} D(f_k, f_j), \quad A_k = \frac{c}{\delta_k \gamma_k} \quad (11)$$

where $0 < \gamma_k < 1$ is tabulated in Table 3.1 at [26, 29].

For concrete data, using (10)–(11), the asymptotic characteristics for m-testing can be calculated. It should be noticed that the essence and benefits of any sequential algorithm strongly depend on the choice of the threshold which defines the decision region for testing [26, 29]; the data processing algorithm can be: coherent (incoherent), energy detection, etc. which are well known [26].

For the concrete case of a Gaussian channel for all multiusers, where the decoding problem for multiusers depends on their SNR, QoS, amplitudes, average power, etc. the formal scenario is as follows: let $k = 0, m-1$ for hypothesis testing $\{H_k\}$ and x_1, x_2, \dots is a sequence of independent Gaussian random variables with means $\{\theta_k\}$ and variances σ_k^2 , which are known a priori (see also [21, 26]). If $\{x_k\}$ are multiuser amplitudes, the data processing algorithm is obvious: $\sum_{i=0}^n x_i$, and the results must be compared with the asymptotic thresholds for each “ k ” as follows [28]:

$$\frac{n(\theta_k + \theta_{k+1})}{2} + \frac{\log A_k}{\theta_{k+1} - \theta_k} \frac{n(\theta_k + \theta_{k+1})}{2} - \frac{\log A_{k+1}}{\theta_{k+1} - \theta_k} \quad (12)$$

Where $k = \overline{0, m-1}$.

It is interesting to express here a remarkable issue: these asymptotic algorithms correspond exactly to the set of simple binary algorithms for testing: H_0 vs. H_1 ; H_1 vs. H_2 and so forth, i.e. are “ad hoc” (see above). This corresponds totally with the intuitive processing of the m-tests as a straightforward generalization of the binary sequential test (called “ad-hoc” [25, 28, 29]) that was known long ago and shown at [29] as an asymptotically optimum for m-hypothesis testing.

Therefore, in the Gaussian case the m-decoding asymptotic algorithm is nothing else but a “block” of cells each for the sequential testing of the different binary hypotheses of the multiusers, see **Figure 3**.

The examples of numerical results, for this testing can be found at [25], which show that for such kinds of algorithms the number of samples (time of analysis) can be reduced 2 or 3 times compared with the optimum algorithm for the fixed time testing. The latter follows exactly from the convergence of the m testing to the (m-1) set of “binary” algorithms well known several decades ago and rigorously presented first by A. Wald.

It is worth mentioning that robust features to the multiuser statistics follow due to the asymptotic character of the proposed algorithms. But the latter requires some further investigation.

6. Conclusion

It was shown earlier that because of the numerous impairments and distortions that take place in Double Selective channels, it is rather “hard” to obtain high values for characteristics, such as noise immunity and spectral efficiency in Doubly Selective Channels which usually appears in 5G and beyond networks for information transmission from HSV terminals.

The material presented above is devoted to two new options for users’ separation in hybrid NOMA /OMA schemes related to the power CR-NOMA information transmission over-application of NOMA to improve the spectrum efficiency paradigm in SISO channels. It has been demonstrated that non-linear filtering is effective to separate OMA/NOMA users in hybrid schemes.

Moreover, two possible approaches for SISO channels were proposed for mitigation of the multiuser’s interferences, namely a Chaos-based filtering approach and an approach based on the m sequential hypothesis testing. Both, show several attractive invariant features for application over Doubly Selective SISO channels such as high fidelity for multiuser decoding, robustness, and reduced decision time, which allows recommend them not only for Doubly Selective channels but also for the “conventional” channels as well, besides a large number of already reported algorithms for them (see [25–29] and references therein).

Previously published papers, where chaotic filtering is used for other applications [19–21], show that proposed algorithms here can be effectively implemented in hardware.

Proposals for future research

It is worth mentioning the existence of a solid number of unsolved problems for OMA/NOMA separating users, particularly for Doubly Selective channels. They are as follows:

- Both proposed methods need to be exhaustively compared for a broad range of impairment features that might exist at Doubly Selective channels.
- Generalizations of CR-NOMA for MIMO Doubly Selective channels and Massive MIMO. It seems, that besides the SIC is a pre-processor block before the main receiver unit (the latter is already well known [14, 15, 30]), for applications at MIMO over Doubly Selective channels, the before mentioned algorithms might require significant modifications.
- The power NOMA paradigm (see also CR-NOMA) must be sufficiently generalized by application of invariant methods of incoherent modulation and demodulation (see [15], etc.)

- It seems extremely promising to complete NOMA transmission for the Double-Selective Channels with block-chain access for application in Massive MIMO networks to improve the Spectrum Efficiency Algorithms for m-hypothesis of the transmission both from the physical channel and network access.
- Algorithms for m hypothesis testing (see Section 5) need to be precisely investigated for their invariant properties in Doubly Selective Channels.

Author details

Carmen Beatriz Rodríguez Estrello^{1*}, Fernando Ramos-Alarcón²
and Valeri Kontorovich²

1 ESIME Zacatenco IPN, CDMX, Mexico

2 CINVESTAV-IPN, CDMX, Mexico

*Address all correspondence to: cbrodriguez@ipn.mx

IntechOpen

© 2022 The Author(s). Licensee IntechOpen. This chapter is distributed under the terms of the Creative Commons Attribution License (<http://creativecommons.org/licenses/by/3.0>), which permits unrestricted use, distribution, and reproduction in any medium, provided the original work is properly cited. 

References

- [1] Ding Z, Schober R, Poor HV. Unveiling the Importance of SIC in NOMA Systems—Part II: New Results and Future Directions. *IEEE Communications Letters*. 2020;**24**: 2378-2382
- [2] Ding Z, Schober R, Poor HV. Unveiling the importance of SIC in NOMA systems—part 1: State of the art and recent findings. *IEEE Communications Letters*. 2020;**24**: 2373-2377. DOI: 10.1109/lcomm.2020.3012604
- [3] Iswarya N, Jayashree LS. A survey on successive interference cancellation schemes in non-orthogonal multiple access for future radio access. *Wireless Personal Communication*. 2021;**120**: 1057-1078. DOI: 10.1007/s11277-021-08504-1
- [4] Elbayoumi M, Hamouda W, Youssef A. A Hybrid NOMA/OMA Scheme for MTC in Ultra-Dense Networks. *GLOBECOM 2020—2020 IEEE Global Communications Conference*. Taipei, Taiwan: 2020. pp. 1-6. DOI: 10.1109/globecom42002.2020.9322207
- [5] Ebrahim A, Celik A, Alsusa E, Eltwil AM. NOMA/OMA Mode Selection and Resource Allocation for Beyond 5G Networks. 2020 IEEE 31st Annual International Symposium on Personal, Indoor and Mobile Radio Communications. London, UK; 2020. DOI: 10.1109/pimrc48278.2020.9217161
- [6] Nguyen H-N, Le S-P, Le C-B, Nguyen N-L, Nguyen N-T, Do D-T, et al. Cognitive Radio Assisted Non-Orthogonal Multiple Access: Outage Performance. 2019 42nd International Conference on Telecommunications and Signal Processing (TSP). Budapest, Hungary; 2019. DOI: 10.1109/tsp.2019.8768873
- [7] Liu X, Wang Y, Liu S, Meng J. Spectrum Resource Optimization for NOMA-Based Cognitive Radio in 5G Communications. *IEEE Access*. 2018;**6**: 24904-24911. DOI: 10.1109/access.2018.2828801
- [8] Saito K, Benjebbour A, Harada A, Kishiyama Y, Nakamura T. Link-Level Performance of Downlink NOMA with SIC Receiver Considering Error Vector Magnitude. 2015 IEEE 81st Vehicular Technology Conference (VTC Spring). Glasgow, Scotland; 2015. DOI: 10.1109/vtcspring.2015.7145913
- [9] Alberto R, Monteiro FA. Downlink MIMO-NOMA With and Without CSI: A Short Survey and Comparison. 2020 12th International Symposium on Communication Systems, Networks and Digital Signal Processing (CSNDSP). Porto, Portugal; 2020. DOI: 10.1109/csndsp49049.2020.9249527
- [10] Xu T, Darwazeh I. Non-Orthogonal Frequency Division Multiple Access. 2020 IEEE 91st Vehicular Technology Conference (VTC2020-Spring). Antwerp, Belgium; 2020. DOI: 10.1109/vtc2020-spring48590.2020.9128663
- [11] Kontorovich V, Lovtchikova Z. Nonlinear filtering of chaos for real time applications. In: Kyamakya K, Halang WA, Mathis W, Chedjou JC, Li Z, editors. *Selected Topics in Nonlinear Dynamics and Theoretical Electrical Engineering*. Berlin, Heidelberg: Springer Berlin Heidelberg; 2013. pp. 41-59. DOI: 10.1007/978-3-642-37781-5_3
- [12] Ali KS, Hossain E, Hossain MJ. Partial non-orthogonal multiple access (NOMA) in downlink poisson networks. *IEEE Transactions on Wireless Communications*. 2020;**19**:7637-7652. DOI: 10.1109/twc.2020.3014625

- [13] Ruegg A, Tarable A. Iterative SIC receiver scheme for non-orthogonally superimposed signals on top of OFDMA. 21st Annual IEEE International Symposium on Personal, Indoor and Mobile Radio Communications. Istanbul, Turkey; 2010. DOI: 10.1109/pimrc.2010.5671952
- [14] Pena-Campos F, Parra-Michel R, Kontorovich V. Incoherent DPSK diversity reception in doubly selective channels based on virtual trajectories. *IEEE Transactions on Vehicular Technology*. 2018;**67**: 7744-7748. DOI: 10.1109/tvt.2018.2821173
- [15] Ramirez-Arredondo G, Pena-Campos F, Parra-Michel R, Kontorovich V. Invariant incoherent MIMO reception over doubly selective channels. *IEEE Access*. 2021;**9**: 67776-67785. DOI: 10.1109/access.2021.3077554
- [16] Pena-Campos F, Parra-Michel R, Kontorovich V. MIMO multicarrier transmission over doubly selective channels with virtual trajectories receiver. *IEEE Transactions on Vehicular Technology*. 2019;**68**: 9330-9338. DOI: 10.1109/tvt.2019.2934693
- [17] Tian F. Chen, Xm, Multiple-antenna techniques in nonorthogonal multiple access: A review. *Frontiers of Information Technology Electronic Engineering*. 2019;**20**(1665-1697). DOI: 10.1631/FITEE.1900405
- [18] Wang T, Shi L, Cai K, Tian L, Zhang S. Non-Coherent NOMA With massive MIMO. *IEEE Wireless Communications Letters*. 2020;**9**: 134-138. DOI: 10.1109/lwc.2019.2944620
- [19] Kontorovich V, Ramos-Alarcon F. *Ubiquitous Filtering for Nonlinear Problems*. London, UK. 2020. DOI: 10.5772/intechopen.88409
- [20] Kontorovich V, Lovtchikova Z. Cumulant analysis of strange attractors: theory and applications. In: Kyamakya K, Halang WA, et al., editors. *Recent Advances in Non-Linear Dynamics and Synchronization*. Springer-Verlag; 2009. pp. 77-115
- [21] Ilitzky Arditti D, Alcocer Ochoa A, Kontorovich Mazover V, Barroso FRA. Adaptive mitigation of platform generated radio-frequency interference. Patent US 2015.0 051 880A1; 2015. Available from: <https://bit.ly/2Pesh6G>
- [22] Van T, H. *Detection estimation, and modulation theory: Detection, estimation, and linear modulation theory*. N.Y, U.S.A: Wiley Ed; 2001. DOI: 10.1002/0471221082
- [23] Jazwinski AH. *Stochastic Processes and Filtering Theory*. Mineola, N.Y., U.S.A: Academic Press; 1970. Available from: <https://bit.ly/34iDlnz>
- [24] Malek S, Chow KY, Ghavamzadeh M. Sequential Multiple Hypothesis Testing With Type I Error Control. Vol. 54. *Proceedings of the 20th International Conference on Artificial Intelligence and Statistics USA*. Lauderdale, FL, USA; 2017. pp. 1468-1476
- [25] Woodroffe M. *Nonlinear Renewal Theory in Sequential Analysis*. Michigan, USA: SIAM; 1982. DOI: 10.1137/1.9781611970302
- [26] Novikov A. "Optimal Sequential Multiple Hypothesis Tests". 45, 2. Prague, Czech Republic: Kybernetika; 2009. pp. 309-330
- [27] Afser H. Statistical classification via robust hypothesis testing. *arXiv*. 2021; 28:2112-2116
- [28] Baum CW, Veeravalli VV. A sequential procedure for multihypothesis testing. *IEEE Transactions on*

Information Theory. 1994;**40**(6):
1994-2007. DOI: 10.1109/18.340472

[29] Devroye L, Gyorfi L, Lugosi G. A note on robust hypothesis testing. IEEE Transactions on Information Theory 2002;**48**:2111–2114. DOI: 10.1109/tit.2002.1013154.

[30] Pena-Campos F, Parra-Michel R, Kontorovich V. A low complexity multi-carrier system over doubly selective channels using virtual-trajectories receiver. IEEE Transactions on Wireless Communications. 2016;**15**: 5206-5217. DOI: 10.1109/twc.2016.2555305

Multiplexing Techniques for Applications Based-on 5G Systems

Nguyen Huu Trung

Abstract

Multiplexing is an important technique in modern communication systems that allows simultaneous transmission of multiple channels of information on the same transmission media. Fifth-generation (5G) mobile communication systems allow Enhanced Mobile Broadband (eMBB), Ultra Reliable Low Latency Communications (URLLC), and Massive Machine Type Communications (mMTC). 5G has carrier frequency bands from sub-1 GHz to mid-bands and millimetre waves. The sub-1 GHz frequency band is for mobile broadband, broadcast and massive IoT applications. The mid-bands (between 1–6 GHz) offer wider bandwidths, focusing on mobile broadband and mission-critical applications. The frequency bands above 24 GHz (mmWaves) support super wide bandwidth applications over short, line-of-sight coverage. For each application on a corresponding frequency band, 5G allows defining of an optimized waveform from a family of waveforms. 5G uses massive MIMO, NOMA and network slicing techniques which allows spatial multiplexing and multibeam multiplexing. Multiplexing techniques play a major role in 5G systems in terms of data rate and bandwidth efficiency. This chapter presents multiplexing techniques for applications based-on 5G systems.

Keywords: 5G NR, duplexing schemes, spatial multiplexing, MIMO schemes, CSI framework, service-based multiplexing

1. Introduction

From the first generation (1G) that were introduced in 1979 by Nippon Telegraph and Telephone (NTT) to today's fifth generation (5G), mobile communication networks are constantly improving the speed and efficiency of bandwidth usage to support various applications with diverse requirements such as latency, high data rates and real-time support for random traffic demands [1].

The increasing number of not only smart phones, tablets and laptops but also the huge number of other devices such as IoT (Internet of Things) nodes, wearable devices for healthcare will demand significant challenges in 5G systems to manage a huge amount of devices and connections [2]. Besides, the exponential growth of mobile video services (e.g., live video streaming, online video gaming, mobile TV) requires wider bandwidth and higher spectral efficiency than that of 4G systems [3].

Such a huge volume of data traffic and connections will lead to 5G systems to use new and higher frequency bands [4]. Some other factors such as ultra-low latency (less than one millisecond), fast-tracking will also be considered in the design of 5G

system architecture. 5G systems support radio connections and end-to-end network connectivity at ultra-high speed, lower latency, higher reliability and massive connectivity [5].

1.1 Scope and contributions

This book chapter gives the reader an up-to-date multiplexing techniques that are implemented in 5G systems. The contributions of this book chapter are listed below:

- First, this book chapter provides a brief introduction of 5G system architecture for the readers to understand the components of 5G systems.
- Second, provides an overview of basic multiplexing techniques as a foundation for 5G systems to implement FDD, TDD modes.
- Finally, it describes MIMO service and data multiplexing operations from a mathematical background, physical antenna configurations, channels and signals, procedures for downlink and uplink MIMO schemes.

1.2 5G system architecture

Today we see the evolution of Industry 4.0 manifested in smart factories, where collaborative robots are instantly connected. The entertainment industry advances dramatically with AR/VR technologies. People are using Zero Search with intelligent personal digital assistants. The Intelligent Transportation Systems (ITS) require all cars connected via C-V2X protocol. The Industrial Internet of Things (IIoT) is used in smart cities and smart agriculture. This is the business ecosystem of 5G systems [6]. 5G systems enable people for living in an intelligently connected world. The 5G system architecture is illustrated in **Figure 1**. At the highest level, the 5G system consists of 5G NR RAN (gNB), 5G Core Network (5GCN)/EPC and different kinds of UEs for three kinds of service including Enhanced Mobile Broadband (eMBB), Ultra-reliable and Low-latency Communications (uRLLC), and Massive Machine Type Communications (mMTC) in a business ecosystem [7].

1.2.1 5G NR RAN (gNB)

5G NR (New Radio) is the global standard for the air interface of 5G networks developed by 3GPP with operation from below 1 GHz up to more than 40 GHz and massive MIMO beamforming capability [8].

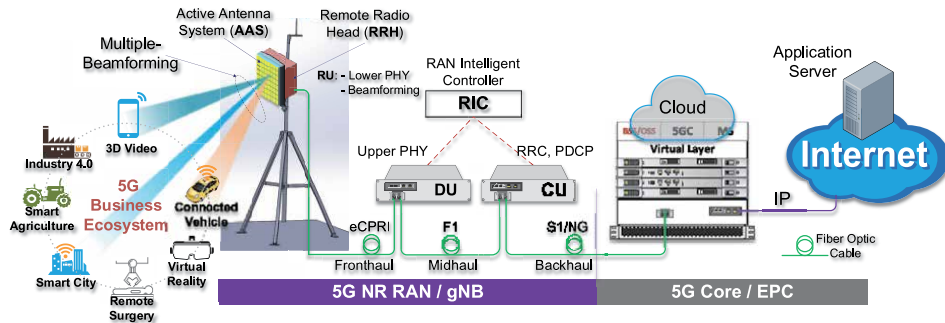


Figure 1.
5G system architecture (vRAN approach).

RAN stands for Radio Access Network. RAN provides radio access and coordinates network resources across User Equipment (UE). For more general, the RAN is divided into two parts. The first part is the lower layer RAN split including the antenna integrated Radio Unit (RU) and the Distributed Unit (DU). The second part is the higher layer RAN split, a 3GPP standard F1 interface between the DU and the Centralized Unit (CU). DU and CU constitute Baseband Unit (BBU) [9].

Legacy LTE uses Evolved Node B (eNodeB or eNB) like Base Station (BTS) in GSM networks. Similarly, gNodeB (gNB – next generation Node B) is 5G Base Station. gNB features Software Defined Radio (SDR) with various MIMO options described in session 3 of this chapter [10].

In 5G NR, RU handles digital front end (DFE), part of the physical layer (low physical) and multiple beamforming operation. RU consists of a Remote Radio Head (RRH) and Active Antenna System (AAS) [11]. Antennas in AAS for 5G NR make use of the shorter element sizes at high frequencies to incorporate a larger count of radiating elements. These antenna arrays are essential for MIMO beamforming operations that play a vital role in 5G systems [12]. The RRH performs all RF functions like ADC/DAC, digital up/down-conversion, filtering and transmitting and receiving signals to the BBU including beamforming. RRH can also provide monitoring and control functions to optimize system performance.

In LTE systems, RRH is connected to the antenna by RF coaxial cable and is usually mounted near the antenna to reduce transmission line losses. In 5G NR, RRH and AAS are integrated in a small and compact form factor [6].

Common Public Radio Interface (CPRI) is the standardized interface that sends data from the RRHs to the Base Band Unit (BBU). CPRI is a very high-speed connection on fiber optic cable. eCPRI is enhanced CPRI which is used to reduce the burden on the fiber. The connection between the RUs and the DU is called fronthaul and it is fiber optic cable.

DU stands for Distributed Unit. DU is placed close to RU and runs RLC, MAC, parts of the Physical layer. This function consists of signal processing, network access. DU is controlled by CU (Centralized Unit). DU also supports FFT/IFFT functions [13].

CU provides support for the higher layers of the protocol stack such as SDAP, PDCP and RRC. Practically, there is a single CU for each gNB. A CU can control multiple DUs (can be more than 100 DUs). Each RU corresponds to one cell. Each DU can support one or more RUs, so in 5G systems, one gNB can control hundreds of cells. 5G NR cell can be femtocell, smallcell or macrocell [14]. 5G Small Cell Radio Nodes can be installed on walls or ceilings with network connectivity and power are provided over Ethernet. Midhaul connects the CU with the DU via F1 interface. Backhaul connects the 5G core to the CU. The 5G core may be up to 200 km away from the CU.

RIC is RAN Intelligent Controller which is responsible for all RAN operation and optimization procedures such as radio and resource connection management, mobility management, QoS management to support the best effective network operation.

There are three different approaches to design a RAN as abstracted in **Table 1** [15].

1.2.2 5G Core network

According to the definition of 3GPP, 5G has two networking modes: SA (Standalone) and NSA (Non-Standalone). 5G system Service-based

	Centralized/Cloud RAN (C-RAN)	Virtual RAN (vRAN)	Open-RAN (O-RAN)
RU	Proprietary		GPP COTS hardware (e.g., SDR)/ OEM vendor
BBU hardware	Centralized functionality, proprietary hardware, software	Generic hardware platforms (e.g., COTS Server with virtualized software), BBU splits into DU and CU.	
BBU software	Proprietary	Virtualized	Virtualized with open API
Interface	Proprietary		Open
Interoperability	Single vender for RU and BBU	Single vender for RU and software	Multiple venders

COTS: commercial-off-the-shelf.

Table 1.
RAN classification.

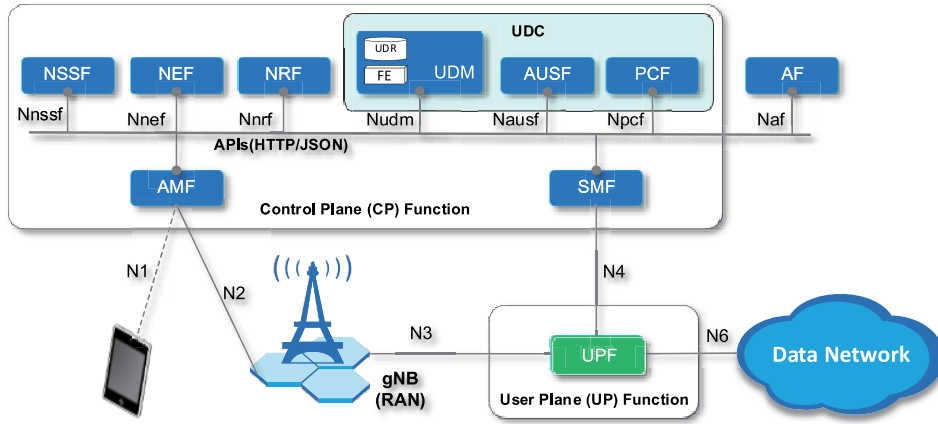


Figure 2.
5G system service-based architecture with core network functions.

architecture is illustrated in **Figure 2** and corresponding functions are described in **Table 2** [16].

The EPC (Evolved Packet Core) network consists of MME (Mobility Management Entity), S-GW (Service Gateway) and PDN gateway. EPC performs functions such as mobility management, IP connection, QoS management, and billing management.

1.3 Chapter structure and organization

The structure and organization of this book chapter are illustrated in **Figure 3**.

2. Basic multiplexing techniques

The term “multiplexing” refers to the sharing of a *system resource* (SR) to a set of users. There is a subtle distinction between multiplexing and multiple access, while multiplexing means the SR sharing is “fixed” (*static* multiplexing) or adaptive

Main functions		
NSSF	Network Slice Selection Function	Selects the Network Slice Instance (NSI) based on information provided during UE attach.
NEF	Network Exposure Function	Facilitates secure, robust, developer-friendly access to the exposed network services.
NRF	Network Repository Function	Provides a single record of all network functions.
UDM	Unified Data Management	Authentication Credential Repository, Access Authorization.
AUSF	Authentication Server Function	Authentication and Authorization.
PCF	Policy Control Function	Ensures policy and charging control, authorized QoS.
AMF	Access and Mobility Management Function	NAS Signaling TerminationMobility ManagementNetwork Slicing.
SMF	Session Management Function	Selection and control of UP function, UE IP address allocation and management.
UPF	User Plane Function	Packet routing and forwarding, QoS handling.
SMF	Session Management Function	Responsible for interacting with the decoupled data plane, creating updating and removing PDU sessions and managing session context with the UPF.

Table 2.
Core network functions.

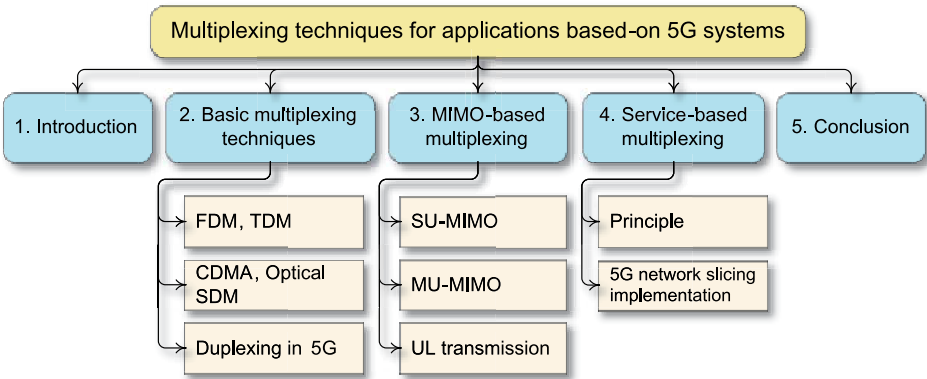


Figure 3.
Structure and organization of the book chapter.

change (*dynamic* multiplexing), multiple access techniques are those techniques that enable multiple users to share limited SRs remotely.

Multiplexing allows multiple channels/users to share the same SR. Multiplexing helps to increase the efficiency of using the SR and the transmission capacity of the system. Dynamic multiplexing makes the allocation of the SR more efficient.

5G NR systems also use “duplexing schemes” for Uplink (UL) and Downlink (DL) data transmission.

The traditional multiplexing techniques are:

1. *Frequency Division Multiplexing (FDM)*: Specified subbands of frequency are allocated. Suitable for analog signal transmission, widely used in analog broadcast radio and television.

2. *Time Division Multiplexing (TDM)*: User data are assigned in periodically recurring timeslots. Suitable for digital signal transmission, commonly used in digital telephone systems.
3. *Code Division Multiplexing (CDM)*: Specified orthogonal spread spectrum codes are allocated.
4. *Wavelength Division Multiplexing (WDM)*: WDM is used in fiber-optic communications. In WDM, several optical carrier signals are multiplexed onto a single optical fiber by using different wavelengths.
5. *Space Division Multiplexing (SDM)*: Transmitting separate data streams in parallel using the same time/frequency resources. The receiver side also requires multiple antennas to the same level (degrees of freedom) as the number of streams or layers to spatially decorrelate, demodulate and decode.
6. *Polarization Division Multiplexing (PDM) or dual polarization frequency reuse*: Orthogonal polarizations are used to transfer signals, allowing for reuse of the same frequency band.

We are now considering basic multiplexing techniques.

2.1 Frequency division multiplexing

Frequency division multiplexing (FDM) is the division of total channel bandwidth into multiple, non-overlapping subbands. Each of these subbands is assigned to a user or a signal by modulating with the appropriate carrier frequency.

The multiplexer from the transmit side is responsible for multiplexing the modulated signals with different carrier frequencies into a total signal for transmission. The demultiplexer at the receiver is responsible for separating the total signal into signals of different users by different frequencies.

Example 1. Primary FDM system (**Figure 4**) with total frequency bandwidth from 60 kHz to 108 kHz is divided into 12 subbands, each subband has a bandwidth of 4 kHz. At the transmitter, the signal of a user is transmitted through a low pass filter (LPF) which is then a single side band (SSB) modulated with an appropriate carrier frequency. At the receiver, the total signal passes through a band pass filter (BPF) and a single side band demodulator to obtain a signal for the corresponding user.

FDM has some disadvantages:

- Analog system: noise accumulates in each hop if we use repeaters.
- Difficult to fabricate high-Q bandpass filters.
- Low multiplexing factor.

2.2 Time division multiplexing

Time Division Multiplexing (TDM) is a technique for the serial transmission of user data over a common medium such as a coaxial cable.

At a time, only one user's data are transmitted serially in a time slot. TDM allows each user to use the entire system bandwidth.

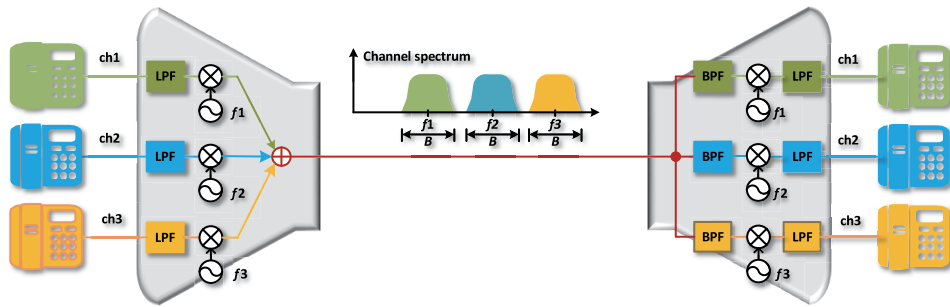


Figure 4.
 Frequency division multiplexing.

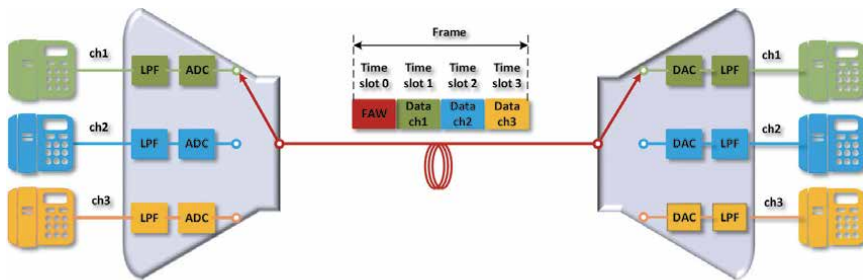


Figure 5.
 Time division multiplexing.

In addition to user data, signaling and frame alignment word (FAW) are inserted into the frame. At the receiver, there is clock recovery and frame synchronization to recover data for each channel (**Figure 5**).

2.3 Optical space-division multiplexing for MIMO systems

Space-Division Multiplexing (SDM) is a multiplexing technique for optical data transmission where multiple spatial channels are utilized. **Figure 6** shows a generic optical MIMO-SDM system. At the transmitter, the user data signals are encoded, modulated, E/O converted and then multiplexed onto different wavelengths ($\lambda_1, \lambda_2 \dots \lambda_N$) in a WDM multiplexer [17].

At the receiver, the transmitted signals are recovered using MIMO digital signal processing consisting of an $N \times N$ array of equalizers by DSP (digital signal processor). First, the N channels signal is demultiplexed by an SDM demultiplexer. Then

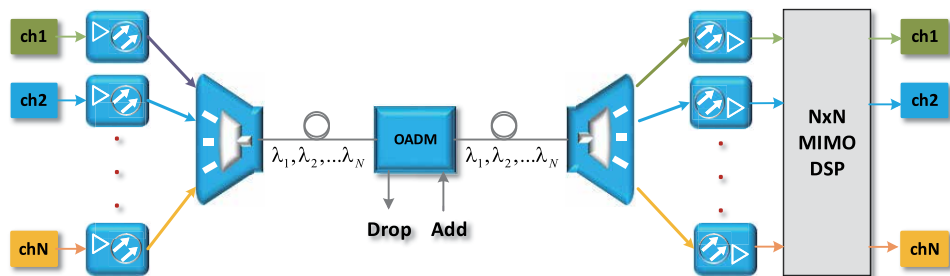


Figure 6.
 Space-division multiplexing for optical communications and application to 5G systems.

the separate signals $r_1 \dots r_N$ are fed into the $N \times N$ MIMO DSP block that is capable of eliminating all linear impairments of the transmission system and giving the reconstructed signals as output. Optical fibers are utilized at fronthaul, midhaul and backhaul of 5G systems. Data from RUs (at smallcells, for example) are multiplexed and transmitted to DU via fronthaul by optical fiber [18]. At present, a dense optical wavelength-multiplexing system has a transmission capacity of more than 1 Tera bit/s (1000 Gbit/s) per wavelength [19].

2.4 Code division multiplexing or code division multiple access

Code Division Multiple Access (CDMA) is a multiple access method that allows multiple users to share the same time and frequency resources.

In a CDMA system, each user is assigned with specific spreading code, and all users can send information simultaneously over a single communication channel. Since CDMA is based on the spread spectrum principle, each transmitter will use a pseudo-random code to modulate the data, and the receiver decodes the modulated signal using its own pseudo-random code. The principle of CDMA is illustrated in Figure 7.

2.5 Duplexing schemes in 5G NR

5G NR supports both Frequency Division Duplex (FDD) and Time Division Duplex (TDD) schemes. TDD is the main duplexing mode for higher frequencies while FDD is used for lower frequencies as the interference problems with large cells is reduced by having different frequencies in UL and DL. FDD is similar to FDM, UL and DL use separate carrier frequencies. Data are transmitted in both directions simultaneously. TDD is similar to TDM, only one carrier frequency is used. Transmission/Reception in UL and DL is assigned by different time slots.

2.5.1 5G NR frame structure

Since TDD is the main duplexing mode of a 5G NR, we will discuss more detail about TDD. We start with 5G NR frame structure. Just like the TDM system, 5G NR is frame structured. A frame has a fixed duration of 10 ms which consists of 10 subframes of 1 ms duration. Each subframe can have 2^μ slots.

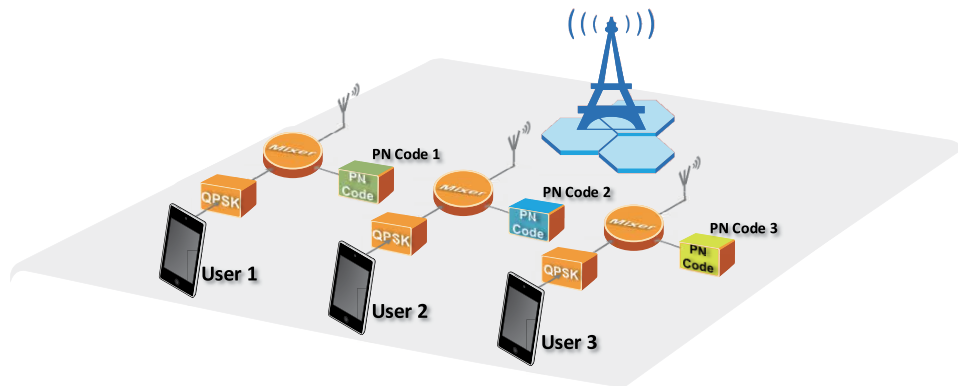


Figure 7.
Code division multiple access.

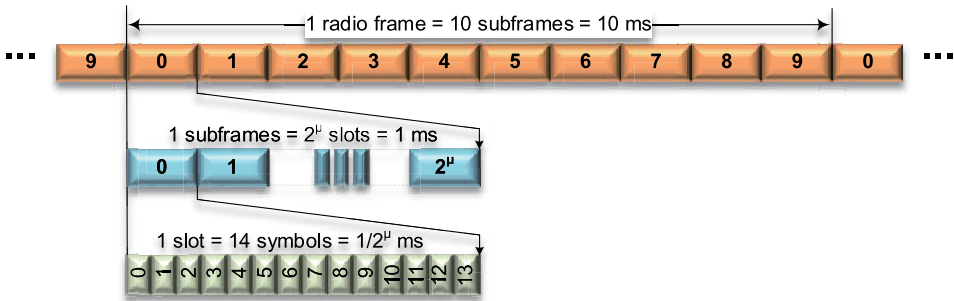


Figure 8.
5G NR frame structure.

Figure 8 shows the 5G NR frame structure. The number of slots per subframe (i.e., 2^μ), hence the slot duration depends on subcarrier spacing (SCS). 5G NR supports two frequency ranges FR1 (Sub 6GHz) and FR2 (millimeter wave range, 24.25 to 52.6 GHz). 5G NR uses flexible SCS derived from basic 15 KHz used in LTE to values of 30, 60, 120 KHz. For SCS of 15 KHz, a subframe has 1 slot of 1 ms duration. For SCS of 30 KHz, a subframe has 2 slots of 500 μ s duration as shown in **Table 3** and **Figure 9** [20].

Each slot is comprised of either 14 OFDM symbols or 12 OFDM symbols based on normal Guard Period (GP) and extended GP respectively. However, mini slots (2, 4, or 7 symbols) can be allocated for shorter transmissions. Slots can also be aggregated for longer transmissions.

SCS	μ	Number of slots per subframe	Slot duration	Number of slots in a frame	Guard Period
15 KHz	0	1	1 ms	10	Normal
30 KHz	1	2	500 μ s	20	Normal
60 KHz	2	4	250 μ s	40	Normal/Extended
120 KHz	3	8	125 μ s	80	Normal

Table 3.
Number of slots per subframe, slot duration, number of slots in a frame and guard period for reference SCS.

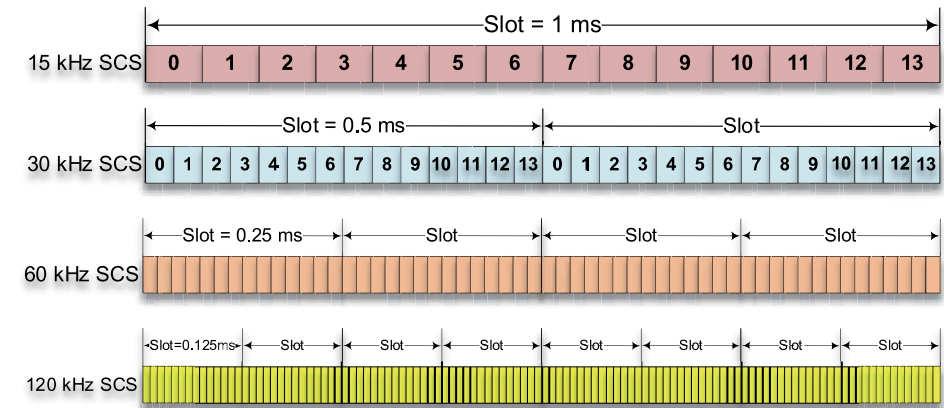


Figure 9.
5G NR scalable slot duration.

2.5.2 5G NR UL-DL pattern

Now we know the frame structure. When operating in TDD mode, we have to specify the exact timing for the uplink and downlink transmission. So, how do we define the time slots for uplink and downlink transmission?

Timeslots for uplink and downlink transmission are organized into DL-UL patterns. In LTE TDD, there are 7 predefined patterns for UL and DL allocation in a radio frame. There is no predefined pattern for 5G NR, but we can define a flexible pattern thanks to parameters in TDD UL/DL Common Configuration (*tdd-UL-DL-configurationCommon*) as shown in **Table 4** below.

You may ask yourself what is the difference between the DL-UL pattern and radio frame? The *dl-UL-TransmissionPeriodicity* parameter, for example 5 ms, defines the periodicity of the DL-UL pattern. So, a radio frame of 10 ms contains 2 DL-UL patterns.

From the above parameters, we can define TDD DL/UL configuration, aka. DL-UL pattern for 5G NR radio transmission as shown in **Figure 10**. In 5G NR, the slot

Field	Description
referenceSubcarrierSpacing	Reference SCS used to determine the number of slots in the DL-UL pattern. Only the values 15, 30 or 60 kHz (FR1), and 60 or 120 kHz (FR2) are applicable.
dl-UL-TransmissionPeriodicity	Periodicity of the DL-UL pattern in ms. This time results in even number of slots depending on the SCS. Possible values are: 0.5 ms, 0.625 ms, 1 ms, 1.25 ms, 2 ms, 2.5 ms, 5 ms and 10 ms.
nrofDownlinkSlots	Number of consecutive full DL slots at the beginning of each DL-UL pattern.
nrofDownlinkSymbols	Number of consecutive DL symbols in the beginning of the slot following the last full DL slot (as derived from nrofDownlinkSlots). The value 0 indicates that there is no partial-downlink slot.
nrofUplinkSlots	Number of consecutive full UL slots at the end of each DL-UL pattern.
nrofUplinkSymbols	Number of consecutive UL symbols in the end of the slot preceding the first full UL slot (as derived from nrofUplinkSlots). The value 0 indicates that there is no partial-uplink slot.

Table 4.
5G NR TDD DL/UL common configuration parameters.

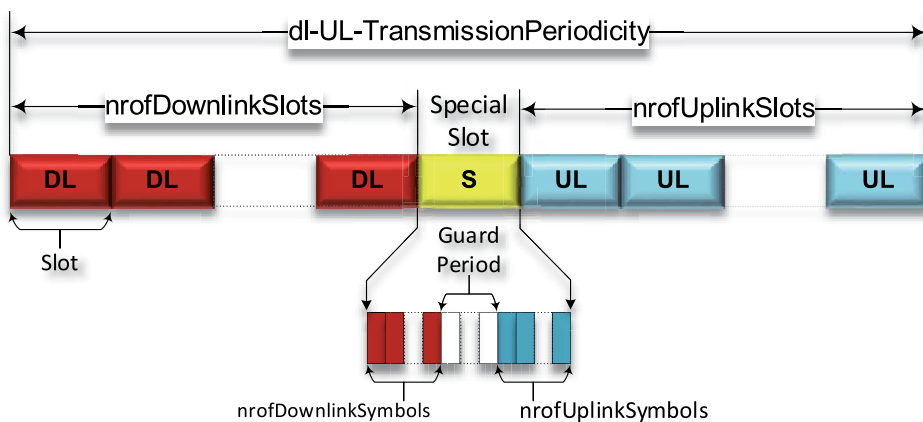


Figure 10.
5G NR TDD UL/DL common configuration frame structure.

configuration is flexible and can be changed from time to time while maintaining the focus on inter-cell interference aspects [21].

Then, the next question is how to design a transmission pattern? We know that time slots allocation for UL and DL depends on UL and DL traffic. We call that UL/DL traffic load ratio. To adapt with actual traffic, 5G NR supports 3 different TDD configurations as follows:

Static TDD configuration: For static TDD, the UL/DL traffic ratio is usually decided by the statistical UL/DL traffic load ratio among multiple operators in a specific country or region. The slots and symbols are defined over a period of time that are dedicated to either the UL or DL based on the UL/DL traffic ratio.

Semi-Static TDD configuration: This configuration is more flexible than the static TDD. We have a certain number of UL and DL slots within a transmission periodicity (defined by *dl-UL-TransmissionPeriodicity*). The remaining slots, which are neither UL nor DL, can be considered ‘Flexible’ with the help of another IE *TDD-UL-DL-ConfigDedicated*.

Dynamic TDD configuration: This is the most flexible configuration for UL/DL transmission for dynamic assignment and reassignment of time-domain resources between the UL and DL transmission. Dynamic TDD is used to adapt to actual traffic but requires coordination to avoid interference between cells, so that there is no fixed UL/DL allocation. With the popularity of video streaming increasing, it is forecast that the proportion of DL content will grow even further in the future, hence it is natural that more resources should be allocated to the DL.

Example 2. The DL-UL pattern design. Assuming SCS = 30 kHz and the carrier is FR1 with 100 MHz bandwidth.

Field name	Value
dl-UL-TransmissionPeriodicity	2.5 ms
nrofDownlinkSlots	3
nrofDownlinkSymbols	10
nrofUplinkSlots	1
nrofUplinkSymbols	2

Since slot duration for reference SCS of 30 kHz is 0.5 ms, the number of slots in DL-UL periodicity would be

$$\text{NumSlotsDLULPeriodicity} = \frac{\text{dl} - \text{UL} - \text{TransmissionPeriodicity}}{\text{Slot length}} = \frac{2.5\text{ms}}{0.5\text{ms}} = 5 \text{ slots, and}$$

$$\begin{aligned} &\text{NumberOfGuardSymbols} \\ &= \text{TotalSymbolsInPattern} - \text{TotalSymbolsWithTypeSpecified} \\ &= (14 * \text{NumSlotsDLULPeriodicity}) \\ &\quad (\text{numDLSlots} * 14 + \text{numDLSyms} + \text{numULSyms} + \text{numULSlots} * 14) \\ &= 2 \text{ symbols.} \end{aligned}$$

This DL-UL pattern is illustrated in **Figure 11**. This pattern repeats itself in the timeline.

3. 5G NR MIMO multiplexing operation

Perhaps the most challenging part of the 5G NR system is the MIMO operation modes. Let us start with SU-MIMO and MU-MIMO. SU-MIMO stands for Single-

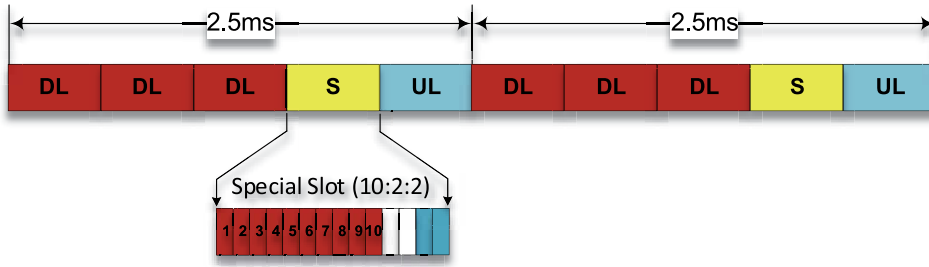


Figure 11.
Example on design a TDD downlink frame structure.

User MIMO. In Single User MIMO, both the base station and UE have multiple antennas, and the base station can transmit multiple data streams simultaneously to the UE using the same time/frequency resources. By doing so, it doubles (2×2 MIMO), or quadruples (4×4 MIMO) the peak throughput of a single user.

MU-MIMO stands for Multi User MIMO. The base station serves more than 2 UEs simultaneously. Since in MU-MIMO, the base station sends multiple data streams, one per UE, using the same time-frequency resources, MU-MIMO mode increases the total cell throughput, i.e., cell capacity. MU-MIMO is not a new concept. We have MU-MIMO in LTE (Transmission Mode 5 - TM5) and WLAN (802.11ad). However, in 5G NR the scale of MU-MIMO will be much larger and deployment will also be more common. 5G NR uses massive MIMO.

Massive MIMO employs a large number of transmit and receive antennas, improves spectral efficiency and increases the transmission data rate through spatial multiplexing to deliver multiple streams of data within the same resource block (time and frequency). Massive MIMO is also called Large Scale MIMO.

By now, you may ask a question: *Why massive MIMO, and how many antenna elements are needed to be called massive MIMO?* In conventional 4G LTE using a normal MIMO, the maximum number of the antenna is 2×2 or 4×4 and even 8×8 is mentioned. We know that the larger the number of antennas, the narrower the beam width. It means the coverage of a specific beam would be smaller. We need a more precise beam control algorithm, but in return, the achievable data rate will be higher. The number of antennas in massive MIMO should be $\gg 8$ [22].

3.1 Mathematical background

Figure 12 shows a typical MIMO system equipped with N_T transmit antennas and N_R receive antennas. The data are encoded in both space and time domains and then transmitted by N_T transmit antennas through a MIMO propagation channel.

The relationship between the input and output of a MIMO system can be written as follows

$$\mathbf{y} = \mathbf{H}\mathbf{x} + \mathbf{n}, \quad (1)$$

where.

$\mathbf{x} = [x_1, x_2, \dots, x_{N_T}]^T$ is transmitted signal,

$\mathbf{y} = [y_1, y_2, \dots, y_{N_R}]^T$ is received signal,

$\mathbf{n} = [n_1, n_2, \dots, n_{N_R}]^T$ is AWGN,

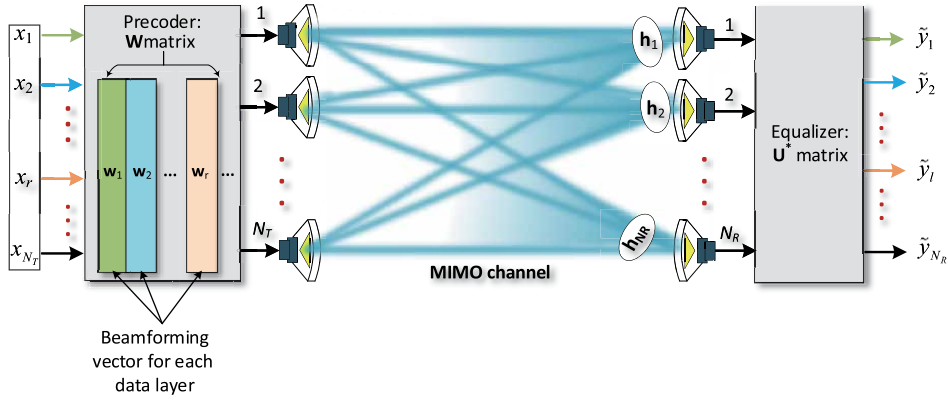


Figure 12.
 System and channel model for spatial multiplexing.

$$\mathbf{H} = \begin{bmatrix} h_{11} & h_{12} & \dots & h_{1N_T} \\ h_{21} & h_{22} & \dots & h_{2N_T} \\ \vdots & \vdots & \ddots & \vdots \\ h_{N_R1} & h_{N_R2} & \dots & h_{N_RN_T} \end{bmatrix} \text{ is channel matrix,}$$

where $h_{i,j}$ is an element of the i^{th} row and the j^{th} column in the matrix \mathbf{H} , denotes a channel from the j^{th} TX antenna to the i^{th} RX antenna.

If the channel matrix \mathbf{H} is known at both base station (gNB) and UE (i.e., Channel state information - CSI) then we could take *singular value decomposition* (SVD) on channel matrix \mathbf{H} as

$$\mathbf{H} = \mathbf{U}\mathbf{D}\mathbf{W}^*, \quad (2)$$

where $\mathbf{U} \in \mathbb{C}^{N_R \times N_R}$ and $\mathbf{W} \in \mathbb{C}^{N_T \times N_T}$ are orthogonal unitary matrices and $\mathbf{D} \in \mathbb{R}^{N_R \times N_T}$ is diagonal matrix, whose diagonal elements are non-negative real numbers and whose off-diagonal elements are zero. The diagonal elements of matrix \mathbf{D} $\lambda_1 \geq \lambda_2 \geq \dots \geq \lambda_r$ are the ordered singular values of channel matrix \mathbf{H} , where $r = \min\{N_T, N_R\}$ is rank of \mathbf{H} .

Assume the receiver knows the \mathbf{U} matrix and the transmitter knows the \mathbf{W} matrix. The transmitted data \mathbf{x} is precoded by \mathbf{W} matrix and the received data \mathbf{y} is equalized by \mathbf{U} matrix, we have

$$\begin{aligned} \tilde{\mathbf{y}} &= \mathbf{U}^* \mathbf{y} = \mathbf{U}^* [\mathbf{H}\tilde{\mathbf{x}} + \mathbf{n}] = \mathbf{U}^* [(\mathbf{U}\mathbf{D}\mathbf{W}^*)\mathbf{W}\mathbf{x} + \mathbf{n}], \\ \tilde{\mathbf{y}} &= \underbrace{[\mathbf{U}^*\mathbf{U}]}_{\mathbf{I}} \underbrace{[\mathbf{D}\mathbf{W}^*\mathbf{W}]}_{\mathbf{I}} \mathbf{x} + \mathbf{U}^* \mathbf{n}, \\ \tilde{\mathbf{y}} &= \mathbf{D}\mathbf{x} + \mathbf{U}^* \mathbf{n}, \\ \tilde{\mathbf{y}} &= \mathbf{D}\mathbf{x} + \tilde{\mathbf{n}}, \end{aligned} \quad (3)$$

where $\tilde{\mathbf{n}} \in \mathcal{CN}(0, N_0 I_{N_R})$ has the same distribution as \mathbf{n} . Thus, we have an equivalent representation as a parallel Gaussian channel

$$\tilde{y}_i = \lambda_i \tilde{x}_i + \tilde{n}_i, i = 1, 2, \dots, r. \quad (4)$$

$\mathbf{W} = [\mathbf{w}_1 | \mathbf{w}_2 | \dots | \mathbf{w}_{N_T}]$ is a precoding matrix. Each symbol x_i is precoded by precoding vector \mathbf{w}_i .

From the Eq. (4), we can see that the base station can transmit simultaneously maximum of r data streams to the target UE, increasing the channel throughput. This is called spatial multiplexing (SM). MIMO spatial multiplexing takes advantage of multipath effects, where a transmitted signal arrives at the receiver through several different paths. Each path can have a different time delay, and the result is that multiple instances of a single transmitted symbol arrive at the receiver at different times [23].

If SNR is high, the number of data streams and data rate for each stream is chosen by the *waterfilling* algorithm [24]. In the opposite case, with low SNR, the best thing to do is to simply choose one subchannel with the highest singular value. This is called beamforming [25, 26]. We can rewrite the Eq. (3) as

$$\tilde{y}_1 = \mathbf{u}_1^* \mathbf{H} \mathbf{w}_1 x_1 + \mathbf{u}_1^* \mathbf{n}. \quad (5)$$

Instead of transmitting a vector of symbols, we just transmit a single symbol at a time. The \mathbf{w}_1 vector defines the beamforming weights and \mathbf{u}_1 here defines the receive beam.

Now we know how to transmit multiple data streams to a UE. We consider the way 5G NR implement MIMO modes.

Clearly, to implement SM, the network (gNB and UEs) should know the channel matrix \mathbf{H} then calculate the 3 matrixes \mathbf{U} , \mathbf{D} , \mathbf{W} out of \mathbf{H} . The transmitter applies \mathbf{W} as a precoder and the receiver apply \mathbf{U} for processing of the received signal. For downlink transmission, gNB is a transmitter and UE is receiver and vice versa for uplink transmission.

3.2 Basic terminologies

The first thing we have to know is the codebook. The **codebook** is a set of predefined precoders (precoding matrices). Why codebook? Consider DL transmission, gNB has to calculate a precoder from a reference signal or selects a predefined precoder with a requested index from UE before transmitting data. The first case is called non-codebook and the second is called codebook-based precoding.

Codebook type in 5G NR: There are two types of codebooks specified in 5G NR. Type I is designed for SU-MIMO and selected by UE report and RRC Configuration. Type II is designed mainly for MU-MIMO and is based on a more detailed CSI report. Type I codebook has predefined matrices based on the number of layers and CSI-RS ports. Type II codebooks contain mathematical formula for selecting a set of beams and then specifying relative amplitudes and phases to generate a weighted combination of beams for each layer of transmission.

The requested index into a set of predefined matrices, a so-called codebook is a **precoding matrix indicator** (PMI). PMI is used for DL transmission, conditioned on the number of layers indicated by the RI. In the uplink direction, the PMI is denoted by **Transmit Precoder Matrix Indicator** (TPMI) to differentiate it from the downlink PMI.

Together with the codebook, **the number of layers** is the number of simultaneous data streams. The number of layers is less than or equal to the rank of the channel matrix that we mentioned before. The number of layers depends upon the channel condition between receiver and transmitter antennas. Low correlation propagation paths increase rank and the number of layers and vice versa. **Rank indicator** (RI) defines the number of possible transmission layers for the downlink and uplink transmission under specific channel conditions. However, gNB does not need to transmit RI as requested by the UE.

Channel state information (CSI) are parameters related to the state of a channel including the channel quality indicator (CQI), precoding matrix indicator (PMI) and rank indicator (RI). UE reports CSI parameters to gNB as feedback in CSI-RS mode.

Channel quality indicator (CQI) is an indicator of channel quality. The CQI index is a scalar value from 0 to 15 representing the highest modulation-and-coding scheme (MCS) to achieve the required block error rate (BLER) for given channel conditions.

CSI-RS resource indicator (CRI), used in conjunction with beamformed CSI reference signals. The CRI indicates the beam the device prefers in case the device is configured to monitor multiple beams.

SRI is an SRS resource indicator.

3.3 Physical antenna configuration versus antenna ports

It is very important to understand the physical antenna configurations, the antenna port and the relationship between them. The antenna system in 5G NR is an Active Antenna System (AAS). Typical active antennas are made up of a matrix of subarrays. Each subarray consists of individual dual-polarized elements. Each polarization is controlled by a beamforming (BF) coefficient. Therefore, the number of columns is doubled.

For example, **Figure 13a** shows 8T8R configuration with 4 columns, 1 row (4x1) consisting of 4 (1x8) subarrays. **Figure 13b** shows 64T64R configuration which is made up of 8 columns, 4 rows of (1x2) subarrays.

Figure 14a shows single panel antenna. 5G NR supports both single panel and uniform (b) and non-uniform multi-panel (c). In 5G NR, logical antenna configuration is described by 3 parameters: N_g is the number of panels, N_1 is number of columns and N_2 is the number of rows in a panel.

In association with N_1 and N_2 , 3GPP defines DFT oversampling factors O_1 and O_2 to determine the sweeping steps of a beam during the beam management (beam tracking). O_1 determines the sweeping step in the horizontal direction and O_2 determines the sweeping step in the vertical direction.

We have:

- Number of polarizations = 2,
- Number of CSI-RS antenna ports = $(2 * N_1) * N_2$,

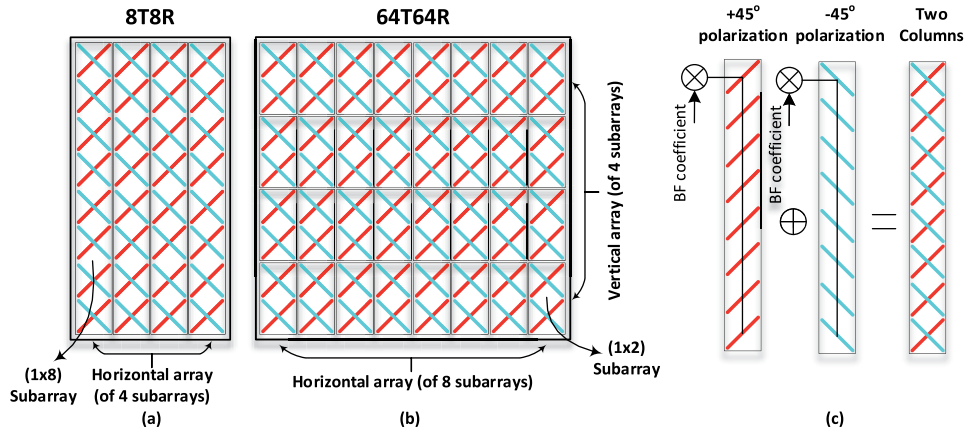


Figure 13.
Physical antenna configuration.

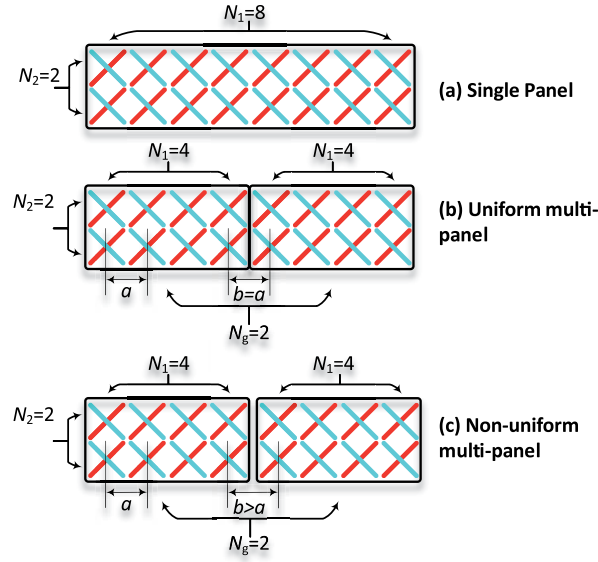


Figure 14.
Single panel and multi panel antenna configurations.

- Number of beams in a column = $N_1 * O_1$,
- Number of beams in a row = $N_2 * O_2$,
- Number of beams = $(N_1 * O_1) * (N_2 * O_2)$ = from 8 to maximum 256 beams.

Antenna port: This is a logical concept and different from the physical one that you see on the antenna tower. You can find the definition of antenna port from the 3GPP specification as “an antenna port is defined such that the channel over which a symbol on the antenna port is conveyed can be inferred from the channel over which another symbol on the same antenna port is conveyed” [27]. We can understand the antenna port like socket and port concept which is used on Internet. For example, port 80 is used for the HTTP protocol, port 20 for FTP, port 22 is for SSH, port 25 is for SMTP. We use “antenna ports” to transmit and receive data. Why the definition of antenna port of 3GPP is related to the channel because we have to estimate the channel model before decoding transmitted data. The channel model has estimated thanks to reference signals. Each antenna port is assigned by a dedicated reference signal. Each antenna port represents a specific and unique channel model. The receiver can use a reference signal transmitted on an antenna port to estimate the channel model for this antenna port and this channel model can subsequently be used for decoding data transmitted on the same antenna port.

Each antenna port carries its own resource grid. One resource grid is transmitted on a given antenna port, subcarrier spacing configuration and transmission direction (downlink or uplink). The resource grid consists of a number of RBs (Resource Blocks) for one subframe.

3.4 Physical channels and signals

Physical Channels and Signals for DL, UL and corresponding antenna port addresses are as follows (**Table 5**):

Downlink channels		Function	Antenna port starting from:
PDSCH	Physical downlink shared channel	Carry user data in the downlink direction	1000 (1000 Series)
PDCCH	Physical Control Channel	Carry DCI (Downlink Control Information) e.g., downlink scheduling assignments and uplink scheduling grants.	2000 (2000 Series)
CSI-RS	Channel State Information - Reference Signal	For DL CSI acquisition. CSI-RS is configured specifically to UE. But multiple users can also share the same resource.	3000 (3000 Series)
SS-Block/ PBCH	Physical broadcast Channel	The combination of SS and PBCH is known as SS-Block (SSB). PBCH carries very basic 5G NR system information for Use (Downlink System BW, Timing information in the radio frame, SS burst set periodicity, System frame number).	4000 (4000 Series)
Uplink Channels		Function	Antenna port starting from:
PUSCH/ DMRS	Physical Uplink Shared Channel / Demodulation Reference Signal	It is used by a 5G NR receiver to produce channel estimates for demodulation of the associated physical channel.	1000 (1000 Series)
SRS, precoded PUSCH	Sounding Reference signal	It is used for UL channel sounding. In contrast to LTE, it is configured specifically to UE.	1000 (1000 Series)
PUCCH	Physical Uplink Control Channel	transport UCI (Uplink Control Information) e.g., HARQ feedback, SR (Scheduling Request) and CSI report (CQI, PMI, RI, Layer Indicator LI).	2000 (2000 Series)
PRACH	Physical Random Access	Carry random access preamble from UE towards gNB (i.e., 5G NR base station). It helps gNB to adjust the uplink timings of the UE in addition to other parameters.	4000 (4000 Series)

Table 5.
Physical channels and signals and corresponding antenna port addresses.

3.5 Mapping antenna ports to physical antennas

There is no strict mapping of antenna ports to physical antenna ports. **Figure 15** indicates the mapping between antenna ports and physical antennas. One antenna port can be mapped to single or multiple physical antenna(s). Due to each antenna port representing a specific and unique channel model, the number of layers in the physical layer may reach the number of antenna ports. The number of layers may range from a minimum of one layer up to a maximum number of layers equal to the number of antenna ports. The layers are then mapped to the antenna ports.

3.6 Downlink MIMO schemes

Legacy LTE supports 9 transmission modes (TM). To avoid sophisticated transmission mode handover for different scenarios, 5G NR uses the term *unified transmission mode* [28]. However, according to the channel state information (CSI) acquisition method, downlink MIMO schemes are categorized into (**Figure 16**):

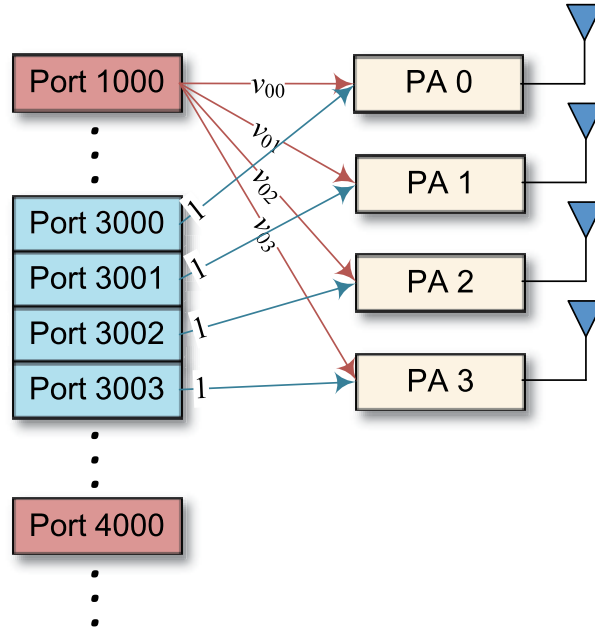


Figure 15.
Mapping antenna ports to physical antennas.

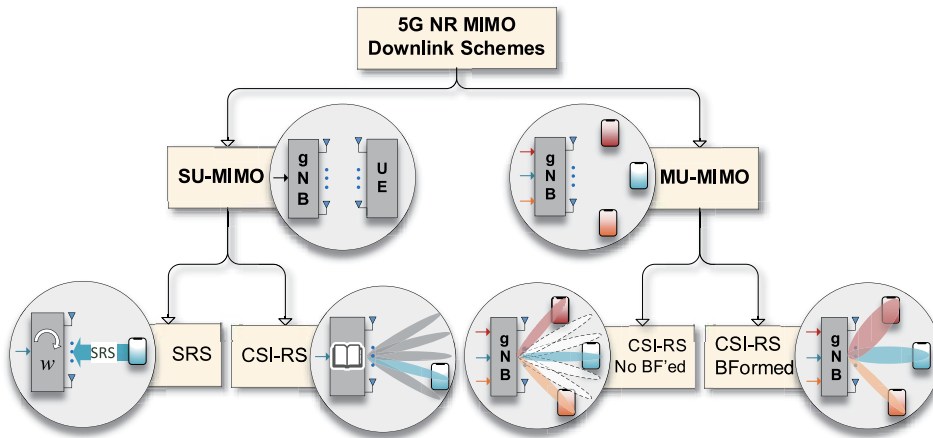


Figure 16.
Downlink MIMO schemes.

Single User MIMO (SU-MIMO):

- SRS-based (sounding reference signal)
- CSI-RS-based (CSI - reference signal, codebook type I, Single / Multi panel)

Multi User MIMO (MU-MIMO):

- CSI-RS without Beamforming (codebook type II Single Panel)
- CSI-RS Beamformed (codebook type II Port Selection)

DL and UL channels are considered reciprocal. From a channel calculation perspective, in SRS-based Single User MIMO scheme, channel calculation obligation belongs to gNB, the remaining schemes rely on UE's CSI report from its channel calculation. The device's capability and channel condition decide the best MIMO mode among the above schemes.

3.7 Single user MIMO schemes

3.7.1 Procedure for SRS-based single user MIMO

1. UE transmits sounding reference signals through each of its antenna ports.
2. gNB estimates the channel (e.g., downlink precoding weights) based on received sounding reference signals
3. gNB transmits PDSCH using a calculated precoder.

This scheme is illustrated in **Figure 17a**, and very simple but due to size and power at the UE are limited, the number of the antenna of UE is smaller than that of gNB and adding more RF chains to UE is difficult, SRS resources are transmitted on antenna ports one by one by transmit antenna switching (TAS).

3.7.2 CSI-RS based single user MIMO

Figure 18 shows a typical downlink transmission CSI-RS based SU/MU-MIMO scheme. First of all, UE needs to know the \mathbf{H} matrix. The gNB is obligated to transmit CSI-RS ports so that UE can observe the full MIMO channel matrix. UE calculates the channel matrix and reports PMI, RI and CQI to gNB.

In the equivalent MIMO channel, we have N_L data streams, corresponding to N_L layers. Each i -th diagonal element of \mathbf{D} , λ_i , represents the i -th layer's channel magnitude; \mathbf{w}_i , the i -th column vector of \mathbf{W} , is the beamforming weights for the i -th layer.

UE reports gNB its preferred PMI but gNB is not obligated to apply the precoding indicated by the PMI, and the gNB does not provide the UE with explicit

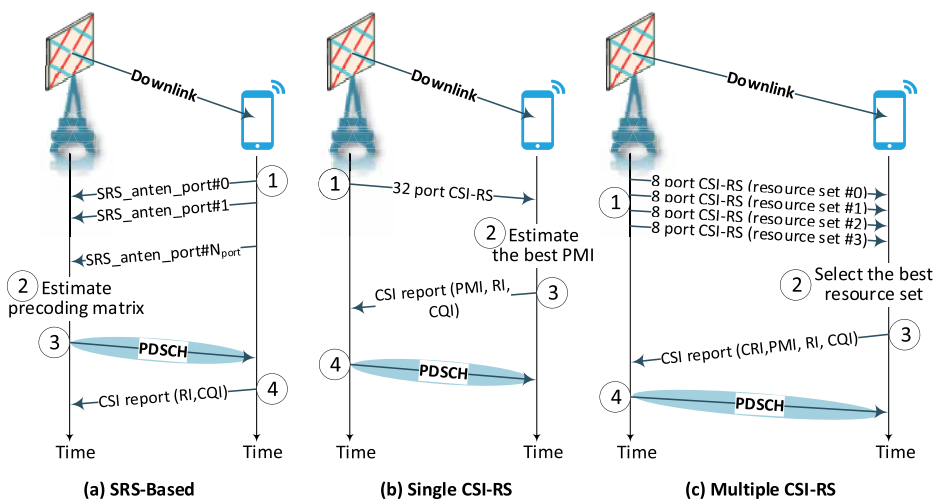


Figure 17.
Downlink single user MIMO operation.

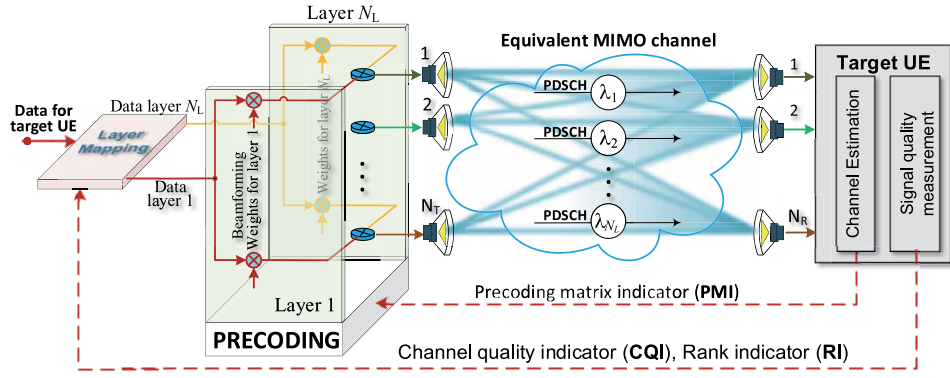


Figure 18.
CSI reporting and equivalent channel for SU-MIMO.

information regarding the precoding procedure. The UE relies upon using the Demodulation Reference Signal (DMRS) when decoding the PDSCH.

CSI-RS single user MIMO scheme uses type I codebook which is based upon a specific set of assumed antenna configurations. The antenna configurations are Single Panel and Multi Panel as described in **Tables 6** and **7**.

For codebook type I single panel: MIMO ranks: 1 to 8; CSI RS Ports: 2, 4, 8, 12, 16, 24, 32.

For codebook type I multi panel: MIMO ranks: 1 to 4; CSI RS Ports: 8, 16, 32.

3.7.3 Procedure for CSI-RS based single user MIMO

1. gNB transmits **32** CSI-RS ports to UE (**Figure 17b**). If DL antenna ports for CSI measurement is limited to ≤ 8 , for example = 8, gNB has to transmit 4 CSI-RS sets of resources of 8 ports (**Figure 17c**)
2. UE estimates the channel based on the received CSI-RS resources, selects the best PMI.
3. UE reports PMI, RI, CQI to gNB.
4. gNB decides a precoder to transmit PDSCH.

3.8 Multi-user MIMO schemes

In Multi User MIMO schemes, gNB tries to communicate simultaneously with a set of UE through the same time/frequency resources. MU-MIMO schemes uses Type II codebook to provide more details about Channel State Information. MU-MIMO schemes support to a maximum of 2 layers per UE. This is smaller than that of SU-MIMO (up to 8 layers for type I single panel) but the maximum number of layers per cell is higher to allow multiple UE to use 2×2 MIMO simultaneously.

DL MU-MO Type II codebook allocates a set of beams to each UE. Each set of the beam is the weighted combination of beams with relative amplitudes and co-phasing phase shifts.

Beamformed CSI-RS relies upon the gNB having some advanced information to allow beamforming of the CSI Reference Signal transmissions.

Procedure for beamformed CSI-RS as follows: gNB transmits one or more CSI-RS, each in different “directions”. UE computes and reports CRI/PMI/CQI to gNB.

Number of CSI-RS antenna ports	4	8	12	16	24	32
(N_1, N_2)	(2,1)	(2,2)	(4,1)	(4,2)	(8,1)	(8,2)
(O_1, O_2)	(4,1)	(4,4)	(4,4)	(4,4)	(4,1)	(4,4)
					(12,1)	(16,1)
					(6,2)	(4,4)
					(4,4)	(4,4)

Table 6.
Single panel antenna configuration.

Number of CSI-RS antenna ports	8	16	32
(N_g, N_1, N_2)	(2,2,1) (2,4,1)	(4,2,1) (2,2,2) (2,8,1)	(4,4,1) (2,4,2) (4,2,2)
(O_1, O_2)	(4,1) (4,1)	(4,1) (4,4) (4,1)	(4,1) (4,4) (4,4)

Table 7.
Multi panel antenna configuration.

3.9 Uplink transmission modes

5G NR supports uplink PUSCH precoding up to 4 layers. However, in the case of DFT-based transform precoding, only single-layer transmission is supported. The transmitted symbols are layer mapped and then precoded at the UEs.

If gNB instructs UE on PDCCH regarding the choice of precoding matrix selected from a codebook: codebook based (**Figure 19a**). Otherwise, UE measure DL CSI-RS signal to determine precoding weights (not constrained to a codebook): Non-codebook based (**Figure 19b**).

3.9.1 Procedure for non-codebook-based transmission mode

1. UE measures DL CSI-RS signal to design suitable precoders for the SRS transmission.
2. UE transmits up to four SRS resources where each resource has one antenna port.
3. gNB determines one or multiple SRIs based on the received SRSs, number of layers for PUSCH. In this example, SRS1 and SRS3 are selected. TRI is equal to the number of SRIs.

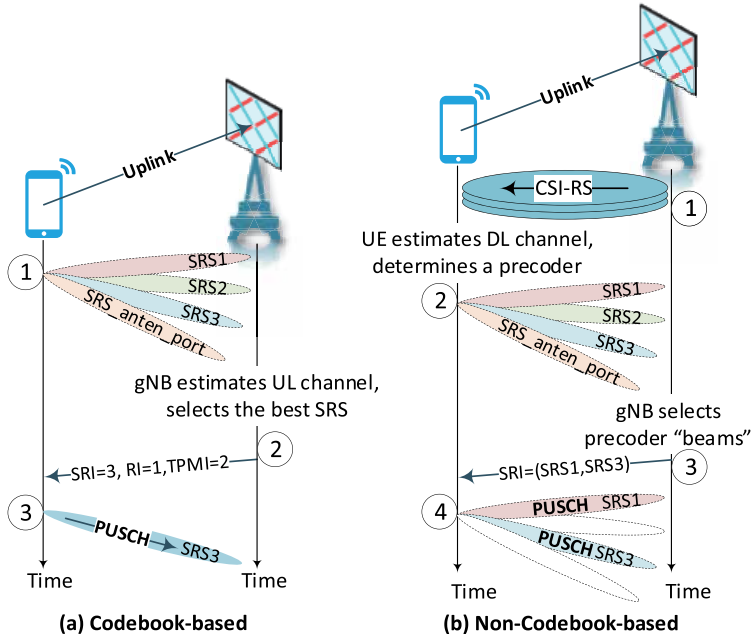


Figure 19.
Uplink MIMO operation.

4. UE uses selected resources to transmit PUSCH.

3.9.2 Procedure for codebook-based transmission mode

1. UE transmits SRS from each of its antenna ports.
2. gNB estimates UL channel based on the received SRSs to select the best SRS for antenna port, appropriate rank and precoding matrix. gNB transmits SRI (SRS resource indicator), RI and TPMI to UE.
3. UE uses selected resources to transmit PUSCH from the indicated antenna port, the number of layers and precoding matrix.

4. Service-based multiplexing

4.1 Principle

5G networks are designed for a wide variety of use cases including urban mobile broadband, massive machine-type communications, ultra-reliable low latency communications, applications such as remote surgery, autonomous driving, a massive number of sensors communicating with the network, 3D video streaming.

The problem is that the physical infrastructure resources are limited. The need for data, services and operators working on the same network increase. The solution is network slicing (NS). NS will create virtual network segments for the different services within the same 5G network. NS will divide the physical network into independent logical subnets for different kinds of services, each of which has a size and structure suitable for dedicated service [29].

NS is one of the key features of 5G NR. NS allows operators to support efficiently different use cases and enterprise customers on a dedicated 5G network. NS leverages the running of multiple logical subnets on top of physical network, multiplexes data services over physical infrastructure.

The concept of network slicing is illustrated in **Figure 20** showing two slices. One slice supports smartphones with 3D streaming, virtual reality (VR) connections with guaranteed throughput slice, the other supports automotive connectivity, IIoT for smart factory with low latency slice on the same network infrastructure [30].

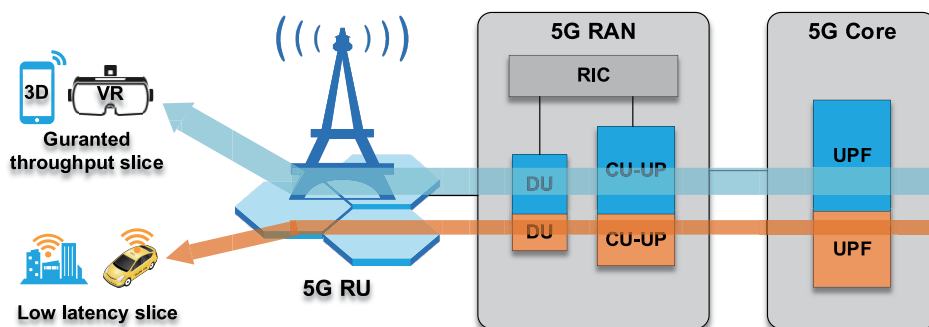


Figure 20.
 Service multiplexing by network slicing.

4.2 5G network slicing implementation

An End-to-End (E2E) Network Slice consists of RU, RAN and Core Transport subnets. Basically, we have to designed Slice Profiles (for RAN, Core and Transport subnets) including the slice characteristics and requirements needed to support the service requested by the UE. Procedure for slicing is as follows:

1. Create slice profile:

The customer will provide their service requirements they want to run on a network slice including bandwidth, capacity, and latency. The operator creates a service level agreement, and allocates the necessary capacity and bandwidth for the slice by NSSAI (Network Slice Selection Assistance Information). NSSAI consists of up to 8 S-NSSAI (Single –NSSAI). The S-NSSAI contains two components: the SST (Slice/Service Type) and an optional SD (Slice Differentiator).

2. UE gathers information for slices when registering for the network:

The UE gathers information for the available slices when registering for the network via NAS signaling. A single UE may be assigned up to eight difference slices [31].

3. Determines the candidate AMF(s) or AMF Set to be used to serve the UE:

Once a PDU session is set up, the UE is then signaled to the NSSAI, assuming this has been provided earlier to the UE.

4. Selects which slices the UE can connect:

Based on required NSSAI and registered information, the network will select the appropriate slice instance and related resources, with the AMF coordinating the actions in the 5G core network. There is one AMF that is common for all the slices a single UE has.

5. Conclusion

This chapter presented multiplexing techniques utilized in 5G systems. Duplexing is one of the key factors affecting the performance of 5G NR in terms of their wide-area coverage. The Frequency Division Duplex (FDD) and Time Division Duplex (TDD) schemes utilized in 5G NR are inherited from FDM and TDM, providing flexibility for designing UL/DL patterns.

Spatial multiplexing supports multi layer transmission. Multiple beamforming will transmit data through targeted beams and advanced signal processing that could speed up data rates and boost bandwidth and reduce interference for nearby users. 5G NR permits to use different waveforms on subbands with scalable subcarrier spacing and transmission time interval operating on one frequency band. Network slicing creates independent logical subnets for different kinds of services.

With these multiplexing techniques, 5G systems could provide data rate up to 20 Gbps and capacity increase by 1000 times and flexible platform for the services like massive Industrial Internet of Things (IIoT), connected society, smart factories.

It is expected that 5G combined with artificial intelligence can improve social life, make life better, more productivity, and safety.

Author details

Nguyen Huu Trung
Hanoi University of Science and Technology, Hanoi, Vietnam

*Address all correspondence to: trung.nguyenhuu@hust.edu.vn

IntechOpen

© 2022 The Author(s). Licensee IntechOpen. This chapter is distributed under the terms of the Creative Commons Attribution License (<http://creativecommons.org/licenses/by/3.0>), which permits unrestricted use, distribution, and reproduction in any medium, provided the original work is properly cited. 

References

- [1] 5G Americas. The 5G Evolution: 3GPP Releases 16-17 [Internet]. 2020. Available from: <https://www.5gamericas.org/wp-content/uploads/2020/01/5G-Evolution-3GPP-R16-R17-FINAL.pdf> [Accessed: 2021-10-01]
- [2] Qureshi HN, Manalastas M, Zaidi SMA, Imran A, Al Kalaa MO. Service level agreements for 5G and beyond: Overview, challenges and enablers of 5G-healthcare systems. *IEEE Access*. 2020;**9**:1044-1061. DOI: 10.1109/ACCESS.2020.3046927
- [3] Jong Gyu O, Won YJ, Lee JS, Kim Y-H, Paik JH, Kim JT. A study of development of transmission systems for next-generation terrestrial 4 K UHD and HD convergence broadcasting. *EURASIP Journal on Wireless Communications and Networking*. 2015; **128**:1-16. DOI: 10.1186/s13638-015-0362-x
- [4] Ullah H, Nair NG, Moore A, Nugent C, Muschamp P, Cuevas M. 5G Communication: An overview of vehicle-to-everything, drones, and healthcare use-cases. *IEEE Access*. 2019; **7**:37251-37268. DOI: 10.1109/ACCESS.2019.2905347
- [5] Technical Specification: Service Requirements for the 5G System. TS 22.261 V16.12.0. 2020
- [6] Samsung Technical White Paper: Massive MIMO for New Radio. 202.
- [7] Technical Specification: NR and NG-RAN Overall Description; Stage-2. TS 38.300 version 16.2.0. 2020
- [8] Technical Specification: NR Physical Layer Procedures for Data. TS 38.214 V16.2.0. 2020
- [9] Technical Specification: NG-RAN; Architecture Description. TS 38.401 V16.0.0. 2019
- [10] Akyildiz IF, Wang P, Lina S-C. Softair: A software defined networking architecture for 5G wireless systems. *Computer Networks*. 2015;**85**:1-18. DOI: 10.1016/j.comnet.2015.05.007
- [11] Alba AM, Janardhanan S, Kellerer W. Enabling dynamically centralized RAN architectures in 5G and beyond. *IEEE Transactions on Network and Service Management*. 2021;**18**:3509-3526. DOI: 10.1109/TNSM.2021.3071975
- [12] Beccaria M, Massaccesi A, Pirinoli P, Khac KN, Trung NH, Manh LH. Innovative MIMO antennas for 5G communication systems. In: 2018 IEEE International Conference on Environment and Electrical Engineering and 2018 IEEE Industrial and Commercial Power Systems Europe (EEEIC / I&CPS Europe); 12-15 June 2018. Palermo, Italy: IEEE; 2018. DOI: 10.1109/EEEIC.2018.8493747
- [13] Xiao Y, Zhang J, Ji Y. Energy-efficient DU-CU deployment and lightpath provisioning for service-oriented 5G metro access/aggregation networks. *Journal of Lightwave Technology*. 2021;**39**:5347-5361. DOI: 10.1109/JLT.2021.3069897
- [14] De Ree M, Mantas G, Radwan A, Mumtaz S, Rodriguez J, Otung IE. Key management for beyond 5G mobile small cells: A survey. *IEEE Access*. 2019; **7**:59200-59236. DOI: 10.1109/ACCESS.2019.2914359
- [15] Gavrilovska L, Rakovic V, Denkovski D. From cloud RAN to Open RAN. *Wireless Personal Communications*. 2020;**113**:1523-1539. DOI: 10.1007/s11277-020-07231-3
- [16] Gupta A, Jha RK. A survey of 5G network: Architecture and emerging technologies. *IEEE Access*. 2015;**3**: 1206-1232. DOI: 10.1109/ACCESS.2015.2461602

- [17] Corcoran B, Tan M, Xingyuan X, Boes A, Jiayang W, Nguyen TG, et al. Ultra-dense optical data transmission over standard fibre with a single chip source. *Nature Communications*. 2020;**11**:1-7. DOI: 10.1038/s41467-020-16265-x
- [18] Huang M-Y, Chen Y-W, Shiu R-K, Wang H, Chang G-K. A bi-directional multi-band, multi-beam mm-wave beamformer for 5G fiber wireless access networks. *Journal of Lightwave Technology*. 2021;**39**:1116-1124. DOI: 10.1109/JLT.2020.3042052
- [19] Miyamoto Y, Takenouchi H. Dense space-division-multiplexing optical communications technology for petabit-per-second class Transmission. NTT Technical Review. 2014;**12**:1-7
- [20] Technical Specification: NR Physical Layer Procedures for Control. TS 38.213 V16.2.0. 2020
- [21] Sun S, Moon S, Fwu J-K. Practical link adaptation algorithm with power density offsets for 5G uplink channels. *IEEE Wireless Communications Letters*. 2020;**9**:851-855. DOI: 10.1109/LWC.2020.2973152
- [22] Trung NH, Binh DT. Large-scale mimo MC-CDMA system. *Vietnam Journal of Science and Technology*. 2018;**56**:102-112. DOI: 10.15625/2525-2518/56/1/9204
- [23] Zeb K, Zhang X, Zhenguo L. High capacity mode division multiplexing based MIMO enabled all-optical analog millimeter-wave over fiber fronthaul architecture for 5G and beyond. *IEEE Access*. 2019;**7**:89522-89533. DOI: 10.1109/ACCESS.2019.2926276
- [24] Gary X, Li Y, Yuan J, Monroe R, Rajagopal S, Ramakrishna S, et al. Full dimension MIMO (FD-MIMO): Demonstrating commercial feasibility. *IEEE Journal on Selected Areas in Communications*. 2017;**35**: 1876-1886. DOI: 10.1109/JSAC.2017.2711150
- [25] Trung NH, Anh NT, Duc NM, Binh DT, Tan LT. System theory based Multiple Beamforming. *Vietnam Journal of Science and Technology*. 2017;**55**: 653-665. DOI: 10.15625/2525-2518/55/5/9149
- [26] Le T-T, Nguyen T-H, Nguyen H-T. User grouping for massive MIMO terrestrial broadcasting networks. In: 2020 IEEE Eighth International Conference on Communications and Electronics (ICCE); 13–15 January 2021. Phu Quoc Island, Vietnam: IEEE; 2021. DOI: 10.1109/ICCE48956.2021.9352134
- [27] Technical Specification: Physical Channels and Modulation. TS 38.211 V16.2.0. 2020
- [28] Schulz B. LTE Transmission Modes and Beamforming. White Paper, 1MA186_2e, 2015
- [29] Barakabitze AA, Ahmad A, Mijumbi R, Hines A. 5G network slicing using SDN and NFV: A survey of taxonomy, architectures and future challenges. *Computer Networks*. 2020; **167**:1-40. DOI: 10.1016/j.comnet.2019.106984
- [30] Popovski P, Trillingsgaard KF, Simeone O, Durisi G. 5G wireless network slicing for eMBB URLLC and mMTC: A communication-theoretic view. *IEEE Access*. 2018;**6**:55765-55779. DOI: 10.1109/ACCESS.2018.2872781
- [31] Technical Specification: NR User Equipment (UE) Procedures in Idle Mode and in RRC Inactive State. TS 38.304 V16.2.0. 2020

Edited by Somayeh Mohammady

The idea of sharing a medium between signals originated sometime in the late 18th century and first appeared in wired telephone systems in the United States in the early 19th century. Multiplexing (MUX), a method by which multiple analog or digital signals are combined into one signal over a shared medium, increases the capacity of the communication channel by dividing it into several logical channels, one for each message signal or data stream to be transferred. On the receiver side, the reverse process known as de-multiplexing (DEMUX) helps to extract the original channel. This book examines recent advances and novel applications in MUX and DEMUX. It discusses how MUX is applied in free-space optics (FSO) applications and how 5G and 6G signals benefit from MUX, among other topics.

Published in London, UK

© 2022 IntechOpen
© The7Dew / iStock

IntechOpen

